The Role of Geophysics in the Investigation of Contaminated Land

Anna C. Vickery

Doctor of Philosophy University of Edinburgh 1999

ABSTRACT

The full potential of non-invasive geophysical methods and their application to polluted sites is seldom recognised. There are over 32,000 hectares of known or suspected contaminated land in England and Scotland which, under the contaminated land provisions contained in the 1995 Environment Act, will require location and inspection by local councils. In consequence, the promotion of shallow, non-invasive geophysical surveying is imperative.

After an extensive desk study and a number of trial surveys, electrical and electromagnetic techniques were chosen for the geophysical investigation of 2 ex-oil distribution terminals in West Granton, Edinburgh, which the City of Edinburgh Council aim to acquire for remediation and redevelopment. An electromagnetic survey of the site was conducted, using a Geonics EM31 conductivity meter, as part of a complete assessment of the surface pollution. A 2-D resistivity survey was later employed to image the geology beneath the site with the aim of locating potential contaminant pathways.

The EM31 is directionally dependent and yields different results when its boom is either parallel or perpendicular to subsurface linear anomalies. Use of the second derivative of unidirectional measurements clarified the response of a labyrinth of underground pipes easing interpretation by geophysicists and non-geophysicists alike. The electromagnetic survey also successfully located a number of shallow oil plumes emanating from the ends of buried, broken pipes.

The computer controlled 2-D resistivity imaging method provided rapid coverage of the Granton site returning a large number of 2-D apparent resistivity pseudosections. The subsurface pipe network had a significant effect on the resistivity measurements and masked the response of the background geology. In order to reconstruct the background resistivity distribution, the effect of a subsurface linear conductor was quantified using a known analytical solution. Pipes could then be located and their effects removed from apparent resistivity pseudosections. Contour plots (plan views) of the background resistivity distributions across the complete site were then constructed by extracting resistivity data points from all modelled profiles at equivalent depths. These contour plots proved invaluable for the assessment of the integrity of the superficial clay coverage, for the location of faults and for resolving complex geology.

A pseudo 3-D model of the resistivity distributions beneath the Granton site was constructed from the contour plots. To test the validity of the model, 3-D forward modelling was employed to produce a synthetic 2-D response to compare with the observed data. The forward modelled pseudosections in response to the 3-D model compare favourably with the measured

responses and match these data more closely than the calculated response to 2-D models. This demonstrates the increased accuracy of the 3-D rather than the 2-D representation.

The conclusions obtained from non-invasive geophysical surveying over the Granton site far exceed any interpretations that could be drawn from the invasive survey alone. As a result of the work, the Granton site remediation plans have been substantially redesigned and the benefits of geophysics have been promoted.

DECLARATION

This thesis has been composed solely by myself. The work presented is my own except where otherwise acknowledged.

ACKNOWLEDGEMENTS

This work was carried out during the tenure of a Natural Environment Research Council studentship and field work was conducted under contract to Edinburgh City Council (ECC) and Lothian and Edinburgh Enterprise Limited.

I have been fortunate enough to receive help and support from a huge number of friends and colleagues during my time in Edinburgh. I would like to thank them all and, in particular, I would like to extend thanks to the following people:

To Bruce Hobbs for his excellent supervision and thanks also to his family for teaching him how to recognise a crisis moment which requires immediate cake or chocolate.

To Rebecca Lunn for arriving just in time armed with her hydrogeology expertise. For all her hard work in negotiating with ECC to ensure the department's contribution to the Granton project which provided me with the majority of the data included in this thesis. I must thank her also for her speedy reading and swimming.

To Pete Styles for believing in me and offering me some fantastic opportunities to discover more about geophysics beyond the oil business, Geordie songs and South America!

To Richard Bates for introducing me to environmental geophysics in the 'real world' at Black-hawk Geosciences and, after a lengthy stay with him and his family in Colorado, becoming a good friend and a great geophysics sounding board.

To the computing officers, the technicians and all my long suffering field assistants. To Klaus Spitzer for the use of his 3-D forward modelling program. To Richard Holme for (stealing a quote from previous acknowledgements) his 'mathemagics'. To Zoe for saving me ridiculous amounts of time with her extensive knowledge of the evil Corel Draw. To Alan Pike for providing help and entertainment on fieldwork and to Mark for his constructive (if a little insensitive!) criticism and for being the most loyal friend anyone could wish for.

Finally, I would like to offer my thanks to a number of people who wisely avoided the science and offered their support in many different ways.

To Dan for opening my eyes to many beautiful things. To Jo for her wonderful, inspirational friendship. To my family, including Davina and the Skertchlys, for their love and to Matthew for achieving the impossible and making writing up one of the happiest times I've known.

CONTENTS

LIST OF FIGURES

List of Symbols

A	Cross-sectional area of a sample	m^2
c	Pipe diameter	m
d	Distance of pipe from current source in y direction	m
g	Gravitational constant	$9.81 ms^{-2}$
H	Total hydraulic head	m
h	Pipe depth	m
I	Electric current	A
K	Hydraulic conductivity	ms^{-1}
k	Hydraulic permeability	m^2
p	Pressure	Pa
Q	Volume flow rate	$m^3 s^{-1}$
v	Voltage	V
x	Horizontal space coordinate	m
y	Horizontal space coordinate	m
z	Vertical space coordinate; elevation head	m
μ_f	Fluid viscosity	Pa s
ρ_f	Fluid density	kg m^{-3}
ρ	Electrical resistivity	Ωm
Φ	Porosity	dimensionless
Ψ	Angle between the electrode array and the perpendicular to the pipe	degrees
Ω_p	Primary potential	V
Ω_s	Secondary potential	V

1 INTRODUCTION

1.1 Rationale for Geophysical Investigations of Contaminated Land

The contaminated land provisions contained in the 1995 Environment Act will soon require local councils to be responsible for inspecting and locating contaminated land within their areas. To enable enforcement of this act 'Statutory Guidance and Regulations on Contaminated Land' will be produced by the Department of the Environment; these provide guidelines which the enforcing authority (local council) must follow in accordance with (Environment Act, 1995). The guidance includes a formal definition of contaminated land and outlines the local authority's responsibilities toward land within their area.

Contaminated land is defined as:

> any land which appears to the local authority in whose area it is situated, to be in such a condition, by reason of substances in, on or under the land, that
>
> 1. significant harm is being caused or there is a significant possibility of such harm being caused (by identified pathways to identified receptors or targets); or
> 2. pollution of controlled waters is being, or is likely to be caused.

It will be the job of the enforcing authority to:

- Determine whether or not land is contaminated land;
- Decide what, if any, remediation is required;
- Establish liabilities for the remediation of contaminated land.

For the first time in the UK, local authorities will have a specific definition of contaminated land and procedure for securing remediation when such land is identified (Environment Act, 1995). In consequence, site investigation strategies are becoming increasingly important to provide a reliable, cost-effective method for the detection of sites requiring remediation.

There are over 32,000 hectares of potentially contaminated land in England and Scotland (29,000 in England (House of Commons, 1990) and 3,162 in Scotland (Scottish Office,

1996).) For each area of contaminated land, historical information must be collected and, if land may be contaminated, those liable must be identified and an invasive site investigation carried out to determine the extent and nature of the pollution prior to any remediation. Non-invasive site investigation methods can provide a valuable tool for reducing site investigation costs whilst yielding detailed information on the nature of the subsurface transport pathways and the extent of existing pollution plumes. Nevertheless, shallow geophysical techniques are still relatively unused within commercial environmental investigations despite the rapid site coverage they provide which in turn yields significant time and cost benefits. In the main, companies rely on spot sampling and chemical analyses. Potential users of geophysics would profit from guidelines stating which geophysical technique suits a particular environmental problem as each contaminated site poses different problems and so no one technique is appropriate for all surveys.

At present, the full potential of geophysics and its application to polluted sites is little understood beyond the scientific community. There is a need for more published research highlighting the contributions of using the appropriate geophysical methods in the first stage of site evaluation. Hence the aim of this research is to present the benefits of geophysical surveying with specific reference to the investigation of two ex-oil distribution terminals.

1.2 Specific Aims and Objectives of this Research

The two ex-oil distribution terminals are only a small part of some 100 hectares of land that Edinburgh City Council aim to acquire and redevelop. Before acquisition, it is necessary to define the nature of the site for the purpose of planning remediation procedures. The existing site information for the ex-oil distribution terminals consists of a small number of borehole records, a geological map constructed only from outcrop data and limited information of the potential contamination of the ground. The aim of this research, therefore, is to use geophysics to locate any subsurface contamination and define the possibility of pollution of the Forth estuary, the shores of which lie approximately one hundred metres north of the site. The historical use of the site, and new on-site boreholes, show the primary contaminant target to be diesel-related organics. Because non-aqueous phase liquids NAPLs (of which diesel is an example) frequently exhibit anomalous subsurface electrical properties this research concentrates on electrical and electromagnetic techniques. The research aims firstly to assess the ability of the techniques to locate and map NAPL contaminants and subsurface man-made structures that are often prevalent on old industrial sites. Secondly, it is intended that the data be interpreted to describe the geology of the site concentrating on those features that are likely to be influential to contaminant migration. Finally, the main objective of this research is to define procedures that allow the user to extract the maximum information from a data set. The information should then be presented in a format that can be easily interpreted by a non-geophysicist who may have to act on the results of a geophysical survey.

1.3 Summary of Principal Achievements

During the investigation of 2 ex-oil distribution terminals, a number of methods for the interpretation and presentation of electrical and electromagnetic data were developed. The major problems encountered and their derived solutions are summarised in the following points:

1. Some electromagnetic surveys are directionally dependent e.g. frequency domain Slingram type surveys. When the line between the source and receiver coils is parallel to a linear conductor (pipe) the resultant resistivity profile has a notable signature. When the line between the coils is orientated perpendicular to the pipe, a very different signature is measured. Thus, profiles over the same causative body can have very different appearances which is extremely difficult to interpret by a non-geophysicist who may need to use the data. In order to eliminate this directional dependence, the second derivative of the data set is taken yielding a single signature regardless of source/receiver coil orientation (Vickery and Hobbs, 1998a).

2. Buried pipes have a significant effect on the measurement of subsurface resistivity. This effect masks information about background geology. Using an analytical solution (Wait, 1982), a program has been written to calculate the effect on a resistivity image of an infinitely long conducting cylinder of variable diameter, depth and orientation with respect to the electrode array (Vickery and Hobbs, 1999). A second program was written to locate the calculated pipe profile within a pipe-affected pseudosection (vertical slice) of apparent resistivity. The main effect of the pipe is then removed leaving a clearer image of the background resistivity and hence the underlying geology.

3. Vertical slices of apparent resistivity can be interpreted in their own right using inversion routines (Loke and Barker, 1996) but it is difficult to summarise information from a large number of profiles when they can only be viewed separately. Horizontal (plan view) resistivity contour plots have been constructed by extracting all modelled true resistivity data points from a chosen depth. This method of presentation allows the user to view the resistivity data of the entire site creating a pseudo three-dimensional (3-D) model. This aids the understanding of how individual profiles relate to each other (Vickery and Hobbs, 1998b).

4. The interpretation of a 3-D problem using two-dimensional (2-D) information must be completed with caution. It is important to test any conclusions to measure their validity in 3-D. A 3-D forward modelling algorithm developed by Spitzer (1995) is used to investigate the complex pseudo 3-D model by producing a synthetic response which may be compared with observed data.

1.4 Thesis Outline

Chapter 1 defines the rationale for this work and sets out the structure of the thesis, highlighting areas of new work. *Chapter 2* introduces the basic theory of groundwater flow and contaminant transport and continues with a summary of the application of geophysics to environmental problems concentrating on the detection of contaminants and their pathways. The final introductory chapter, *Chapter 3*, records typical site investigation strategies and introduces the Granton site, the main field area to be surveyed for this work. The site introduction includes industrial history as well as a description of the geology and hydrogeology of the area.

Chapter 4 is an account of the reconnaissance electromagnetic (EM31) survey employed to locate shallow contamination and subsurface structures beneath the Granton site. The chapter also addresses the problem of directional dependence in the EM31 survey. Section 4.5 introduces a new method of presentation for EM31 data to eliminate the directionality of the survey technique and highlight specific targets.

Chapter 5 introduces a 2-D resistivity imaging technique (Barker, 1992) and its application to Granton for a secondary survey designed to determine the geology of the site and to define rapid contaminant pathways. *Chapter 6* contains almost entirely new work describing the effect of conducting pipes on apparent resistivity measurements. Section 6.2 describes the programming of the analytical solution of apparent resistivity measurements over an infinitely long cylindrical conductor and Section 6.3 sets out the methodology for locating and removing the masking effect of pipes from apparent resistivity data.

Chapter 7 presents the results of the 2-D resistivity imaging survey concentrating on the integrity of the clay coverage, the location of rapid contaminant pathways and the delineation of the saline/fresh water interface. Interpretations are aided by the construction of resistivity contour plots of the entire site, at a chosen depth. Chapter 7 also shows the steps required for the construction of a pseudo 3-D model from 2-D vertical slices of resistivity (modelled by inversion).

Chapter 8 describes a method for testing the validity of the pseudo 3-D resistivity model. In particular, Section 8.3 describes the translation of the pseudo 3-D model from Chapter 7 into the format required for 3-D forward modelling and Section 8.4 quantifies the validity of the model by comparing a simulated field survey with real measurements and giving a value of 'misfit'.

Finally *Chapter 9* presents the major conclusions from throughout the thesis and *Chapter 10* details suggestions for future work.

2 BACKGROUND THEORY AND PREVIOUS WORK

2.1 Subsurface Fluid Flow

The predominant mechanism for migration of pollutants from a site to a nearby target is transport within subsurface water. Water enters the ground via rainfall, flowing through the available void space within the soil or rock. Water within the ground can be divided into two separate flow zones: groundwater flow which is predominantly lateral and occurs where the void space is fully saturated with water; and unsaturated flow which is mainly vertical and describes the gravity driven flow of water from the ground surface to the deeper groundwater (or saturated zone). These two flow mechanisms are each described in more detail below after a summary of the main rock properties which affect flow.

2.1.1 Soil and Rock Properties

Porosity

The amount of ground water stored in a saturated material depends on its porosity. The total porosity is defined as the proportion of a rock or soil which is represented by voids. Primary porosity relates to voids created at the time of rock formation e.g. intergranular spaces, while secondary porosity is a result of subsequent geological or climatic actions. Secondary porosity can occur as faults, fractures and weathered joints which often form the main channels for groundwater flow (Figure 2.1).

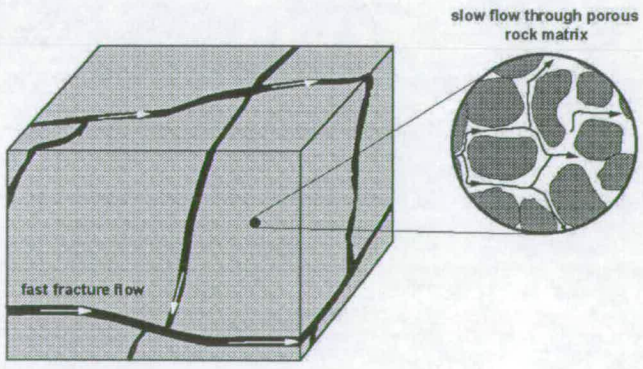

Figure 2.1: Flow through porous media; examples of primary and secondary porosity.

Both laboratory and field studies have shown that crustal rock permeability varies over 14 orders of magnitude (Brace, 1980). This reflects the large variation in pore space characteristics defined by the nature and geological history of the rock. Even within a single rock formation, pore (or crack) size and shape is observed to be heterogeneous (Pittman, 1984).

Permeability

Permeability describes the ease with which liquids (or gases) can pass through rock or soil. The permeability depends on the grain size and the packing of the grains. Assuming isotropic rock, permeability k is related to the saturated hydraulic conductivity K as given by the equation:

$$K = \left(\frac{\rho_f g}{\mu_f}\right) k \tag{2.1}$$

where ρ_f is the density of the fluid, μ_f is the dynamic viscosity of the fluid and g is the gravitational constant. High permeability units create preferential pathways for fluid flow.

It is common to find high estimates of permeability for high porosity materials (e.g. sandstone) but a porous medium can contain voids that are not interconnected inhibiting movement of pore fluids. Clay is a special example of a high porosity, low permeability material. The low permeability of clay can, in part, be explained by the adsorption of soil fluids onto the solid particles. Adsorption occurs mainly due to electrostatic forces in which the polar water molecules become attached to the charged soil particle surface. The high surface area of clay particles means that greater quantities of soil fluid can be adsorbed. Consequently, it is probable that contaminated soil water will reside in clay layers for a significant length of time even after long periods of drying.

2.1.2 Unsaturated Flow

Above the saturated zone, unsaturated flow occurs. The unsaturated flow is predominantly controlled by forces either at the ground surface (infiltration, evaporation) or from the bottom of the unsaturated zone. This leads to the development of vertical potential gradients across the zone resulting in vertical movement of water with the aid of another controlling force, gravity.

2.1.3 Groundwater

Groundwater is the subsurface water in soils and rocks that are fully saturated. The upper boundary of the zone of saturation varies according to whether the groundwater is confined or unconfined. For unconfined groundwater, the boundary is called the water table, the upper boundary of the zone of saturation, and is the level at which water would rest within a borehole drilled at a given location. The water table tends to follow the contours of the overlying ground surface.

In general, groundwater is recharged at places of higher elevation and the groundwater flow moves mainly laterally under pressure head gradients ultimately discharging in lakes, rivers or at the coast. The flow of groundwater is described by Darcy's law (Darcy, 1856) which may be written as:

$$Q = -KA\nabla h \tag{2.2}$$

where Q is the volume flow rate, K is the hydraulic conductivity, A is the cross-sectional area of the sample and h is the hydraulic head. ($h = p/\rho_f g + z$ where p is the pressure, ρ_f is the fluid density, g is the gravitational constant and z is the elevation head).

A special example of an unconfined aquifer (a geological formation which contains sufficient groundwater to yield significant quantities of water) is perched groundwater where ground water lies above a discontinuous, impermeable or semi-permeable bed (aquitard) that is situated at some height above the water table. In a confined groundwater system, groundwater is confined under pressure (i.e. trapped) by an aquitard. In such a case, if a borehole were to penetrate this layer, water would rise up the hole and come to a resting level above the top of the saturated aquifer. The aquifer systems are summarised in Figures 2.2 and 2.3.

In reality, confined and unconfined aquifers are often linked into one system. Most confined aquifers have an unconfined area of outcrop through which groundwater recharge occurs where the water table represents the upper boundary for the zone of saturation. Furthermore, the overlying boundary layer is rarely completely impermeable so that some interchange will occur.

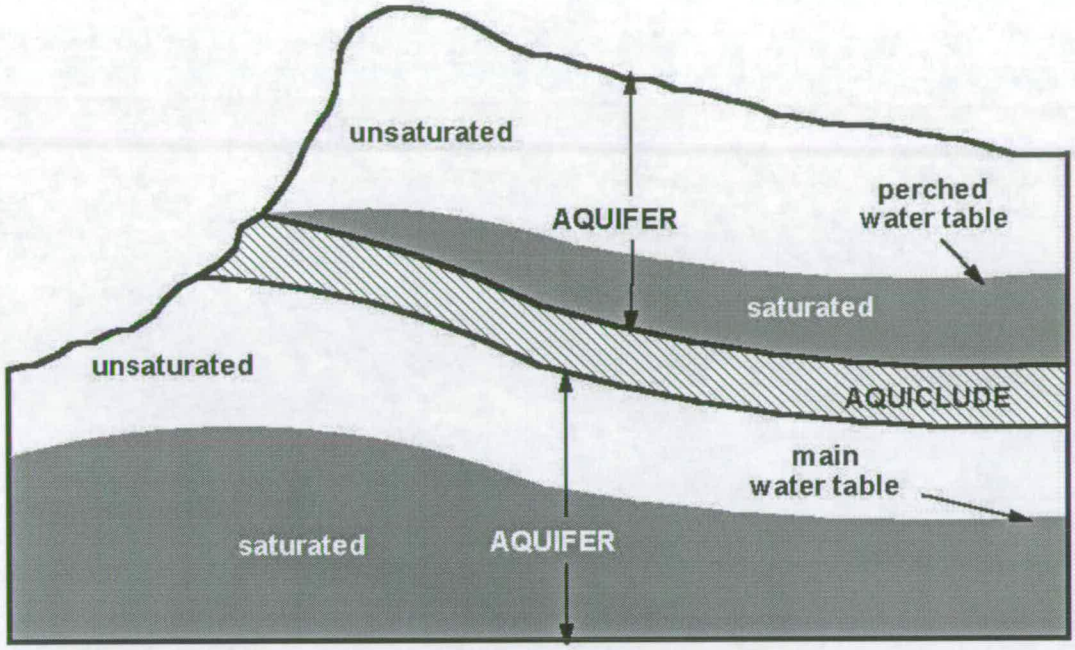

Figure 2.2: Unconfined aquifers.

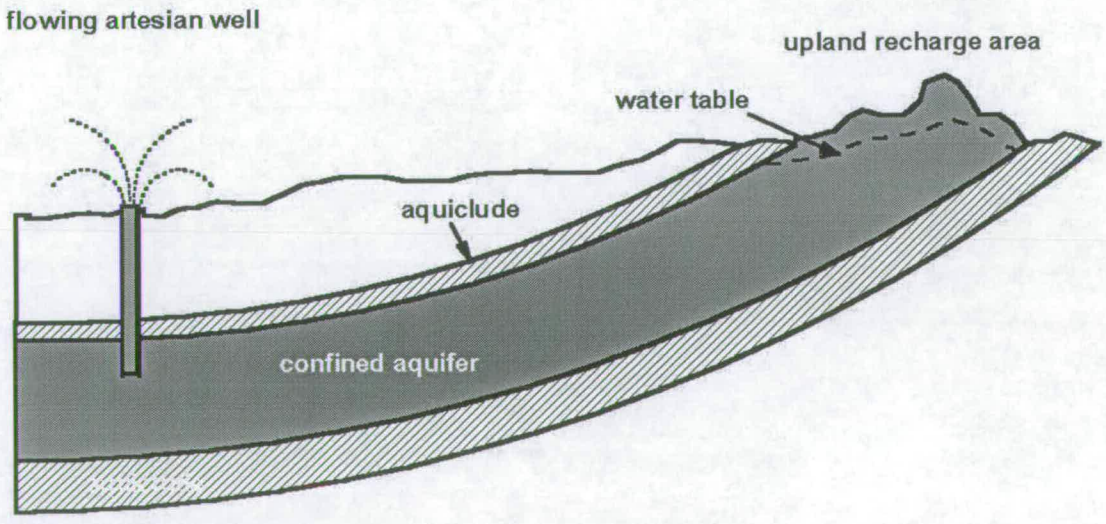

Figure 2.3: Confined aquifers.

2.2 Contaminant Transport

Ground water flow patterns are the key to interpreting contaminant migration. On a metre scale, it is possible to assume homogeneous flow where local fluctuations in the conducting properties are averaged out, thus a volume of rock can be represented by a single parameter (e.g. permeability). But there are several other physical processes which are involved in contaminant transport and these are detailed below.

In the absence of other processes, contaminants will be transported by *advection*; at the same rate as the macroscopic velocity of the groundwater. Advection is the dominant transport mechanism except in very slow flow regimes, however, for detailed mapping of contaminant pathways, it is also vital to consider the heterogeneities in rock permeability. In reality, contaminant transport also varies due to *dispersion*. Dispersion is a consequence of complexities in the pore system and of the tortuosity of pore networks (Figure 2.4). Hydraulic flow is mostly driven in "critical paths" when the pore size distribution is heterogeneous, especially where the pore size distribution has a decreasing exponential-like shape (David, 1993). Flow follows the path of highest permeability producing preferential pathways that result in a sub-network which carries a large part of the total groundwater thus ensuring contaminant mixing.

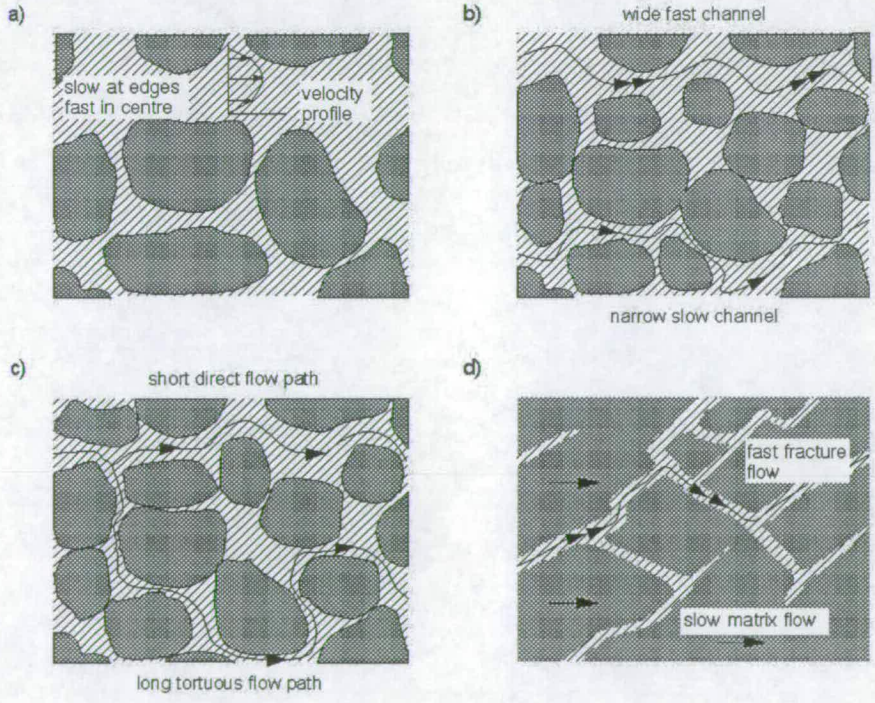

Figure 2.4: Dispersion mechanisms due to: (a) & (b) complexities in the pore system, (c) tortuosity of pore networks and (d) secondary porosity.

Another important mechanism for contaminant migration is flow through fracture networks. Berkowitz and Scher (1996) studied the influence of embedded fractures on contaminant mi-

gration in geological formations by generating percolation clusters to represent the fractures. They found that preferential pathways through these structures and the shortest route between them can so significantly decrease contaminant break through times that previous estimates can be in error by up to an order of magnitude for any given rock formation. As a result, field characterisation of fractured formations is generally considered as a guideline rather than to be exact. It is frequently argued that fractures have little effect unless they form an hydraulically-connected network being a potential pathway for rapid off-site migration of contaminants. However, unconnected fractures, in sufficient proximity to one another still form potential rapid pathways and should not be ignored.

Within low permeability media, *diffusion* is the dominant transport mechanism; ionic or molecular constituents can move under the influence of their kinetic activity in the direction of the concentration gradient. Diffusion is a very slow method of contaminant transport.

Finally, at a site scale, faults can act as flow paths or as barriers to flow depending on whether the faults are open or closed and on the orientation of the faults with respect to the overall groundwater flow. The flow behaviour of faults is governed by alterations in the properties of the pore space i.e. reduction in connectivity due to pressure induced pore closure. The exact role of a fault or fracture cannot be surmised simply by its detection but requires permeability measurements. However, the potential effect of a fault is enormous and must therefore be considered in detail for the mapping of potential contaminant pathways. A comprehensive summary of faulting, fault sealing and fluid flow is given by Knipe *et al.* (1998).

2.2.1 Transport of Non-Aqueous Phase Liquids

The behaviour of a contaminated fluid depends on numerous factors: groundwater flow velocity, porosity, existence of local fracture systems and, of particular relevance to this research, density of contaminant relative to groundwater. The main contaminant types evident on the field site described in this thesis are diesel related organics. Density is the main control determining where Light Non-Aqueous Phase Liquids (LNAPLs) and Dense Non-Aqueous Phase Liquids (DNAPLs) will settle. Figure 2.5 shows the relative behaviour of these two contaminant types.

An LNAPL (less dense than water) spilled into the subsurface travels through the unsaturated zone towards the top of the saturated zone leaving behind a residual component. A sufficiently large LNAPL spill forms a pool upon reaching the top of the saturated zone and eventually depresses it. Along with this free-phase pool of LNAPL, there is an associated gas phase and dissolved phase. Therefore, although the LNAPL pool does not migrate below the water table as a continuous phase, the dissolved phase is a mobile groundwater contaminant.

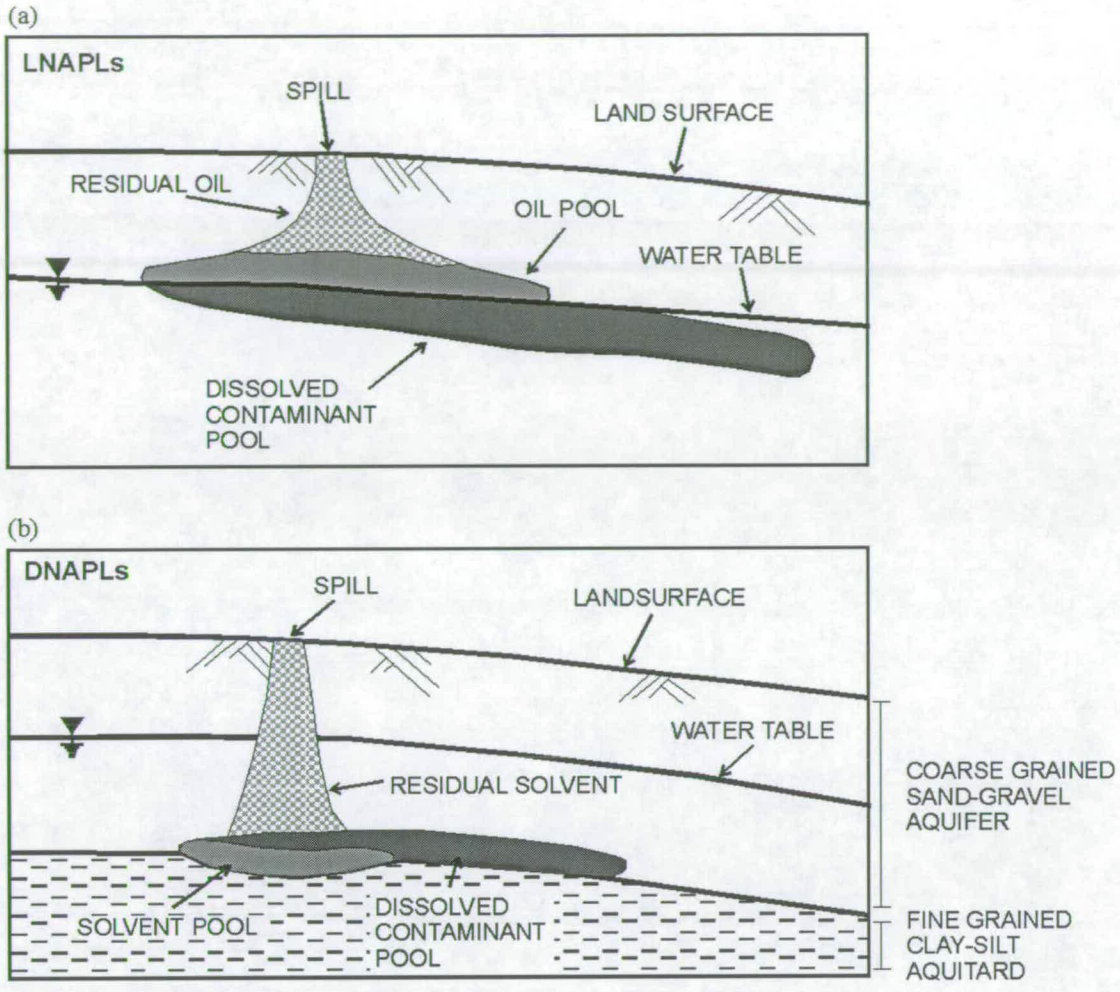

Figure 2.5: Relative behaviour of (a) LNAPL and (b) DNAPL contaminants.

DNAPLs are more dense than water and therefore sink below the water table pooling above the nearest impermeable lithological layer. Here, in the saturated zone, DNAPLs are subjected to the same pressure gradients as groundwater and therefore flow in the same direction (but more slowly), transported with the natural flow of groundwater.

2.3 Detecting Contaminants with Geophysics

2.3.1 Introduction

The initial work carried out for this thesis included a feasibility study on the use of various geophysical techniques for the investigation of contaminated land. Desk studies were carried out into the suitability of a selection of techniques (gravity, magnetics, 2-D resistivity imaging and electromagnetics, including magnetotellurics) and a number of trial surveys re-

sulted from the study. The trial surveys were conducted over a test site; a landfill site between Edinburgh and Glasgow, hereafter named EF Quarry, which contains highly toxic industrial and municipal waste (Vickery, 1996). This review of detecting contaminants with geophysics concentrates on the methods chosen for the desk study and includes examples from EF Quarry where appropriate.

2.4 The Geophysical Response of a Contaminated Site

Many routine geophysical techniques have something to offer towards the characterisation of contaminated sites and there are a number of articles examining the range and applicability of general geophysical surveys (e.g. McCann (1994) and Benson (1993)). McCann (1994) summarises the effectiveness of most of the routine geophysical techniques, with specific reference to landfill sites, in an attempt to aid the choice of an individual method.

Variations in gravity can occur across a landfill due to changes in fill depth and inhomogeneities in the density of fill material but ordinarily a gravity survey is too time consuming for effective coverage of a contaminated site. The desk study of the gravity method did not reveal any record of the technique distinguishing between contaminated and uncontaminated soils and subsequently no trial survey was conducted over EF Quarry. However, gravity can be productively employed where there is a specific target that naturally lends itself to the technique e.g. the detection of abandoned mines (Ghatge, 1993).

The prime use of magnetic surveys is to locate buried ferrous objects or other magnetic materials e.g. magnetic surveys have been used for the location of buried oil drums (Pierce and DeReamer, 1993). Magnetic surveys are often used for the mapping of landfill boundaries due to the high metal content of municipal waste (of order 10% (McCann, 1994)). Roberts *et al.* (1990) collected magnetic data over a waste disposal site which displayed intense magnetic variations. The landfill boundaries enclosed short wavelength anomalies from individual surface iron and steel objects.

The magnetic response of EF Quarry landfill was significantly different from that obtained by Roberts *et al.* (1990) because the fill material behaved as a large, single body (Figure 2.6). One explanation for this may be the age of the site. The fill may become more homogeneous after decomposition and subsequent amalgamation of materials.

The benefits of multidisciplinary surveys are frequently presented, but electrical and electromagnetic methods repeatedly dominate the discussion chapters. As with groundwater studies, the methods have been extensively investigated since the resistivity of a material is a function of the fluids contained within it. Because of this relationship, the remainder of the desk study is centred on electrical and electromagnetic methods.

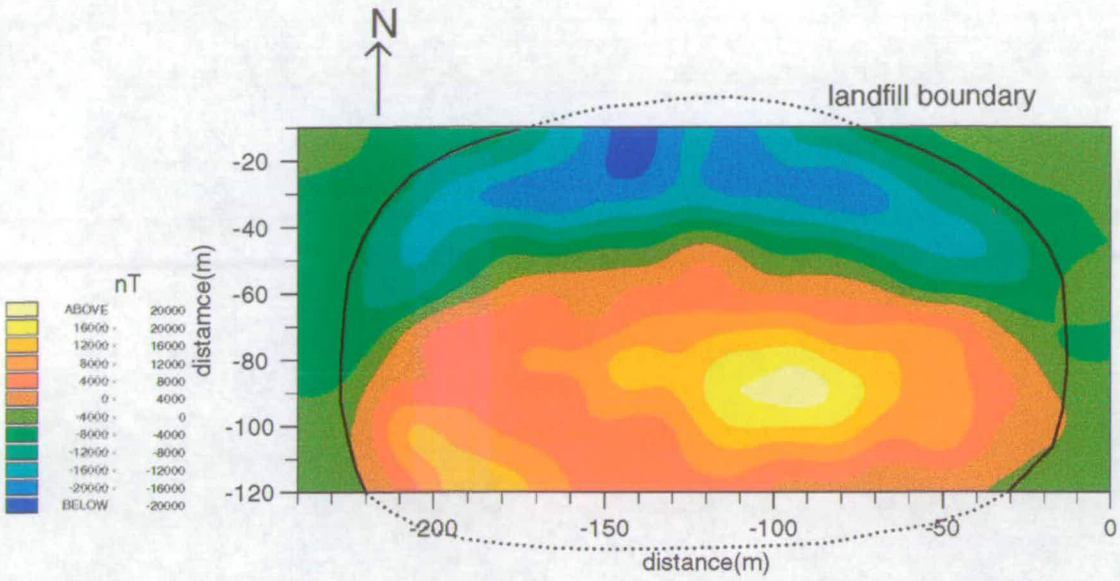

Figure 2.6: The results of a magnetic survey over a landfill containing both industrial and municipal waste.

2.4.1 The Effect of Contaminants on Electrical and Electromagnetic Methods

When considering electrical techniques it is important to understand the likely effect of a particular contaminant on the conductivity of its host. Each contaminant affects the conductivity of the host rock in different ways. Conduction of electricity can occur via movement of ions through saturating brine and/or movement of absorbed ions along the surfaces of pores and cracks. The conductivity of a rock is therefore related to pore geometry, the surface of mineral grains lining the pores and the electrical properties of the mineral grains and pore fluid. The relationships of fluid chemistry, hydraulic properties and measured electrical properties are made through the empirical relationship, Archies Law (Archie, 1942):

$$\rho = \rho_0 \Phi^{-m} S^{-n} \tag{2.3}$$

where ρ is the electrical resistivity, ρ_0 is the electrical resistivity of pore fluid, Φ is porosity, m is cementation factor, S is fraction of pore space that is saturated, n is saturation parameter.

The electrical properties of various contaminants have been studied. For example, in the case of landfill sites, landfill material consists mainly of municipal waste which has a higher conductivity than natural rock. Contaminated fill material has an approximate resistivity value of 15 - 30 Ωm when saturated and 30 - 70 Ωm when unsaturated compared to surrounding rock which is more likely to have a resistivity around 50 - 500 Ωm (McCann, 1994).

Again, of particular interest in this research is the effect on electrical properties of diesel related organics being present within the saturated and unsaturated zones. Monier-Williams (1995) presents a detailed summary of electrical properties, showing how the presence of LNAPLs can increase, decrease or have no effect on the apparent conductivity of the subsurface. Where LNAPLs replace aqueous phases in the vadose zone (zone in which water moves freely under the influence of gravity above the zone of saturation), the apparent resistivity increases but if they replace air, the apparent resistivity decreases due to the enhancement of aqueous connectivity. A combination of both these processes may yield no overall change. It should also be noted that the properties of any liquid could change as its composition changes due to subsurface reactions with other groundwater contaminants and NAPL biodegradation. Sauck *et al.* (1998) suggested that a conductive plume associated with a non-conducting LNAPL may be a consequence of organic acids produced by biogradation of the NAPL.

Schneider *et al.* (1993) test the effectiveness of utilising DC resistivity methods for the detection of different hydrocarbons. The method is successful in delineating both DNAPLs (PCEs) and LNAPLs (kerosene) recognising the relationship described by Monier-Williams (1995). They highlight the benefits of time lapse studies but conclude that for large DNAPL spills, the anomaly is so large that significantly large quantities can be detected without the need for background measurements.

More recently, Darayan *et al.* (1998) conducted laboratory studies into the effectiveness of using electrical techniques (particularly high frequency electromagnetic methods) for the detection of hydrocarbons. Darayan *et al.* (1998) compared the electrical properties of uncontaminated soils and soils contaminated with diesel measuring both the dielectric constant and conductivity of the samples. As previously detected by Monier-Williams (1995) and Schneider *et al.* (1993), the values of these two parameters increased with the addition of diesel oil which replaced the air between pores. The dielectric constant of diesel oil is about twice that of air but this only produces a small change between the dielectric constant of soils before and after oil contamination. However Darayan *et al.* (1998) concludes that the change in dielectric constant is still significant and detectable.

2.4.2 Detecting Contaminants with Geophysics - Relevant Case Histories

Resistivity

The electrical properties of contaminants are frequently anomalous. As a consequence there are numerous examples of electrical and electromagnetic techniques being used for contaminant mapping. One example includes the detection of saline intrusions which pollute fresh water supplies (Barker, 1980). The extreme low resistivity associated with saline water lends itself to electrical surveying. Barker (1980) took results from a significant number of Wenner resistivity soundings to successfully map a body of saline groundwater within a large sandstone unit in Staffordshire, England. With the advancement of the automation of 2-D resistivity surveys (Barker, 1992), subsequent investigations of the same site were carried out with a 2-D resistivity imager to take a vertical slice of resistivity information (Griffiths and Barker, 1993). Pseudosections showed the fresh/saline water interface and a clear picture of the edge of the saline plume.

The same electrical techniques have been used extensively for other problems. Some examples include the evaluation of trace metal contamination in soils (Bauman *et al.*, 1997) and the mapping of landfill leachate plumes (Barker, 1992). A similar survey was conducted as part of this research after the completion of the desk study; a 2-D resistivity imaging survey of the EF Quarry landfill successfully located the boundaries of the landfill but the highly conductive nature of the fill material prevented the survey locating the bottom of the quarry. Resistivity images obtained over 50m away from the quarry, down the hydraulic gradient, revealed highly conductive bodies mapping out a leachate plume moving away from the site.

Electromagnetics

Electromagnetic techniques respond to the same parameters as electrical surveys except that while resistivity surveys are more sensitive to resistive targets, electromagnetic surveys are more sensitive to conductive targets.

Electromagnetic terrain conductivity measurements were collected to assess the extent of groundwater contamination at two swine confinement facilities (Larson *et al.*, 1997). A shallow electromagnetic survey was conducted (using a Geonics EM-34 with a coil separation of 10m) and located anomalous conductivity highs and lows. Test wells were positioned to sample the anomalous regions and proved that, for this case, high conductivity regions were representative of areas with a high degree of water contamination.

Jansen *et al.* (1993) presents 3 cases where frequency domain electromagnetics has been a profitable survey method. One case details the investigation of a municipal landfill with a

Slingram loop-loop system (Max-Min). The results were interpreted with a 1-D inversion package. The best fit was obtained with a three layer model; soil cap, unsaturated fill and saturated fill material. The survey also located a number of leachate pockets and apparent drum disposal areas. In another case, Jansen *et al.* (1993) utilises the Geonics EM31 (soil conductivity meter) to provide evidence for unsubstantiated reports indicating that industrial solvents in steel drums had been dumped into an abandoned landfill. The high conductivity of metal objects makes them easy to detect with electromagnetic techniques. Jansen *et al.* (1993) distinguished discrete accumulations of metal bodies from uniform distributions of small metal objects by studying the anisotropy of the fill.

Time Domain Electromagnetic (TDEM) surveys have been successfully employed in the detection of saline plumes in fresh water (e.g. Mills *et al.* (1988), Goldstein *et al.* (1990)) and for the mapping of leachate plumes near waste disposal sites (e.g. Buselli *et al.* (1990)). TDEM is an extremely valuable technique as it does not require large coil separations to sample deep into the subsurface. The depth penetration is increased by reducing the frequency of the transmitted source field. Despite the favourable desk study, the approach was unavailable for this research and would be included in future work.

A desk study of the SPAM (Short Period Automatic Magnetotelluric) system (developed since 1980 at the University of Edinburgh and therefore readily available) was conducted to assess its applicability to environmental problems. Magnetotelluric (MT) surveying measures both the natural low frequency magnetic fields that flow within and around the Earth and the natural alternating electric fields induced by the magnetic fields. The impedance at each frequency can be calculated from the relationship between the fields. However, SPAM has a limit on the frequencies within which it will operate, in particular the highest usable frequency is 2kHz, thus restricting the amount of detail that can be obtained from shallow depths. Consequently, for the mapping of EF Quarry, it was important to know which frequencies would adequately sample a landfill site. These frequencies were estimated using GEOTOOLS (Vickery, 1996).

GEOTOOLS is a software package designed for the forward and inverse modelling of MT data. Figure 2.7 shows the modelled apparent resistivity versus frequency curves calculated in response to a landfill model. The model was constructed using data from a report on EF Quarry: 4m of liquid waste above 11m of industrial waste and 7m of rubble within consolidated sandstone with a 3m clay cap and 7m of top soil above.

Although highly conductive material, like landfill waste, reduces the frequency required to sample shallow depths, the frequencies usable by SPAM are still too low and penetrate too deeply to reveal significant information about this model. There is a significant amount of detail present at frequencies higher than 2kHz. There may be environmental problems (i.e. deep conductive landfills, deep contaminant plumes) where SPAM can be utilised but the frequency limitations restrict the use of SPAM for shallow investigations.

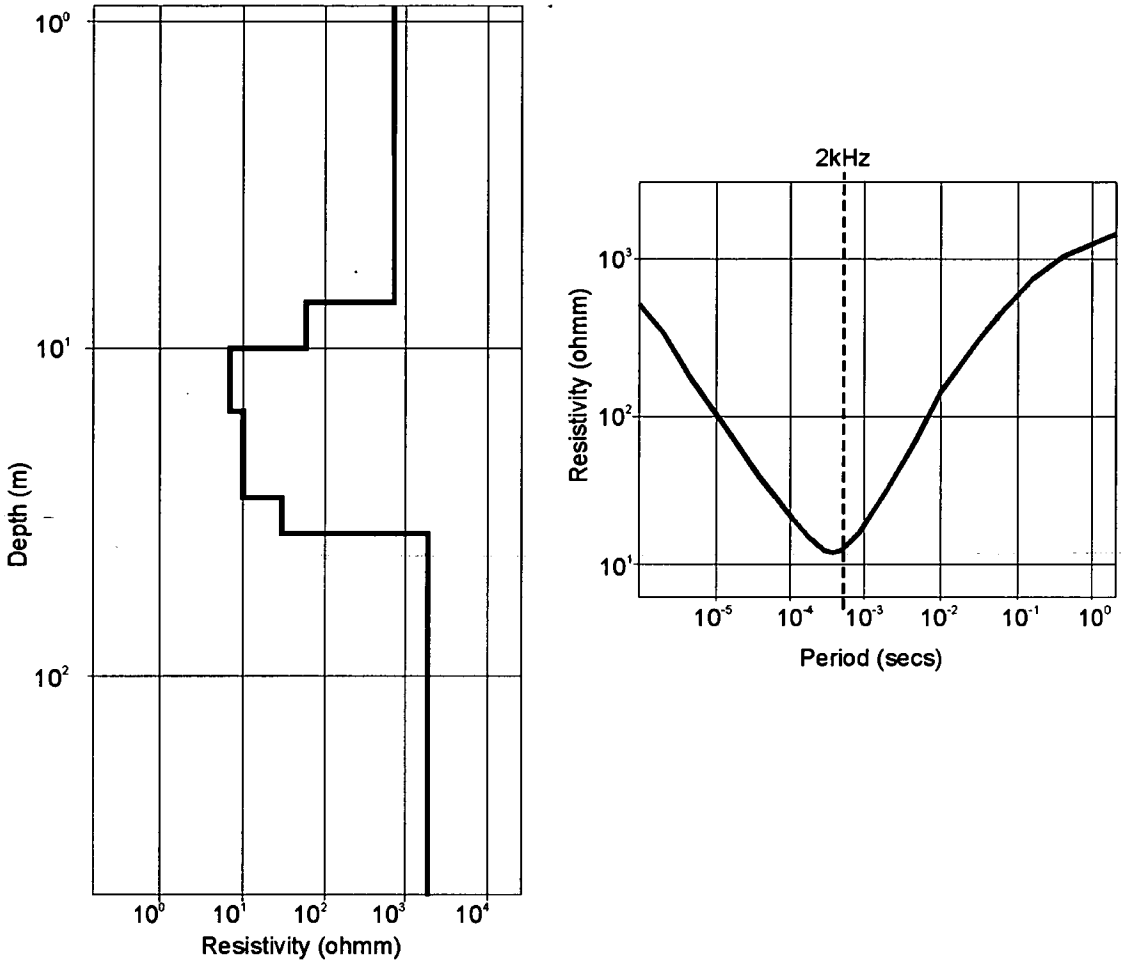

Figure 2.7: Calculated MT response to a model of a landfill.

Ground Penetrating Radar

Ground Penetrating Radar (GPR) surveys can provide high resolution images of contaminated sites and have proved particularly successful at mapping hydrocarbon pools (e.g. Nash *et al.* (1997)). However, the technique can only be employed under certain suitable field conditions. Because of the the shielding effects of clay and the noise inducing effects of uneven, gravelly surfaces, the GPR is inappropriate for use in investigations discussed within this thesis.

2.4.3 Summary

A desk study into the application of different geophysical techniques to environmental investigations highlighted unsuitable methods as well as those likely to succeed: At present, it is not possible to sample the higher frequencies of naturally occurring magnetic and electric fields thus discounting the use of MT surveys. GPR surveys are unsuitable because the ma-

jority of contaminated sites within the UK have some clay coverage and are unlikely to have even ground surfaces. Magnetic surveys are particularly applicable to sites contaminated with metals or subsurface metal structures. A magnetic survey offers rapid ground coverage which is ideal for preliminary site investigations but there is no literature suggesting its sensitivity to non-metal bearing contaminants. Both electrical and electromagnetic techniques have proven to be successful in the detection of the anomalous conductivities likely to arise due to contamination and subsurface structures. As a consequence, the remainder of this thesis will concentrate on electrical and electromagnetic surveying.

2.5 Detecting Rapid Pathways with Geophysics

2.5.1 Introduction

Contaminants are predominantly transported within the natural flow of groundwater (Section 2.2.1). Consequently, mapping contaminant pathways involves recognising particular factors which affect the rate of groundwater flow. In addition to the effects of rock matrix porosity and permeability an important influence is exerted by secondary geological processes such as faulting and folding. If these secondary pathways are open, they are potentially rapid, large scale, planar flowing features which may have a significant effect on the overall flow pattern of a site. A preferred orientation of flow may also be induced by rock matrix anisotropy exerting a similar directional dependence (although not rapid) to that caused by faulting and folding. Ground anisotropy can result from a number of different geological features: Inherent/intrinsic anisotropy caused by preferential alignment of crystals, microcracks or sediments due to fluid flow during deposition; crack induced anisotropy from liquid filled cracks or pores, aligned due to nonlithostatic stress and long wavelength anisotropy due to a regular sequence of thin isotropic layers.

Preferred flow orientations may be studied in a number of ways but, as a consequence of the conclusions from Section 2.3, this review concentrates on the contributions of electrical and electromagnetic techniques.

2.5.2 Hydraulic Conductivity versus Electrical Conductivity

Currently, the transmissivity of an aquifer (hydraulic conductivity x thickness of saturated aquifer) is commonly characterised by measurements taken from drill cores which is expensive and not always convenient. Research has been carried out to find a relationship between electrical current and fluid flow to enable the characterisation of rocks with simple electrical surveys. There is an analogy between the two differential equations describing hydraulic and

electrical flow within rocks demonstrating the relationship between the hydraulic and electrical conductivities of rock. Fluid transport through porous, low velocity materials is found experimentally to obey Darcy's Law (Equation 2.2) as described in Section 2.1.3.

Similarly, the conduction of electric current through a porous, insulating material saturated with an electrolyte, is governed by the expression:

$$I = -\frac{A}{\rho}\nabla v \tag{2.4}$$

where I is the electric current, A is the cross-sectional area of the sample, ρ is the bulk electrical resistivity and v is the electric potential or voltage.

This suggests a relationship between the electrical and hydraulic conductivities of a rock (i.e. volume flow rate $\propto$ current flow). So, surface resistivity measurements are frequently used for qualitative estimates of aquifer properties but their applications in quantitative studies are controversial.

Most research towards defining the relationship between electrical and hydraulic conductivity has concentrated on the analysis of single flow systems. Computer simulations of single fractures have been used to evaluate this relationship between transport of fluid and electric current. The use of a simple parallel plate model to represent a fracture has been discussed by Sibbit and Faivre (1985) and Brown (1989) (Figure 2.8). Sibbit and Faivre (1985) use the model in their computer simulations to evaluate the electrical response of a fracture. They aim to obtain information about the transmissivity assuming transmissivity is proportional to fracture aperture d.

Fracture aperture is the predominant control over transport properties but at smaller apertures the parallel plate model is inadequate. Brown (1989) presents errors arising from the use of the simple parallel plate model. The model assumes the fracture to have smooth, parallel sides whereas the surfaces of a fracture are rough and mismatched at some scale. The shape, size and number of contacts between the surfaces control the mechanical properties (Brown and Sholtz, 1985). Brown (1989) performs simulations on fractures with rough surfaces and finds that local directions of fluid and electrical flow are not the same. However, by introducing tortuosity of the fluid or electric current paths, a relationship can still be developed between the microscopic physics of the transport properties and the macroscopic behaviour described by Darcy's and Ohm's Laws. In general, it is believed that a relationship does exist but electrical conductivity measurements are likely to underestimate the hydraulic conductivity of the rock.

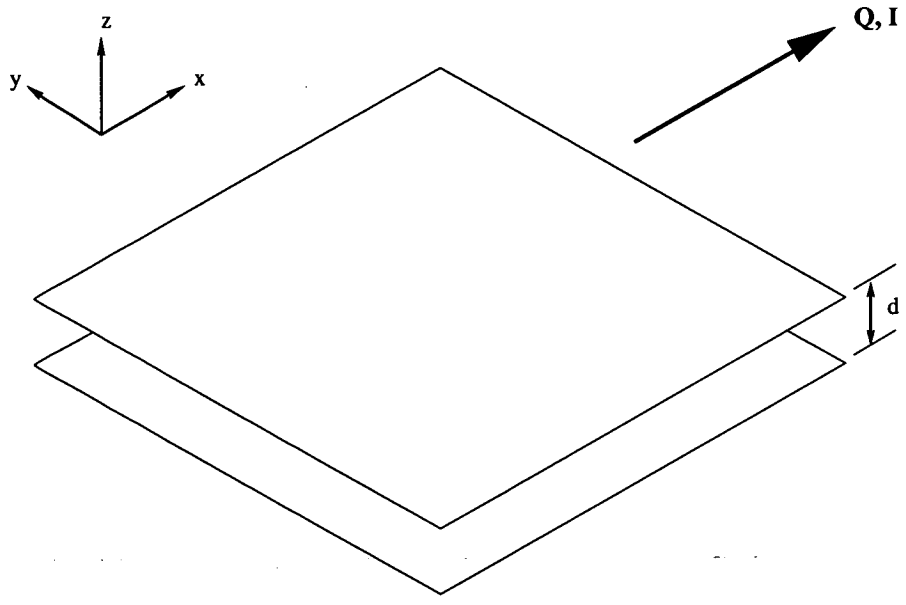

Figure 2.8: Parallel plate model geometry of a fracture with aperture d with volume flow rate Q or electric current I. Taken from Brown (1989).

Field experiments have also been conducted to investigate the relationship between electrical and hydraulic conductivity. Heigold *et al.* (1979) compare vertical electrical soundings with pump test data and find a direct correlation between hydraulic and electrical conductivities for a granular, glacial outwash aquifer. However, this interpretation is supported by only three data points and the authors stress the need for care in developing this relationship. Later work by Kelly and Frohlich (1985) attempts to further quantify the factors controlling the relationship; the paper documents two factors introduced by the influence of layering which both affect field correlations. Firstly, vertical electrical sounding measurements are inevitably influenced by the non-aquifer layers. Secondly, it is also important to consider the direction of current flow during a resistivity measurement. Parameters that are correlated are simply average properties reflecting aquifer layering and the direction of hydraulic flow which is predominantly horizontal, and electrical flow which is horizontal and/or vertical. Figure 2.9 shows the difference between longitudinal and transverse current flow with respect to a layered model. In the transverse case the electrical flow is vertical (orthogonal to the direction of groundwater flow), whereas in the longitudinal case groundwater flow and electrical flow are both horizontal. In the longitudinal case, the measurement of resistivity will be affected by the hydraulic anisotropy of the layer so that field scale relationships between average hydraulic conductivities and average longitudinal resistivities exhibit considerable scatter unless the anisotropy is constant. Different values for conductivity will be obtained depending on the orientation of the measurement within the horizontal plane.

The anisotropy of a layer causes problems in the experiments conducted by Kelly and Reiter

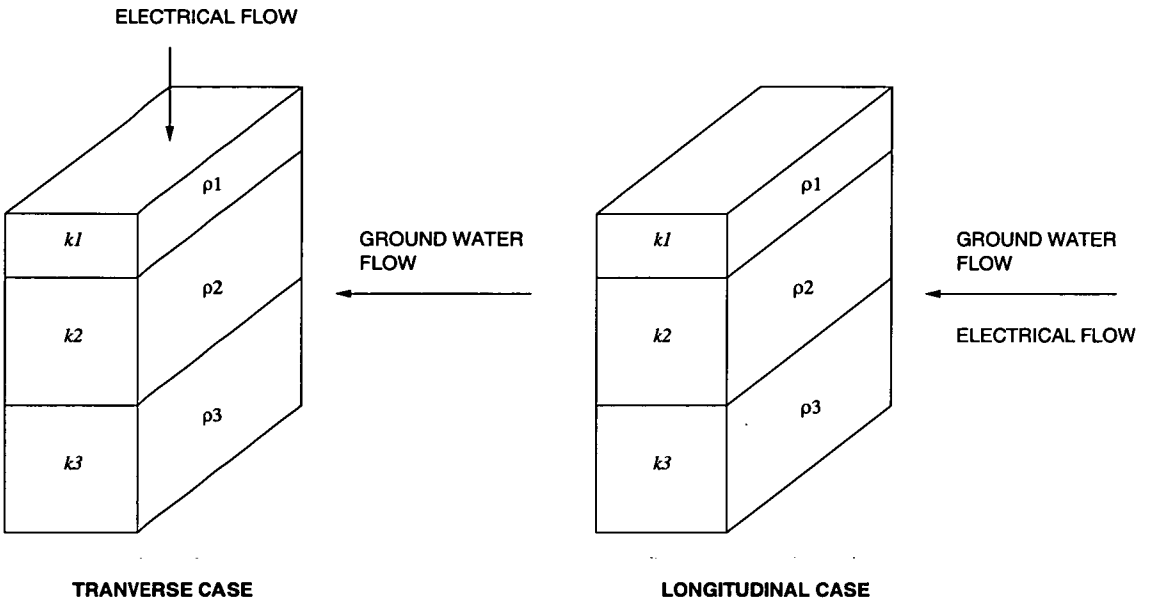

Figure 2.9: Layered models showing electrical and hydraulic flow for the transverse and longitudinal cases. Taken from Kelly and Reiter (1984).

(1984) because measurements are only taken in one orientation which may or may not be aligned with the directional dependence of the rock. In an attempt to overcome this problem, measurements can be taken in a number of orientations to locate the preferred direction of flow.

2.5.3 Detecting Rapid Pathways using Geophysics - Relevant Case Histories

A fault has great potential for providing a rapid contaminant pathway. Previously faults have been successfully located with resistivity techniques. Hobbs and Reading (1994) employed the 5-electrode offset Wenner resistivity system (developed by Barker (1981)) for the location of a fault within coal measures. Hobbs and Reading (1994) found that simply plotting the offset measurements is sufficient to locate the fault while apparent resistivity pseudosections may be misleading with regard to its structure.

Fissured rocks, favourable for accumulation and flow of groundwater, are often characterised by low resistivity zones. Alteration and fissuration causes the resistivity of rocks to decrease. Bernard and Valla (1991) located a conductive, finger-shaped anomaly within the crystalline basement (Figure 2.10) which was explored with drill holes. A drill hole located at the centre of the anomaly intersected 5m of alluvium above a highly altered and fissured crystalline rock of significant thickness which had a high transmissivity. In general, a measure of transmissivity is, however, directional and may be further addressed with azimuthal studies.

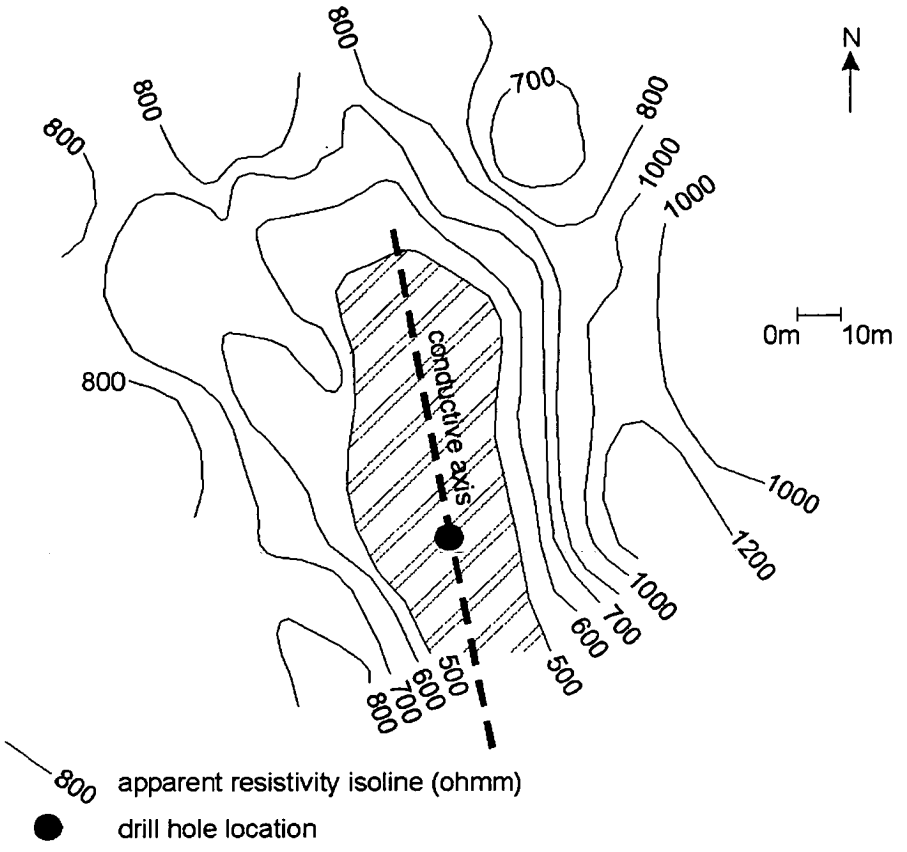

Figure 2.10: A map of iso-ohm contours delineating a conductive zone. Taken from Bernard and Valla (1991)

The measurement of electrical anisotropy requires the sampling of earth resistance in a number of different orientations. Where modest contrasts are encountered, orientational variations of the mean resistivity are small (< 4%) (Habberjam and Watkins, 1967). However, the azimuthal inhomogeneity ratio is often anomalously high and this response can be used to determine anisotropic transmissivity. This method has been proven to work in a number of settings. Ritzi and Andolsek (1992) utilised azimuthal resistivity surveys to determine the principal directions of groundwater flow regimes in shallow carbonates before pumping. The monitoring of fluid flow during pumping supported the interpretations of the resistivity data. However, due to the poor understanding of the method, the technique often produces unexplainable results. Anomalous results have frequently been attributed to overburden. Laboratory experiments show that the direction of anisotropy could rotate 90^o once overburden thickness exceeds a critical value (approximately 20% of the electrode spacing) (Sauck and Zabik, 1992).

In a survey over a fractured landfill cover, Carpenter *et al.* (1994) do not have the problems of overburden but they still conclude that directions of elongation on azimuthal resistivity plots do not always correspond to fracture trends. Here, inaccuracies are explained using a more

complex fracture pattern that has been induced in the covering clay. However, fractured cover materials exhibited greater degrees of anisotropy than unfractured covers. They also present qualitative results on the effect of moisture content on azimuthal responses. In the case of landfill covers, greater anisotropy was apparent during dry periods.

More recent work (Watson and Barker, 1998) challenges the interpretations of many earlier azimuthal resistivity surveys. Directional variations in apparent resistivity are frequently employed to determine fracture orientation ignoring the other, more common potential causes of directional dependence. Variations may also be caused by the presence of a dipping interface, a gradational lateral change in resistivity or a combination of these. Watson and Barker (1998) present a method to distinguish between these causes using the offset Wenner technique (utilising a 5-electrode array) and comparing the resistivity measurements recorded with the left four electrodes and the right four electrodes.

Studies were carried out into the use of azimuthal electromagnetic techniques in preference to the azimuthal resistivity method to speed up the data collection process (Vickery and Hobbs, 1997b). Direct comparisons were made between the two techniques which found the electromagnetic method to be highly successful. New methods of presentation of the data were also investigated to display both the strength and azimuth of directional dependence (Appendix A).

Azimuthal electromagnetic surveys could be used to investigate the role of a fault; the fault may be conducting if it is a fluid filled, open fault suggesting great potential to affect flow paths. The technique is, however, time consuming and therefore not suitable for rapid fault location or site investigation. As a consequence of this conclusion, the research carried out into the azimuthal electromagnetic method is included in Appendix A but is not discussed in the main body of this thesis except where it appears in suggested future work.

2.6 Conclusions

To evaluate a contaminated site it is wise to assess the extent of contamination and determine the likelihood of contaminant migration away from the site. Contaminant migration is controlled primarily by the natural flow of groundwater but can be affected dramatically by the existence of critical pathways e.g. introduced by faulting and folding.

Electrical and electromagnetic techniques are sensitive to any changes in resistivity caused by the introduction of contaminants into a material. Diesel related organics can either increase or reduce the resistivity of a material depending on whether it is replacing water or air in the pore spaces. A shallow electromagnetic technique has been used for a reconnaissance survey of 2 ex-oil distribution terminals because it is a rapid survey method which has the capacity to detect subsurface structures as well as shallow contaminants (Jansen *et al.*, 1993; Larson *et al.*, 1997) (Chapter 4).

Resistivity has proved successful in the location of faults (Hobbs and Reading, 1994) and for resolving complex geology (Griffiths and Barker, 1993). A 2-D resistivity imaging survey has been employed to map out potential rapid contaminant pathways (breaks in clay coverage, high permeability units and faults) beneath the Granton site (Chapter 5 and 7).

3 GRANTON - SITE INVESTIGATION OF TWO EX-OIL DISTRIBUTION TERMINALS

3.1 Typical Site Investigation Strategies

The process of site assessment includes a number of stages. It is standard to undertake a lengthy desk study before embarking on the 'hands-on' site investigation stage. Figure 3.1 shows a typical site assessment process (reproduced from Imperial Chemical Industries plc (1992)) split into 5 stages. The desk study gathers together present day and historical information about plant processes and operations history to define the possible contaminants and the likely extent of contamination. The desk study also looks at available geological information to assess the potential for contaminant migration. Only if this desk study reveals the likelihood of significant contamination will an expensive site investigation commence.

To date, site investigation procedures rarely include the use of geophysical methods despite the time and cost advantages. A typical investigation (taken from a Rust Environmental advertising brochure) may comprise:

- Walk over inspection and grab sampling;
- Shallow soil survey by mechanical or hand auger and probe;
- Ambient vapour monitoring;
- Gas monitoring;
- Shallow soil survey by trial pit;
- Groundwater monitoring and installation of temporary piezometers;
- Soil and groundwater sampling and analytical testing.

These data provide the technical basis on which the decision for action or no action is taken and ultimately defended. This apparently extensive survey procedure consists entirely of spot measurements which can fail to locate contamination 'hotspots'. The invasive site investigation employed at Granton is an example of this (Chapter 4). The remainder of this thesis outlines the complete assessment of the Granton site and the vital role of geophysics.

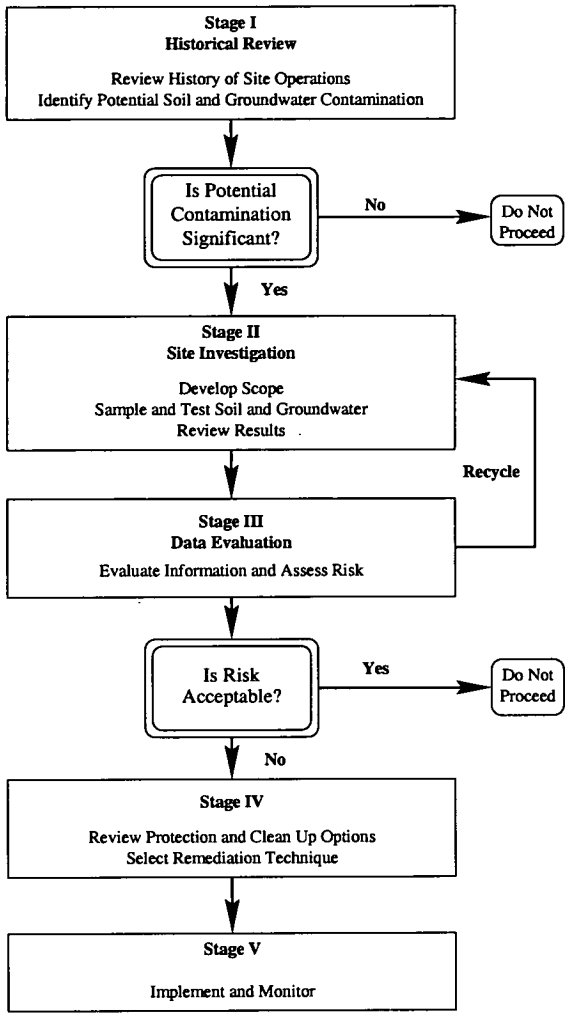

Figure 3.1: Site assessment Process. Reproduced from Imperial Chemical Industries plc (1992)

3.2 The North Edinburgh Project - Desk Study

The City of Edinburgh Council in conjunction with Lothian and Edinburgh Enterprise Limited (LEEL) are undertaking redevelopment of some 100 hectares of land in West Granton, Edinburgh, Scotland (Figure 3.2). The Council aim to acquire a large proportion of the industrial land at Granton for remediation and redevelopment to accommodate new industrial use and/or housing (Couper, 1998). In accordance with the Environment Act (1995) directives, a complete assessment of the surface pollution at Granton is being undertaken for the Council, before purchasing commences. A specialised, preliminary desk study was carried out, for the Council, by the University of Edinburgh in corroboration with the British Geological Survey (BGS), investigating the hydrogeological conditions of the site (Lunn *et al.*, 1997). The major findings from this report are presented below.

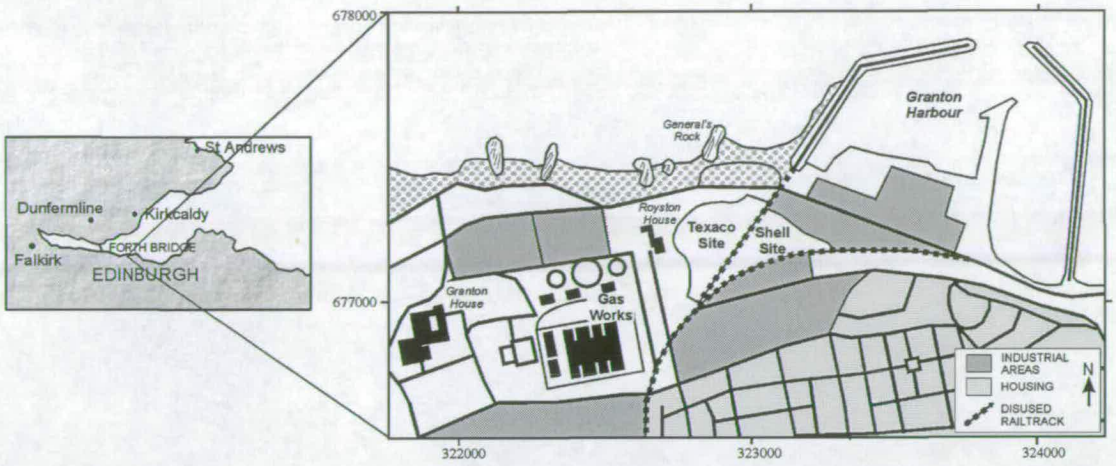

Figure 3.2: Location of the Granton Site, North Edinburgh, Scotland.

3.2.1 Site History

Archive records show that the Granton area has accommodated heavy industrial use for the past 150 years. Old Ordnance Survey map editions of the Granton area show the previous existence of an iron works, an ice works, a printing works, a timber yard and a chemical works. Contamination from all these sources may still reside in the subsurface. Recent industrial use comprises: a British Gas site, Lothian Chemical Co., an old sandstone quarry which has been used as a landfill, and, of particular interest to this thesis, two ex-oil distribution terminals. Figure 3.3 shows the location of the old quarry and the latter two sites including a plan of some historical details of the installations. Figure 3.4 shows an old photograph of the two sites taken from the east with the gas towers of the British Gas site in the distance.

All these industries are potential contaminant sources, in particular dense oil products are likely to have migrated into the subsurface geology and could potentially be transported toward the Forth estuary. Pollution of the foreshore and controlled waters would have serious implications for the Council's redevelopment plans.

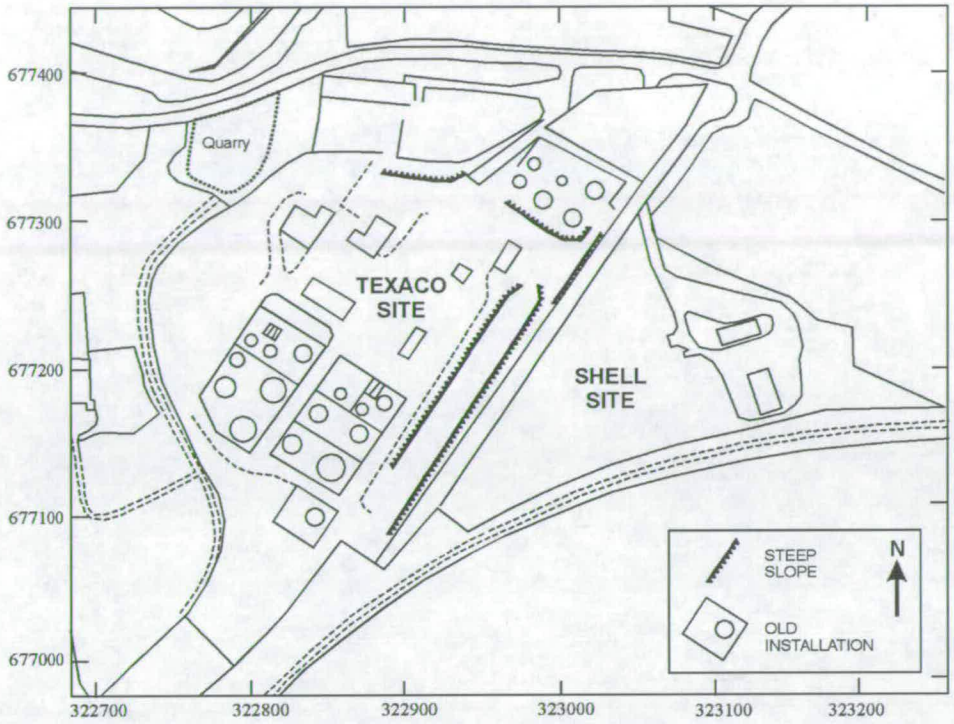

Figure 3.3: The former Shell and Texaco sites with historical map of installations.

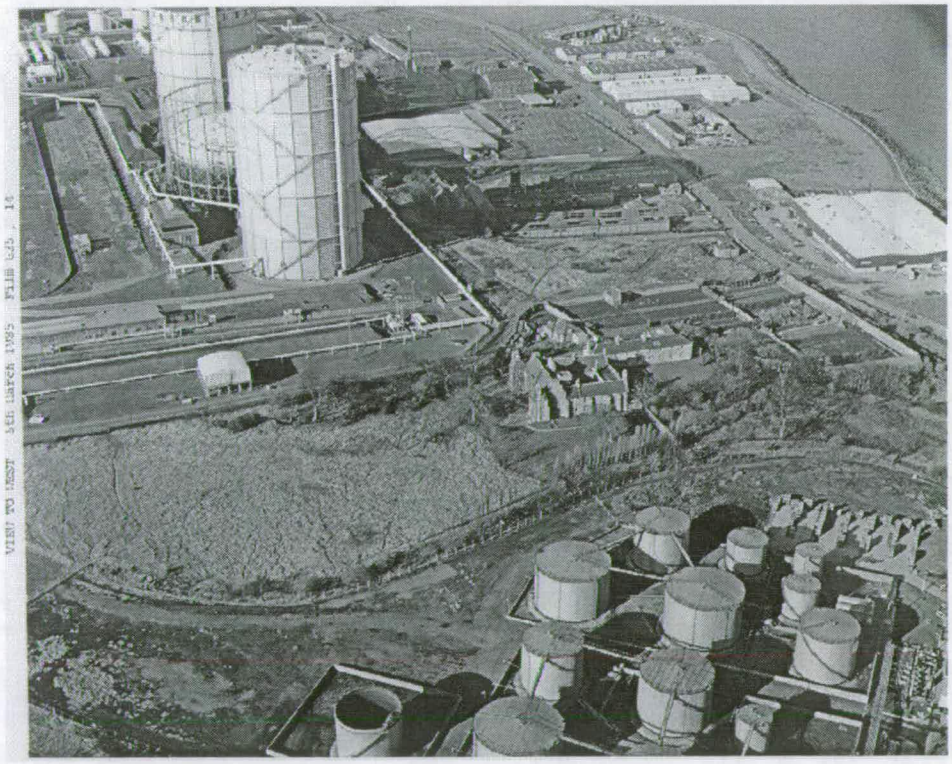

Figure 3.4: Historical photograph of the former Texaco site (taken from the east).

3.3 Geology of the Granton Area

3.3.1 Bedrock Geology

The geology of the Granton area belongs to the **Lower Oil-Shale Group** of the Lower Carboniferous succession in the Edinburgh region. The group is a cyclic sequence in the main consisting of pale coloured, fine to coarse grained sandstone interbedded with grey to black, sometimes bituminous mudstone and siltstone. A map of the main constituent rock types is shown in Figure 3.5 (taken from the current published BGS 1:10,560 Geological Sheet NT27NW). The geological lines portrayed on these maps are conjectural and display an interpretation of the data that was available at the time of compilation. The borehole information available for the Granton area is limited (Figures in Appendix C). The dip of the geological beds varies between 10 and 30 ^{o} which often prevents direct correlation between the widely spaced boreholes.

The youngest sequence on the site is the **Wardie Shales**. They consist of often bituminous (poor oil-shales), grey to black mudstones and grey siltstones with some off-white, fine to medium grained sandstones. Thin beds of limestone, coal seams, volcanic tuff and intrusive dolerite are infrequently present.

The **Granton Sandstones** consist of two sandstone units separated by mudstones. The lower sandstone, a fine grained pale unit known as the **Craigleith Sandstone**, is thought to have a maximum thickness of 105m but is much less at Granton where only ~17m of sandstone were excavated from a local quarry. The upper sandstone, known as the **Ravelston Sandstone**, has a maximum thickness of 38m but again is thought to be less at Granton. Approximately 15m of the Ravelston Sandstone was worked in the old quarry northeast of Royston House (NT 22800 77350) (Figure 3.3). The medium grained, brown rock is exposed on the Granton foreshore.

The Geological structure of the area is dominated by the **Granton Dome** (Mitchell and Mykura, 1962). The dome is an anticlinal fold with a north-south trending axis which plunges downwards to both the north and south causing the closure of the sandstone outcrop in both directions. The Granton site is located at the north eastern side of this dome where the geology dips steeply to the east. The regional geological map also locates a number of faults (Lunn *et al.*, 1997) which complicate the structure and highlight the likelihood of further undetected faults.

A geological map of the area immediately surrounding the Shell and Texaco sites is shown in Figure 3.5. The map has been constructed entirely from the limited surface outcrop data and does not take borehole data into account. The map should thus be treated with caution. Note the fault which was observed in one of the few on land outcrops, in the old quarry northeast of Royston House.

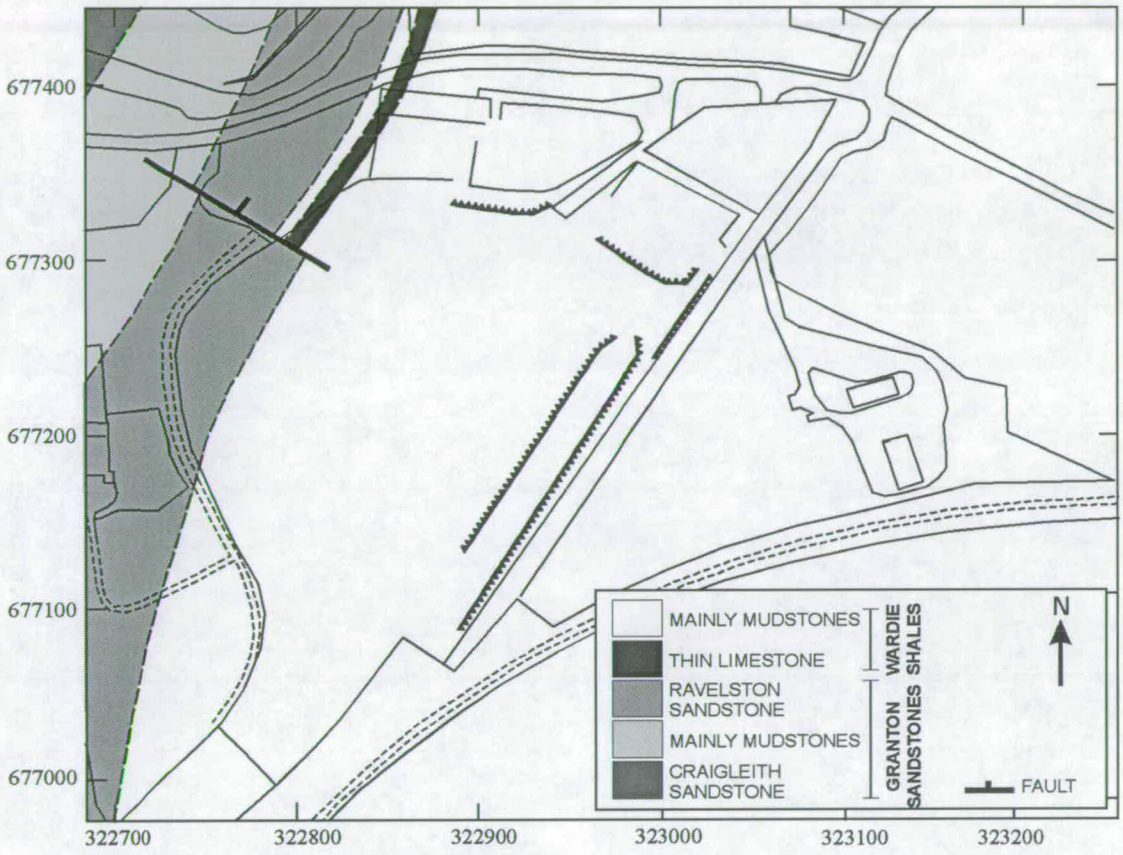

Figure 3.5: Geological map of Shell and Texaco sites constructed from archive data.

3.3.2 Drift Geology

Apart from the foreshore and the old quarry, the bedrock of the Granton site is usually covered by drift deposits with an average thickness between 5m and 6m. These deposits consist of naturally occurring **Quaternary** subsoils and man-made surfaces. Over the two ex-oil distribution terminals, archive records show the bedrock to be overlain by **late-Devensian Raised Beach** deposits. The lithologies of this sequence are highly variable. In places they consist of loose to medium dense sand with some gravel, overlying brown and grey, plastic, soft to firm clays, glacial till or bedrock. The sand and gravel layers have an average thickness of less than 2m (locally up to 6m). The laminated clays have thicknesses locally up to 8m but again have an average thickness of less than 2m.

Modern boreholes now show that the majority of the two sites are topped with 1 - 2 m of *land raise* man-made deposits(Appendix C). These deposits most commonly contain rubble, brick etc.

3.4 Hydrogeology of the Granton Area

Groundwater resides preferentially within granular materials rather than in the finer grained clays and mudstones. Beneath the Granton site the granular units include: the made ground; sand and gravel layers within the till; and sandstone units. The porosity and permeability values of a particular unit are also affected, however, by the secondary void space present due to fissures and fractures. The low permeability mudstones and shales may contain fractures and fissures particularly in the weathered zone and the Granton sandstones are thought to contain widespread bedding plane fissures (Lunn *et al.*, 1997). This increased permeability reduces groundwater travel times towards the sea.

The rate of flow of groundwater beneath the site is also dependent on the difference in hydraulic head, or depth to water table, between the inland area and the coast.

3.4.1 Groundwater in Drift Deposits

The low permeability clays and tills ordinarily act as a barrier against downward migration of surface waters favouring lateral movement towards the sea (following the direction of falling hydraulic head). Ground water can reside as perched water tables above the low permeability layers. Locally the clay coverage is likely to be heterogeneous, especially considering the extent of man-made surfaces and possible sand and gravel layers. If these granular units replace the clays, infiltration into the groundwater system could occur.

The granular drift deposits are particularly influential where they lie below the shallow water table. Here downward migration is not necessary so lateral flow rates will be dramatically increased.

3.4.2 Groundwater in Bedrock

Laboratory studies (Ngwenya, 1998) (which assume no fracturing) show the sandstones to be the only units of significant porosity ($\sim$ 17%). The higher porosities define the sandstones to be the main aquifers. The two Granton sandstones probably act as separate aquifers due to the confining mudstones and shales present above and below. They will, therefore, each have slightly different hydraulic heads.

3.4.3 Groundwater Flow System

At Granton, groundwater is generally moving in a northerly direction away from the higher ground (at higher hydraulic head) in the south towards the sea. Replenishment of water to aquifers takes place on higher ground especially where clay coverage is thin and where the sandstone units are exposed at the surface. Smaller amounts of water infiltrates into the system through superficial cover.

Once the water has entered into the groundwater flow system, travel times depend on the properties of the aquifers, the quantity of fracturing and other channels of concentrated flow. The University of Edinburgh was commissioned to determine flow and transport parameters of the lithologies beneath the Granton site (Ngwenya, 1998). The major conclusions of the laboratory studies found the sandstones to be the only units of significant permeability ($\sim$61mD). From cores of the borehole sections, the permeabilities of the mudstones were considered to be too low to be included in the experiment process. However, these results have no way of including the effects of fracturing or weathering outside the region of the sample, so the possibility of transport through the mudstones should not be disregarded. A number of the sandstone samples could not yield intact cores due to extensive fracturing, this may imply similar weathering of the mudstones. Open fractures and fissures within aquifer units can account for over 90% of the total groundwater flow as a consequence of the high secondary permeability. This highlights the benefits of field testing.

The United Wire Works (NT 23 77) drilled 3 water boreholes between 1960 and 1969. The boreholes were drilled to depths of 32m, 77m and 87m into the Granton sandstones. The two most productive sources pumped water at rates of 3.8 litres/second and 2.8 litres/second. The latter borehole had a fall in the water level of 4.3m during pumping.

The structural geology of the bedrock also affects groundwater flow. Permeability within sandstones tends to be highest parallel to the bedding, so, where the significant dip away from the Granton anticline coincides with the general hydraulic gradient, preferential groundwater flow occurs. The significant faulting in the area complicates flow patterns. Open faults and fissures can connect permeable units to provide extended, preferential flow paths.

Groundwater is normally discharged in areas along low-lying ground. Springs are seen where the water table and/or perched water tables coincide with the ground surface. Discharge will also occur at the saline/freshwater interface. As the groundwater flows towards the saline water of the sea, the fresh water rises to the surface due to the density variations between the two fluids. Figure 3.6 summarises the groundwater flow system hypothesised for the Granton area.

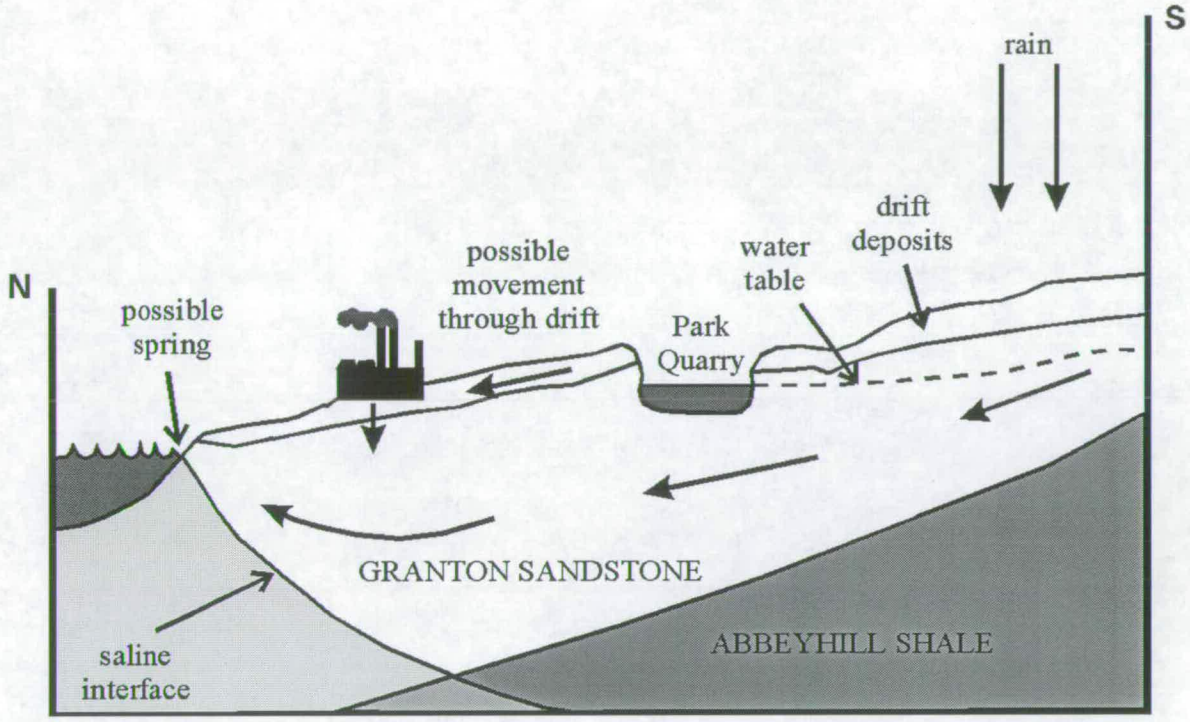

Figure 3.6: Generalised flow system for the Granton Area. (Reproduced from Lunn *et al.* (1997))

4 SURVEY I - RAPID RECONNAISSANCE SURVEY

4.1 Introduction

The Granton site, last used some twelve years ago to house oil distribution terminals, is to be redeveloped following any necessary remediation. Before the start of invasive site investigations, a trial geophysical survey was conducted involving magnetics and electromagnetics. This trial demonstrated that the electromagnetic technique, involving a Geonics EM31 soil conductivity meter, was capable of detecting subsurface metal pipes and contaminant concentrations resulting from the oil terminal works. The success of the trial survey led to the complete survey of the Granton site which proved highly successful (Vickery and Hobbs, 1997a).

The EM31 is directionally dependent and the results it yields depend on the orientation of the boom with respect to subsurface anomalies. This directionality can cause misleading interpretations and necessitated research into new methods of presentation (Vickery and Hobbs, 1998a).

4.2 Granton Site Investigation

The first phase of this Granton Development Project involves investigation and possible remediation of land formerly used as oil distribution terminals by Texaco ($\approx$6 hectares) and by Shell ($\approx$4 hectares). Figure 4.1 shows the location of the sites and includes a plan of some historical details of the installations. These installations are also shown in an old photograph of the Texaco site taken from the east (Figure 3.4).

At the demise of these terminals in the late 1980's, the sites were supposedly cleared - all that remains visible are some hard standing in the former Shell site (which has received a certificate of remediation) and a small group of pipes emerging from the ground to stand approximately 0.5m high at one location in the former Texaco site. Both sites now have rough, mixed vegetation.

Following desk studies and site inspections by the contractors, an invasive investigation comprising a number of trial pits and boreholes was arranged. Prior to the start of that inves-

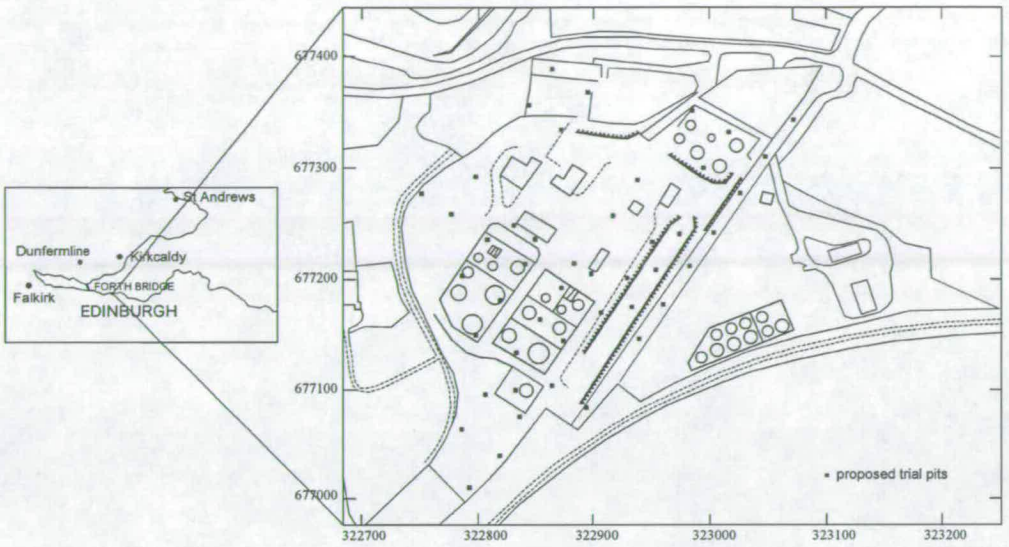

Figure 4.1: Location of the former Shell and Texaco sites.

tigation, it was suggested that non-invasive geophysics could play a useful role in locating anomalous regions indicative of contaminant concentrations and could thereby improve the efficiency and returns from judicious trial pit placements.

Geophysics is not, as yet, a routine procedure for industrial site investigations but, diverging from conventional investigation programmes, the City of Edinburgh Council agreed to a trial survey over part of the former Texaco site. A plan of the Texaco works together with two selected trial areas A and B is shown in Figure 4.2.

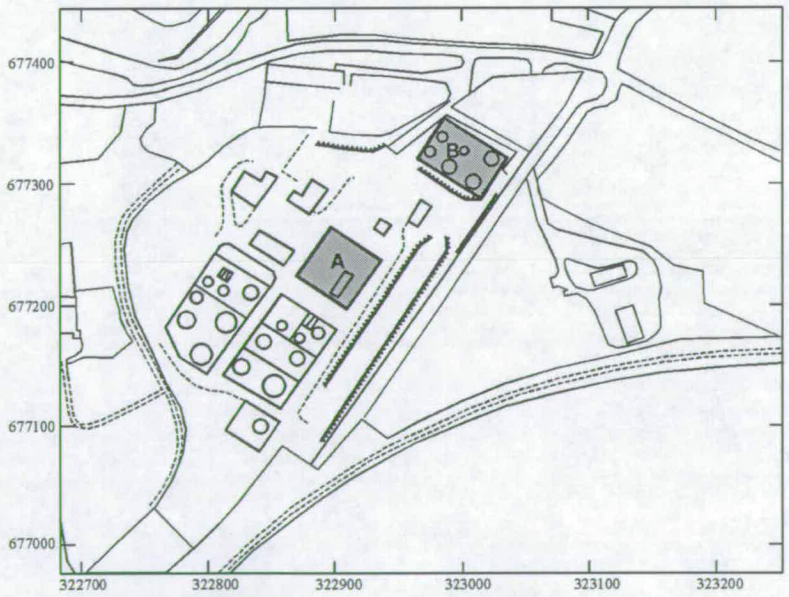

Figure 4.2: Location of trial surveys.

Since contaminants are the prime target, with oil and its derivatives likely, an electromagnetic technique was chosen to map changes in subsurface conductivity. At Granton, where the water table is relatively shallow, the expected contaminants are likely to increase electrical resistivity. Low conductivity values in this trial EM survey would therefore be priority areas for invasive investigation. Also, in view of the several pipes emanating from the ground in the former Texaco site, and despite firmly held beliefs that no subsurface structures still remained, it was felt a search for buried tanks, pipes, foundations etc. would be prudent and to this end total magnetic field gradiometry was also employed in the trial.

4.3 Trial Survey

A soil conductivity meter (Geonics EM31) was employed over area A (Figure 4.2) and a proton precession magnetometer in the gradient mode (Geonics G856) was employed over area B (Figure 4.2) for the trial survey. The techniques were applied to different trial areas due to contractual terms, affording no direct comparison at that stage.

4.3.1 EM31 Trial Survey

Area A, of size 50m by 50m, was positioned to include the visible pipes in its SE corner with a view to determining the anomaly they caused and the tracing of any subsurface connection or extension. Measurements of both in-phase (measured in parts per thousand) and quadrature (measured in mSm^{-1} EM31 responses were made at a grid spacing of 2m x 2m with the boom parallel to the NW-SE grid edge. The 2m X 2m grid was chosen as a compromise to cover the area in sufficient detail within the time constraints stipulated by the City of Edinburgh Council. Figure 4.3 shows the quadrature response which corresponds to soil conductivities in mSm^{-1} when the instrument is in its linear response regime. This linearity condition breaks down in the vicinity of large metal bodies such as pipes. When the EM31 boom is not parallel to the linear conducting body, negative quadrature readings may ensue (Geonics Ltd (1991)). These increase to a maximum negative when the boom is perpendicular to a linear conductor.

The anomaly caused by the visible pipes is seen clearly in Figure 4.3.a as two parallel linear negative regions implying subsurface connections. One of these linear features is seen to extend to the NE and a further linear negative anomaly is seen running diagonally across the trial area.

The theory of the EM31 and its surveying methods are presented in Appendix B. There is no available literature detailing the cause of the different responses of the in-phase and quadrature components to metallic objects, but the EM31 manual (Geonics Ltd, 1991) states that

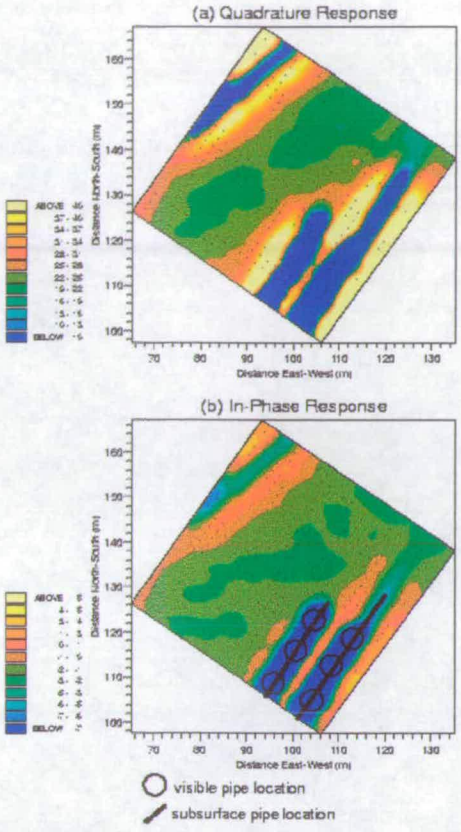

Figure 4.3: Quadrature response and in-phase response over area A.

the in-phase component is significantly more sensitive to metallic objects than the quadrature component. In support of this, numerous field surveys have shown that the in-phase EM31 measurements respond primarily to metal conductors while the quadrature EM31 measurements respond, more generally, to electrical conductors. Consequently, if the same anomaly is seen in both the in-phase and quadrature responses, the causative body is metallic in origin. Figure 4.3.b shows the in-phase measurements corroborating a metallic origin for the linear anomalies. Moreover the strength of the in-phase anomaly extending from the visible pipes is smaller than that directly over the visible pipes (distance to the source is greater) and is of the same order as that over the diagonally trending linear anomaly seen in the NW corner.

The obvious similarities between the anomalies imply a similar causative body. Thus both in-phase and quadrature measurements suggest an interpretation in terms of subsurface metal pipes. This is a plausible interpretation considering the few visible pipes remaining above ground but an unexpected result in view of the supposed site clearance. Figure 4.3.b shows the position of the pipes visible at the surface and shows the location of the subsurface pipes as interpreted from the EM31 data.

The original aim of the EM31 trial was to use conductivity variations as a pointer to possible concentrations of contaminants. The large response of the subsurface pipes (with the chosen boom orientation giving a negative flanked by positives on either side) masks much of the trial area from soil conductivity determinations. However, at the end of what is interpreted as a subsurface pipe (extending from the visible pipes), soil conductivities are seen to be relatively low and the results are evocative of contaminants leaking from the pipe end. (A later trial pit investigation verified this interpretation). If magnetometry had been employed over this area, the metal pipes would surely have been located - however, it is unlikely that any information relating to the contaminants would have been determined.

The dual success of the EM31 trial, pinpointing both subsurface pipes and contaminants, dictated this as the technique to use over the entire former Texaco site. Before embarking on a full survey, investigation was made into whether a coarser grid could be employed without significant degradation of information. Accordingly the 2m x 2m trial grid was subsampled at a spacing of 4m x 4m (i) by taking even-numbered grid points and (ii) by taking odd-numbered grid points. One of the two grids would be relatively displaced by 2m in both directions. Figure 4.4 shows the quadrature results from the two course grids. In Figure 4.4.a the visible pipes and subsurface continuation are seen, but the diagonal anomaly is degraded and contaminant information is less convincing. Displacing the starting point by 2m in both directions results in Figure 4.4.b where information on the subsurface pipe extending from the visible pipes has been lost, along with details of the associated contaminant concentration. It is concluded that the information sought from the former Texaco site required the establishment of a 2m x 2m grid over the entire area.

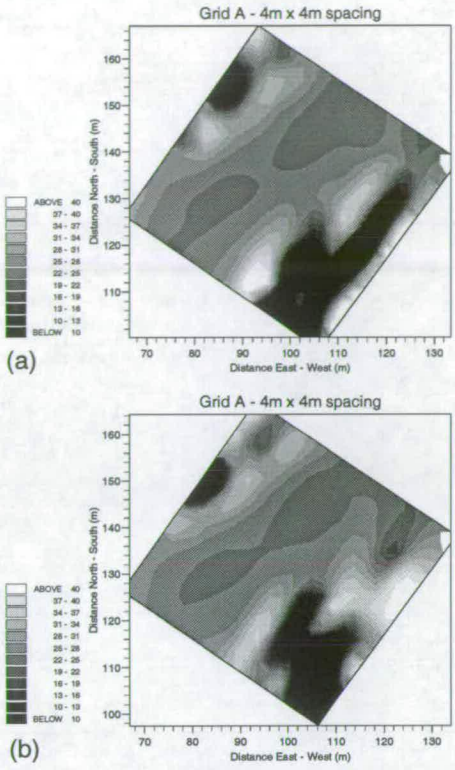

Figure 4.4: Quadrature response over area A with a coarse grid.

4.3.2 Magnetic Trial Survey

Area B (Figure 4.2), of size 60m x 40m, at the northern end of the site was chosen for the trial magnetic survey, which was conducted using a Geonics G856 magnetometer in gradient mode again over a 2m x 2m grid. The area was topographically quite difficult, with several large spoil heaps, and was bordered by a metal fence to the north. The gradiometer results are uninterpretable and values of the total magnetic field, from the top sensor 2.5m above ground surface, are presented in Figure 4.5. The map is dominated by a large anomaly of over 2000nT, which has to be caused by a large metallic underground structure. No evidence of pipes is seen in this area and it was concluded, as above, that use of the EM31, providing dual evidence for metallic conductors and contaminants, would be more rewarding over the entire area. (Subsequent EM31 measurements over area B also revealed the location of the large conducting body detected by the magnetics).

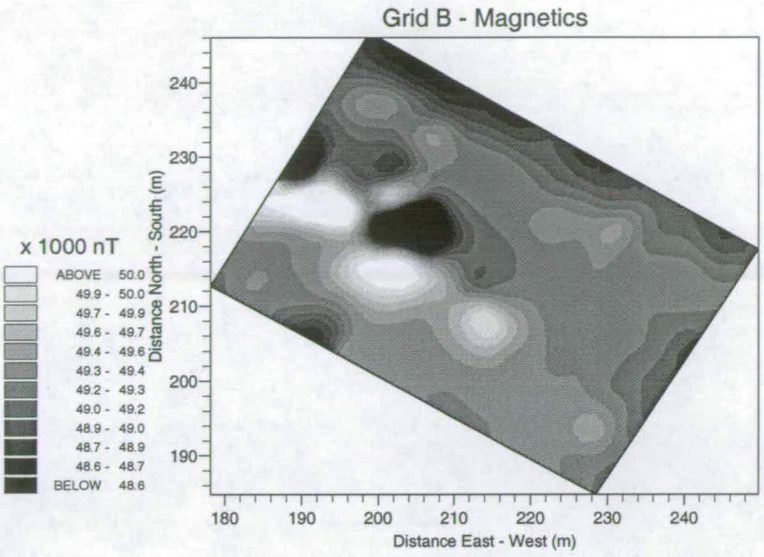

Figure 4.5: Total magnetic field over area B.

4.4 Full Survey

For the full survey, areas encompassing the former Texaco and Shell sites were treated separately. The Shell site to the east had been granted a certificate of remediation and was thereby thought to be relatively free of contaminants. Consequently, the former Texaco site was considered to be of more immediate interest. The trial survey supported this conclusion and full surveying of the former Texaco site was commenced first.

4.4.1 The Texaco Site Results

The former Texaco site was divided into 18 separate grids as shown in Figure 4.6 partly through logistics and partly through the nature of the contract details. Measurements were taken wherever possible including through wooded areas and other dense vegetation where grid lines were positioned using compass bearings. Two specific areas, an embankment (grid O) and a cutting (grid P), the latter formerly used as a railway line, were surveyed separately as extreme topographic gradients prevented measurements being taken between these grids.

A useful technique in EM31 surveying is to take measurements in orthogonal directions by rotating the EM31 boom within the horizontal plane. Differences between these readings are attributed to lateral inhomogeneities in conductivity. In view of the above time constraints and the close grid spacing, measurements at Granton were taken with the boom in a NW-SE orientation only, the same orientation as the trial survey.

Figure 4.6: Location of survey grids on former Texaco site.

In total, 13,274 in-phase and quadrature measurements were taken across the former Texaco site at a grid spacing of 2m x 2m. Figure 4.7 shows a composite contour map of the conductivity (quadrature) measurements. The existence of numerous subsurface linear features is instantly apparent. These features are characterised by conductivity highs (reds and yellows) running in a northwest southeast orientation and by negative values (blues) in a northeast southwest orientation. This directional dependence is the typical response of a highly conductive linear body. When the EM31 boom is parallel to the strike of the body a high conductivity reading ensues whereas when the boom is perpendicular to the strike the quadrature is negative. A similar map, and similar arguments, apply to the in-phase data and so, as in the trial survey, evidence is strong for the interpretation of these linear features in terms of subsurface pipes. The extent of the underground network still remaining over this "cleared" site was somewhat of a surprise to the contractors.

On inspection by a non-geophysicist, the type of display shown in Figure 4.7 is complicated to interpret. Both positive and negative features are attributed to similar causative bodies. Further complications occur with double peak anomalies that arise when the subsurface linear feature is parallel to the EM31 boom and these can be confused, by geophysicists and site engineers alike, as having two causative bodies. If geophysics is to be used as a tool by engineers it is important for any information to be clear and easily interpretable. For this reason an alternative data presentation method is described below.

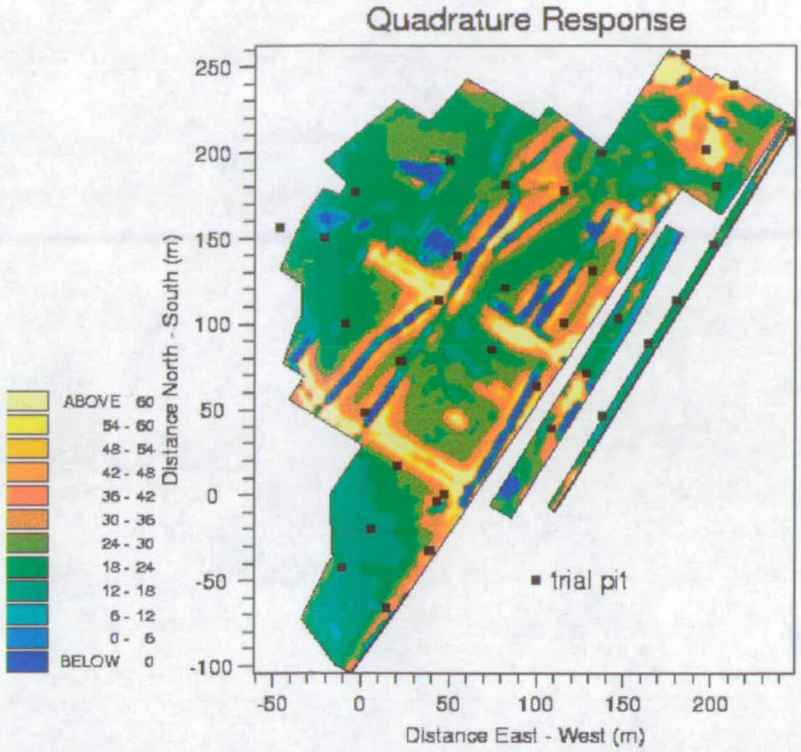

Figure 4.7: Composite map of the quadrature response over the former Texaco site. Includes locations of trial pits.

4.5 Presentation of Data

The EM31 manual (Geonics Ltd, 1991) shows the anomaly across a linear conductive body to be either a positive peak or a negative trough depending on whether the EM31 boom is parallel or perpendicular, respectively, to the strike of the conducting body. However, at present, there is no theoretical explanation of this behaviour. In practice, the Granton data agrees with other EM31 field data (e.g. Reynolds (1997) page 598) which demonstrates that a linear conductor is represented by an 'M' shaped apparent conductivity anomaly. When the EM31 boom is perpendicular to the pipe, a central trough is seen when the transmitter and receiver coils straddle the pipe. When the EM31 boom is parallel to the pipe, the single peak anomaly is seldom seen perhaps because the slightest deviation of the boom, from parallel, causes the coils to straddle the pipe. In the case of the Granton data, the responses of the two boom alignments are distinguished by the severity of the central trough. When the boom is perpendicular, the central trough is negative. When the Boom is parallel, the central trough remains positive. Examples of these different pipe anomalies are presented in Figure 4.8.a. Consequently, whether the central trough is negative or positive, both profiles have the same pattern of peak-trough-peak but they look different on traditional contour plots of conductivity because one trough lies below zero.

The most obvious comparison between the two anomalies is the rapid change in the quadrature response with distance. Figure 4.8.b shows how taking the second derivative transforms both anomalies into a positive peak flanked on either side by negative troughs thus removing boom directionality.

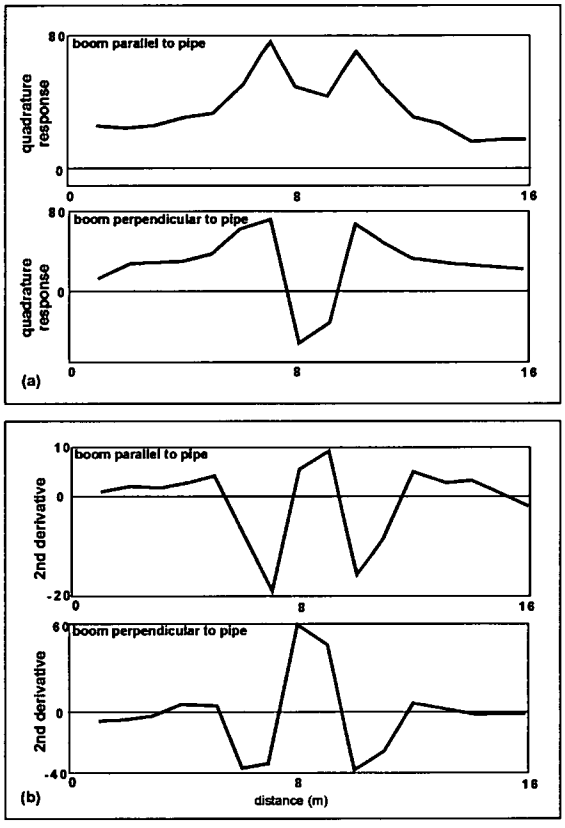

Figure 4.8: Comparison of perpendicular and parallel profiles from the Granton data set. (a) Quadrature response. (b) 2nd derivative of quadrature response

The second derivative of the complete quadrature data set has been taken in orthogonal directions. The data were firstly interpolated onto a 1m x 1m regular grid and then the second derivatives of the interpolated matrix were calculated using a pre-programmed Matlab routine. The output and input matrices are the same size where each output matrix element is equal to the difference between an element of the input matrix and the average of its four neighbours. The second derivative effectively amplifies the high frequency components of the data but the pipe anomalies clearly dominate (Figure 4.9). All conductive linear bodies are now characterised by a positive anomaly flanked on either side by a negative trough. This representation also eliminates the ambiguity between interpreting one causative body or two parallel bodies. Figure 4.10 shows a) the conductivity plot and b) the 2nd derivative contour plot for one such area where previously two pipes were inferred.

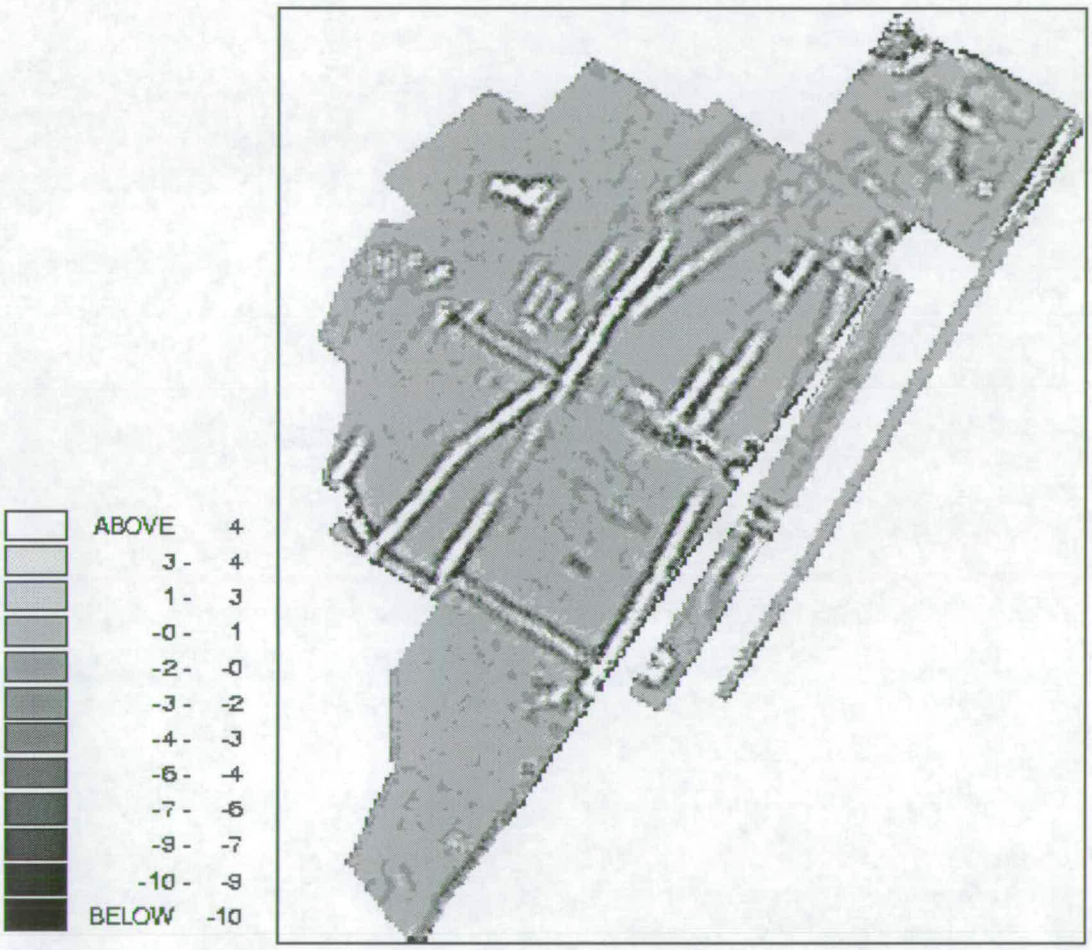

Figure 4.9: 2nd derivative of the complete quadrature response data set over the former Texaco site.

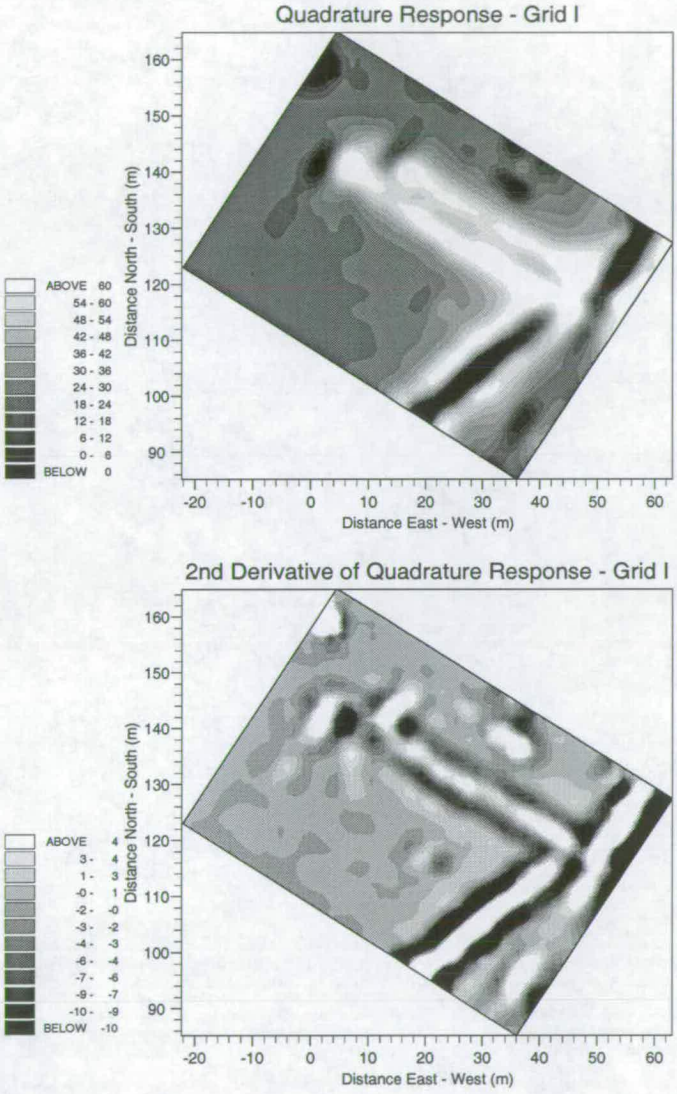

Figure 4.10: Comparison of the quadrature response and 2nd derivative of quadrature response over grid I.

4.5.1 The Shell Site Results

The survey over the former Shell site highlighted very few anomalous regions. During an initial walk over of the site, the response of the EM31, across the site, was thoroughly investigated. No extreme anomalies, frequently representative of man-made structures, were apparent. Hence, in accordance with the time constraints imposed by the contract, a grid spacing of 4m x 4m was concluded to be sufficient to sample the more smoothly varying soil conductivities. (This decision was aided by the knowledge that the Shell site had previously been awarded a certificate of remediation). The Shell site has no difficult topography apart from one shallow drainage channel. The site does, however, include a large concrete standing in the north west region. This standing shows up as negative quadrature readings (saturating the EM31) due to the reinforcing bars within the concrete. Consequently the EM31 method provides no information below the hard standing. This area could have been resurveyed with an alternative technique, such as GPR, if required.

Figure 4.11 presents a conductivity map of the former Shell site and little variation is seen. As expected, the water-filled drainage channel produces a linear higher conductivity anomaly. The few anomalies that showed low resistivity values (marked X on Figure 4.11) possibly compatible with hydrocarbons were ground truthed and, on the whole, were clean. The only area of suspicion is the small negative anomaly in the north east corner which the trial pits missed. However an invasive survey nearby did pick up quantities of hydrocarbons which may have a source at the location of the anomaly e.g. a buried drum.

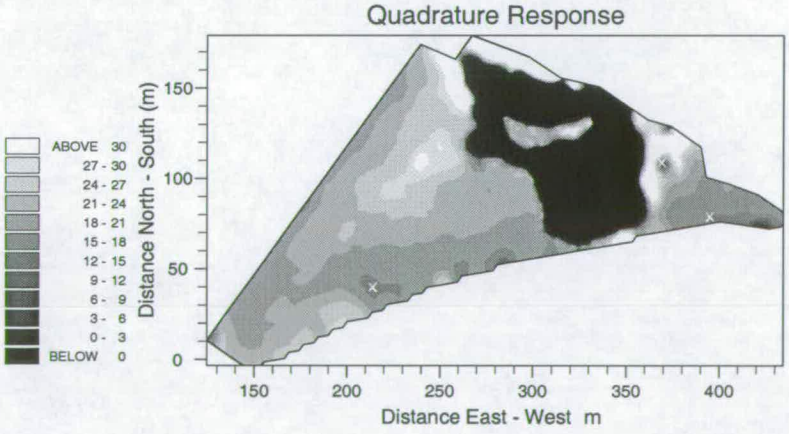

Figure 4.11: Contour map of the quadrature response over the former Shell site.

4.6 Invasive Survey

The original trial pits were positioned using information obtained from a desk study of the site conducted by the contractors. The trial pits were designed to sample the old installations

and areas of known spillages or dumps. None of these trial pits contained any hint that there might be a subsurface pipe network. Figure 4.7 shows the trial pit locations in relation to the geophysics and it can be seen that none of the invasive surveys coincide with the centres of any of the large conductivity anomalies. This 'hit and miss' approach has been experienced before notably with an EM31 survey which located a polluted area which had been missed by a grid of boreholes (Earth Science News (1993)). At Granton, without the geophysics, there would have been no reason to suppose that subsurface engineering structures might be present.

The invasive team were keen to utilise the geophysics and relocated a small number of trial pits in grid areas D, A and J. When a relocated trial pit was dug precisely over the centre of the large linear anomaly trending SW-NE in region D (location (82,35) on Figure 4.7), a 13cm metal pipe was uncovered at a depth of 1m. It is important to be precise when attempting to unearth a 13cm diameter pipe within a 6 hectare site! Figure 4.9 shows two pipes crossing obliquely (location (55,124) on Figure 4.7) and again a trial trench was dug revealing the two pipes.

As was apparent in the trial survey, the large response from a small pipe 1m deep masks a considerable region on either side from soil conductivity determinations. However, despite this masking effect, detailed interpretation of the geophysics was possible in many regions and zones of possible contamination, the original target, could be identified. Here reference is made to the original quadrature maps rather than to the second derivative maps used to highlight the subsurface pipes.

On inspection of the trial survey over area A (Figure 4.3.a), a marked difference is seen between the termination styles of the two parallel pipe anomalies. The end of one pipe is closed in by a conductivity high whereas the other leads to low conductivity values, evocative of contaminants emanating from the pipe end. A trial pit at this location revealed both the pipe and contaminants.

This pattern is present elsewhere, for example in area J (Figure 4.12). Again this anomaly was sampled with an invasive survey and a broken pipe with significant hydrocarbon concentration at the open end was revealed (see Figure 4.13).

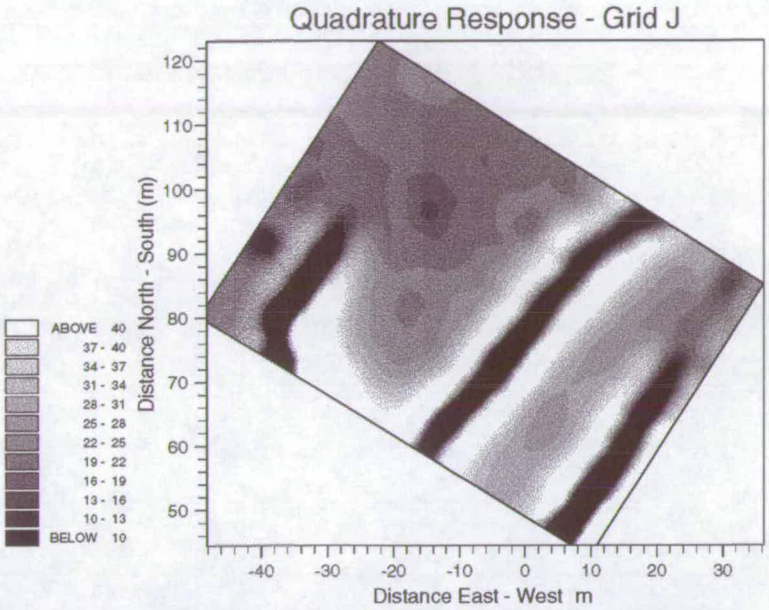

Figure 4.12: Contour map of the quadrature response over grid J.

Figure 4.13: Photo of trial pit revealing the end of a broken pipe.

4.7 Conclusions

The value and effectiveness of geophysical surveying, prior to invasive site investigation, has been clearly demonstrated.

In the case of the former Texaco site, the original aim of the EM31 survey was to locate any anomalous conducting regions for further investigation using trial pits. However, a labyrinth of underground pipes turned out to be a major unexpected discovery. This now necessitates a two-stage approach to remediation in which over 700m of pipe will first have to be removed. With precise positions known, their careful and safe extraction can be effected. The scrap value of the removed pipe work may compensate for the extra remediation step. Over a linear pipe network such as that encountered, directionality of EM31 measurements led to some scepticism of interpretation from contractors. Rather than undertake a more time-consuming survey with orthogonal measurements at each location, use of the second derivative of unidirectional measurements is shown to reveal all the pipes clearly and similarly, i.e all the pipes in Figure 4.9 show as positive anomalies (in white) whatever their direction relative to the EM31 boom. Conductivity plots could also be interpreted in terms of soil contamination in regions away from the masking effect of subsurface pipes and other conductors. Several low conductivity areas were examined by trial pits and trenches and were found to contain oil/tarry contaminants.

For the former Shell site, electromagnetic surveying confirmed the relative cleanliness of the remediated ground. The most anomalous areas, in terms of their conductivity, were highlighted and investigated with trial pits. On the whole, no significant contaminants were found.

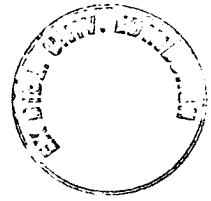

5 SURVEY II - TWO-DIMENSIONAL (2-D) RESISTIVITY IMAGING SURVEY

5.1 Introduction

After the success of the initial reconnaissance EM31 survey at Granton, a second geophysical survey was designed to determine specific details about the subsurface (Vickery and Hobbs, 1998b). The aim of the survey was to assess the risk of contaminant emergence on the foreshore at Granton.

The survey was designed to do the following;

- Evaluate the integrity of the superficial clay deposit which could, if intact, act as an effective barrier reducing the flow of contaminants.
- Locate any potential rapid contaminant pathways. These include significant faults and connected higher permeability sequences.
- Delineate the saline/fresh water interface to predict the zone within which groundwater is likely to rise and discharge at the surface.

To address all these aims, a resistivity technique was chosen because of the expected anomalous electrical properties of all the targets. The 2-D Resistivity Imaging method was chosen in particular for ease of use in the field with high returns of information sampling both lateral and vertical resistivity changes.

5.2 2-D Resistivity Imaging

The resistivity method involves the injection of current into the ground and the measurement of the resulting potential differences at the surface. Homogeneous ground produces particular pattern of potential differences and any deviations from this can provide information on the electrical properties of the inhomogeneities in the subsurface. Calculations will provide the *apparent resistivity* which is a weighted average of the true resistivities sampled by the current.

There are numerous electrode configurations that can be employed for resistivity surveying. For this survey the Wenner configuration was used in which the current and potential electrodes are maintained at an equal separation. Traditional methods utilise the Wenner configuration for vertical electrical soundings (VES) and constant separation traversing (CST). During VES the electrode spacing is systematically increased about a fixed central point and the current penetrates to progressively greater depths. For CST surveys, the electrode separation is fixed and the whole spread is moved along a profile sampling lateral variations of resistivity.

The GEOPULSE resistivity imaging equipment performs both the VES and CST surveys producing a two-dimensional slice through the subsurface when used with the IMAGER cable system (Campus Geophysical Instruments Ltd., 1994a,b). The GEOPULSE is coupled to the IMAGER multicore cable which has 25 take-out points for electrodes. Figure 5.1 shows the arrangement of electrodes and the measurement sequence which is used to build up a Wenner pseudosection in traverse mode. Electrode spacing a determines the apparent depth of investigation. The zone of investigation lies approximately between depths of $a/2$ and $4a$. The imaging module of GEOPULSE is computer controlled which increases the rate of data acquisition and the data are stored ready for interpretation.

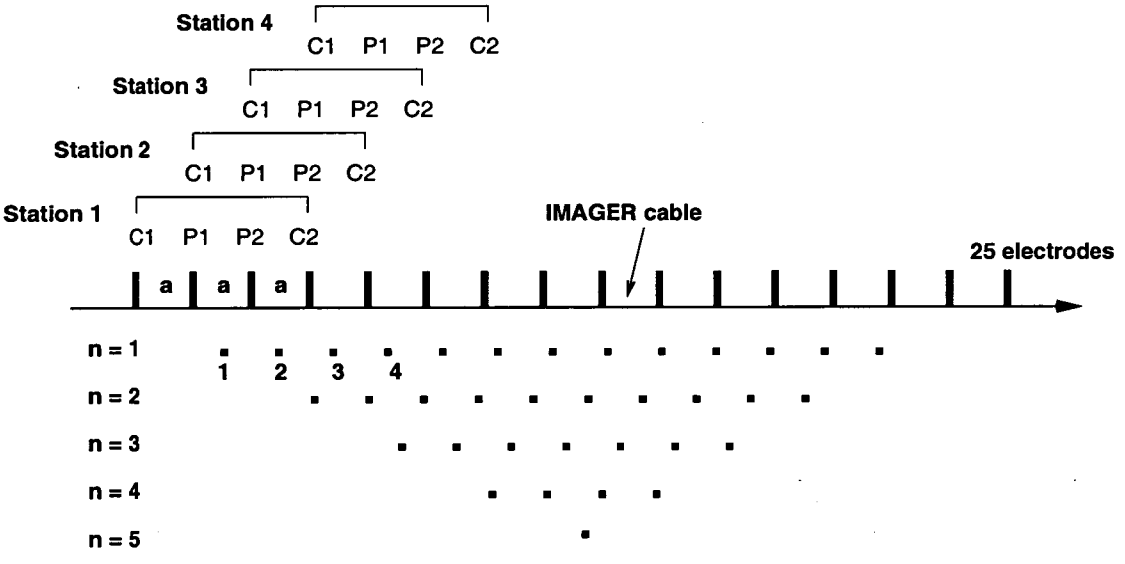

Figure 5.1: Principles of electrical imaging in traverse mode. (C1 and C2 represent the two current electrodes and P1 and P2 represent the two potential electrodes). Redrawn from Campus Geophysical Instruments Ltd. (1994a).

There are two survey methods that can be employed by the GEOPULSE system. First, the traverse mode utilises all 25 electrodes to measure a complete pseudosection. All measurements along n = 1 are measured before starting n = 2 etc. The second method, the roll-on mode, is used when a survey line extends beyond 25 electrodes. The measurement sequence for the roll-on mode is shown in Figure 5.2. Measurements for n = 1-6 are made for station 1 before

continuing for station 2. Measurements are completed up to station 7 before electrodes 1-7 are taken out and moved to the end of the array becoming electrodes 26-32. The IMAGER cable is moved on accordingly and measuring continues. The procedure is continued until no more roll-ons are required and the full pseudosection is completed measuring up to the last station in place.

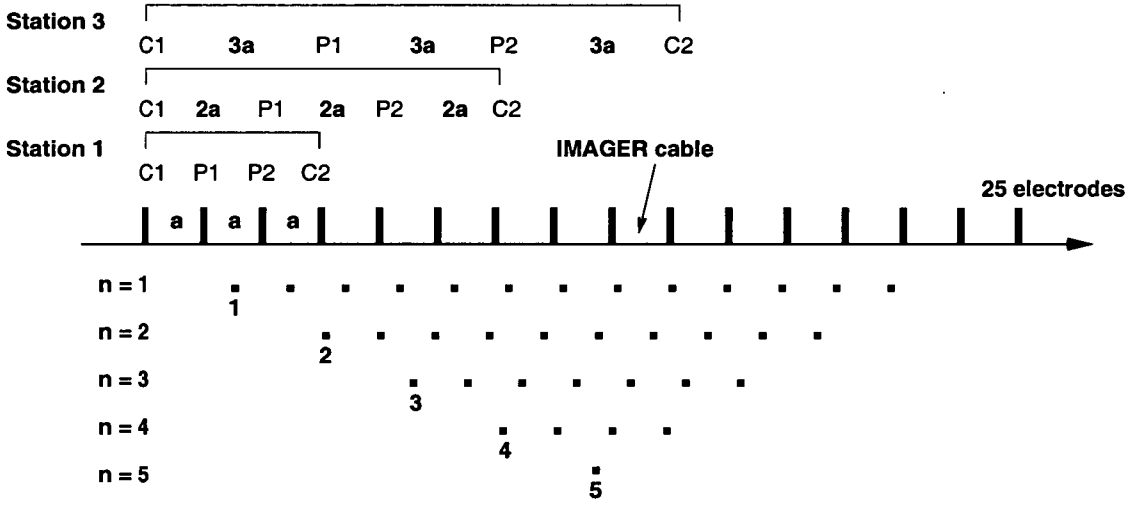

Figure 5.2: Principles of electrical imaging in roll-on mode. Redrawn from Campus Geophysical Instruments Ltd. (1994a).

5.2.1 Resistivity Pseudosections

GEOPULSE data can be displayed as a pseudosection by plotting each apparent resistivity as if it were the resistivity of the point immediately below the centre of the electrode array at a depth equal to half the electrode spacing. The contoured data provide an approximate picture of the resistivity distribution in the plane of the section. The pseudosection can be transformed into modelled resistivity using an inversion program allowing both apparent and modelled resistivity to be displayed in a 2-D plane. Figure 5.3 shows an example of measured apparent resistivity pseudosection with the calculated apparent resistivity pseudosection which would be measured over the resistivity model produced from the inversion program, RES2DECO . It should be noted that the layer numbers (n = 1-8) are converted to a modelled depth scale in the model resistivity section.

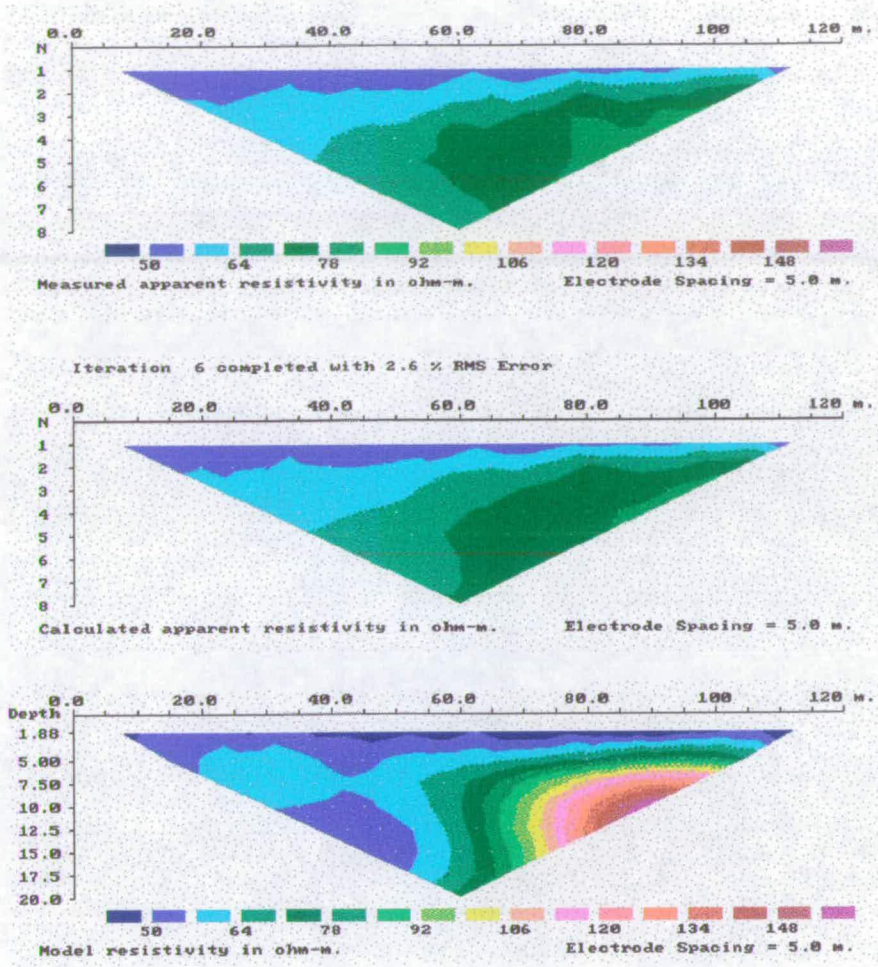

Figure 5.3: Example of measured and calculated apparent resistivity pseudosections with the corresponding resistivity model.

The RES2DECO program (Campus Geophysical Instruments Ltd., 1994c) incorporates an inversion algorithm developed by Loke and Barker (1996) centred around the equation

$$(JJ^T + \lambda F)d = J^T g \tag{5.1}$$

where

$F = f_x f_x^T + f_z f_z^T$

(f_x = horizontal flatness filter and f_z = vertical flatness filter), J is the Jacobian matrix of partial derivatives, g is the discrepancy vector which contains the differences between logarithms of the measured and calculated apparent resistivity values, λ is the damping factor and d is the model change vector.

The inversion algorithm is based on the smoothness least-squares method (deGroot Hedlin and Constable, 1990; Sasaki, 1992). It is modified to speed up the inversion routine and reduce the amount of required memory. The routine quickly produces a 2-D model that approaches a model of the resistivity of the subsurface from the measured resistivity pseudosection. However, the user must be aware that, as with all modelling routines, the inversion suffers from non-uniqueness i.e. there are an infinite number of models that will fit any one data set. Also, models produced by the inversion show sharp boundaries as gradational and resistivity contrasts may not be exact.

The user can define a starting model and control the inversion by defining a number of parameters including damping and flatness filters. Alternatively, defaults are provided for all the above. The damping factor and flatness filter can be adjusted to allow for the particular characteristics of a data set. The damping factor depends on the level of random noise present in the data i.e. the greater the noise level, the larger the damping factor. The flatness filter parameters allow the user to select the ratio of the damping factor for the horizontal flatness filter and the vertical flatness filter i.e. if the anomalies in the pseudosection are elongated horizontally, the user can force the production of horizontally elongated models by increasing the ratio of the horizontal to vertical flatness filter. For the inversion of the Granton data, a single damping factor is used for both filters to allow for the steeply dipping geological units that the borehole information predicts.

Figure 5.4 shows the 2-D model used by the inversion program. The subsurface is divided into a number of rectangular blocks. For the Wenner array, each block, apart from the outer most edge blocks, has a width equal to half the electrode spacing. The thickness of the outer blocks can be defined by the user.

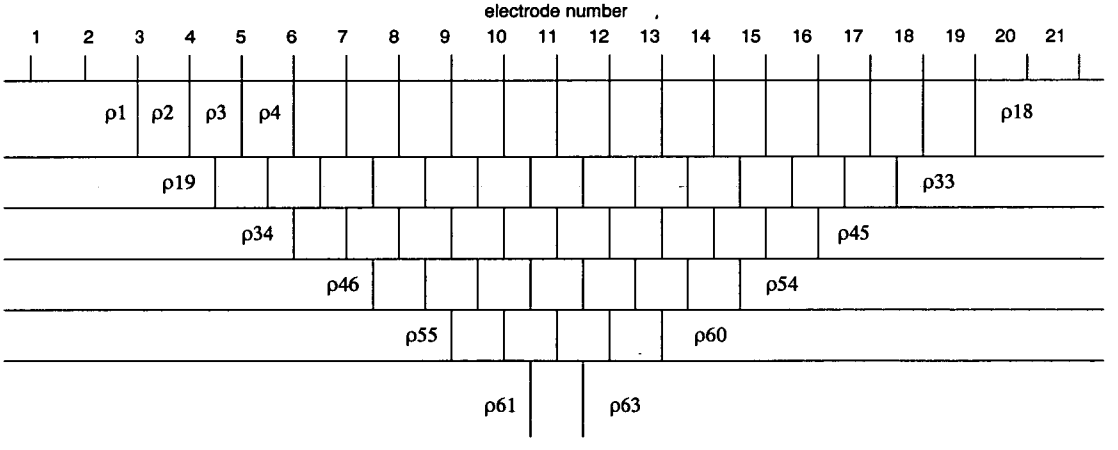

Figure 5.4: Model used by inversion program RES2DECO . (Redrawn from Campus Geophysical Instruments Ltd. (1994c)).

The aim of RES2DECO is to assign each block a resistivity value which will ultimately pro-

duce an apparent resistivity pseudosection which matches the measured field data. The default starting model is calculated using the deconvolution method. This method involves the deconvolution of a homogeneous earth model using a precomputed filter. The method is explained in detail in Loke and Barker (1996). Alternatively, it is possible to enter a user defined model or use the field apparent resistivity values for the initial model resistivities. The effects of all the above parameters were tested by systematic variation. As a result of the tests, the defaults were accepted.

The success of the model is given as a root-mean-squared RMS error which measures the difference between the calculated and measured apparent resistivity values. The optimisation method attempts to reduce the RMS error and produce the closest fitting resistivity model. The RMS error is typically between 2 and 12%.

RES2DECO and a comparable routine RES2DINV are widely used throughout the environmental and engineering geophysics community as a tool to interpret apparent resistivity pseudosections. The inversion algorithm uses N data points to calculate N resistivities which could be unstable if some of the model parameters are poorly determined. The sizes of the blocks in the resistivity model are fixed according to the electrode spacing. If some combinations of model parameters are poorly sampled then the eigenvectors which correspond to the small eigenvalues can have their behaviour dominated by the effects of noise. In an attempt to eliminate the instability, the smoothness of the perturbations to the model parameters is constrained to some constant value. However, the errors introduced in using this method are most likely insignificant in comparison with the errors inherent in the interpretation of resistivity data collected over the real earth.

For interpretation, in order to divide the subsurface into discrete packages, it is necessary to assume that for each package, the resistivity distribution is uniform. The resistivity of any one package is typically heterogeneous varying, for example, due to fracture density, moisture content and mineral distribution. A further consideration is the range of resistivity values of different materials. Resistivities vary by orders of magnitude, broadly defining geological units. Finally, any user of the inversion routine must take into account that the program output is a 2-D model of a 3-D earth. This particular aspect is covered in more detail in Chapter 8.

Despite the problems outlined above, if the user recognises the limitations of RES2DECO and does not attempt to over interpret the data, the routine is one of only a handful of valuable tools for extracting the maximum amount of information from apparent resistivity data.

5.3 Data Acquisition and Field Limitations at Granton

Over 30 profiles were collected using the GEOPULSE system over and around the former Shell and Texaco sites. Figure 5.5 shows the locations of these profiles. The profiles are labelled according to the electrode spacing and the survey method i.e. the prefix R5 denotes a 5m electrode spacing roll-on survey and T10 denotes 10m traverse. The exceptions to this rule include S4, C6, S7A and C10 which are traverses with 5m electrode spacings positioned near boreholes with the same label, and profile AL that was measured as a roll-on with 5m electrode spacings as part of an undergraduate project (Gardiner, 1997). The positioning of the profiles was determined primarily by the size of the available open ground. The extreme topography, concreted areas and fences all presented obstacles to laying out the electrode array. Wider spaced, deeper penetrating surveys were preferentially employed but frequently only the shorter surveys could be accommodated.

Figure 5.5: Location of resistivity traverse (red) and roll-on (blue) profiles across Granton site.

In order to make the greatest use of the available core logs (Section 3.3), the profiles labelled **S4, C6, S7A** and **C10** were sited straggling boreholes to directly correlate resistivity variations with different rock types. This increased confidence in assigning resistivity values to the geological units of interest where no invasive investigations were present.

The majority of the measurements were taken within the former Shell and Texaco sites because the access around the site is restricted by buildings to the south and east and by the road to the north. Steep topography and fences also limit the location of profiles. However, profiles

were taken wherever practicable from outside the site along grass verges, within the private ground to the west, on and near the foreshore and along the dismantled railway line.

5.4 Conclusions

The GEOPULSE system was utilised for a detailed investigation of the Shell and Texaco sites at Granton. The computer controlled resistivity imaging method provided rapid coverage of the entire site returning a large number of 2-D apparent resistivity pseudosections.

The interpretation of these pseudosections is aided with the use of a 'least-squares deconvolution' inversion routine included in the RES2DECO package. However, to extract geological information from the Granton resistivity pseudosections, further data processing is required before inversion can be employed. The extra data processing is introduced to remove the masking effects of the conducting pipes located in the reconnaissance survey (Chapter 4). The processing method is described in Chapter 6.

6 THE EFFECT OF SUBSURFACE PIPES ON APPARENT RESISTIVITY MEASUREMENTS

6.1 Introduction

A conducting subsurface pipe causes a strong response in most electrical geophysical surveys. The pipe signature is well defined in some techniques (e.g. EM31 Vickery and Hobbs (1998a)) such that it can be recognised within survey data and pipe lines can be detected. However, perhaps more frequently, the effect of pipes on a geophysical survey is considered to be noise, rendering the data uninterpretable and surveys are redesigned to avoid pipelines altogether. For example, (Schwarz, 1990) experienced constraints in a resistivity survey due to the electrical interference created by a pipeline which acted as a perfect conductor.

Ordinarily apparent resistivity pseudosections are interpreted directly after inversion, however, in the case of the Granton site investigation, further processing has been necessary to extract the maximum amount of information from the data set. The pipe network detected in the EM31 survey (Section 4) acts as a severe noise source in the resistivity survey, but the extensive pipe network cannot be avoided and the pipe effects are evident in a large number of the resistivity images. As a result, this work has included extensive research to quantify the effect of a conducting pipe on apparent resistivity measurements and a program has been written to locate and remove the effect of the pipes from the apparent resistivity pseudosections.

6.2 Conducting Pipe Located in a Resistive Half-space

6.2.1 The Analytical Solution

When a current I is injected into a homogeneous halfspace of resistivity ρ, the primary potential Ω_p at a point P is given by

$$\Omega_p = \frac{I\rho}{2\pi(x^2 + y^2 + z^2)^{1/2}} \tag{6.1}$$

where x, y and z define the location of P relative to the current source (x and y locate P in the horizontal plane while z determines the depth of P relative to the ground surface.

For the same current source I, a buried, conducting pipe gives rise to a secondary potential Ω_s. Wait's solution (Wait, 1982), shows that for a pipe of diameter c, located at a depth h and a distance d in the y direction from the current source in a homogeneous halfspace, the secondary potential Ω_s is given by

$$\Omega_s = \int_0^\infty P(\lambda) \left\{ K_0 \left[\lambda \left[(z-h)^2 + (y-d)^2 \right]^{1/2} \right] + K_0 \left[\lambda \left[(z+h)^2 + (y-d)^2 \right]^{1/2} \right] \right\} \cos \lambda x \, d\lambda \tag{6.2}$$

where $K_0[r]$ is the modified Bessel function of the second kind for argument r and

$$P(\lambda) = -\frac{I\rho}{\pi^2} \frac{K_0[\lambda(h^2+d^2)^{1/2}]}{[K_0(\lambda c) + (K_0(2\lambda h)]} \tag{6.3}$$

These formula are taken from Wait (1982), equations 245 and 246 with a change of coordinates after making the correction $\cos \lambda z \, d\lambda$ for $\cos \lambda z \, dz\lambda$ in equation 245.

It is now possible to define the location of current sources, current sinks and potential electrodes, relative to a pipe, to set up electrode arrays, e.g. the traditional Wenner array, and then to apply conventional apparent resistivity methods. The electrode array can be at any angle relative to the pipe. The angle Ψ is the angle between the electrode array and the perpendicular to the pipe so that $y = a \cos \Psi$, $x = a \sin \Psi$ and, when P is at the ground surface, $z = 0$ (Figure 6.1).

6.2.2 The Calculation of Pipe Effects

Calculation of the secondary potential (Equation 6.2) requires the numerical integration of modified Bessel functions of the second kind, i.e. integrals of the form

$$\int_0^\infty P(\lambda) K_0(\lambda a) \cos \lambda x \, d\lambda \tag{6.4}$$

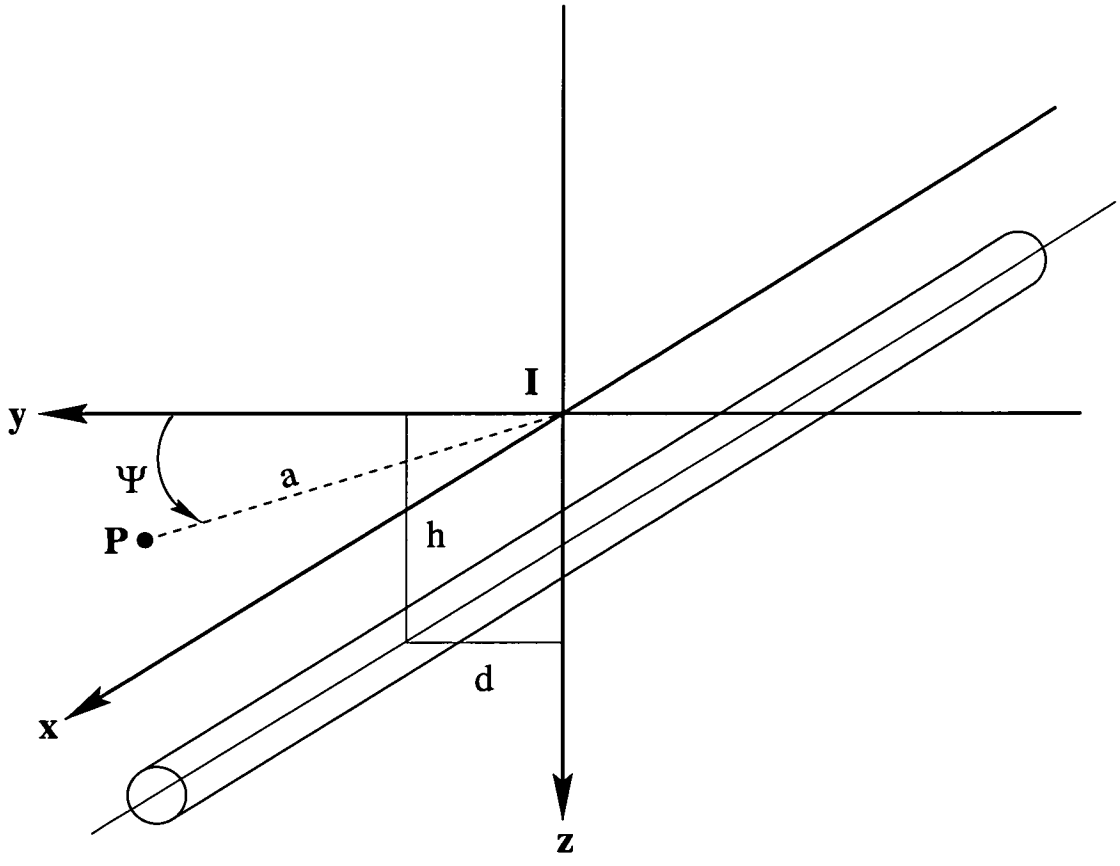

Figure 6.1: Infinitely long cylindrical conductor in a resistive half space.

where $a = \left[(z-h)^2 + (y-d)^2\right]^{1/2}$ or $a = \left[(z+h)^2 + (y-d)^2\right]^{1/2}$

Although $P(\lambda)$ and $\cos \lambda x$ are bounded in $[0, \infty]$, such integrals are improper because of the singularity

$$K_0(\lambda a) \rightarrow -\infty \; as \; \lambda \rightarrow 0 \tag{6.5}$$

at the lower limit of integration. Since this singularity is logarithmic, i.e.

$$K_0(\lambda a) \sim -\ln \lambda \; as \; \lambda \rightarrow 0 \tag{6.6}$$

(Abramowitz and Stegun, 1973), the improper integral may be converted to an ordinary integral using the change of variable

$$\lambda = t^2 \tag{6.7}$$

(Press *et al.*, 1986).

With this change of variable, Equation 6.4 becomes

$$\int_0^\infty P(\lambda)K_0(\lambda a)\cos\lambda x\, d\lambda = \int_0^\infty P(t^2)K_0(at^2)\cos(t^2x)\, 2tdt \tag{6.8}$$

The asymptotic behaviour of the kernel is as follows:

(i) as $t \to 0$

$$\begin{aligned} P(t^2)K_0(at^2)\cos(t^2x)\, 2t &\sim \frac{I\rho}{2\pi^2}\ln(at^2)\cos(t^2x)\, 2t \\ &= \frac{I\rho}{\pi^2}\cos(t^2x)(2t\ln t + t\ln a) \\ &\to 0 \end{aligned} \tag{6.9}$$

and

(ii) as $t \to \infty$ the asymptotic form of the Bessel function approximates to

$$K_0(t) \sim \sqrt{\frac{\pi}{2t}}\, e^{-t} \tag{6.10}$$

so

$$\begin{aligned} P(t^2)K_0(at^2)\cos(t^2x)\, 2t &\sim \frac{I\rho}{2\pi^2}\sqrt{\frac{\pi}{2at^2}}e^{-at^2}\cos(t^2x)\, 2t \\ &= I\rho\sqrt{\frac{1}{2a\pi^3}}e^{-at^2}\cos(t^2x) \\ &\to 0 \end{aligned} \tag{6.11}$$

Thus the transformed kernel is regular and the numerical evaluation of the ordinary integral becomes stable.

It is sufficient to evaluate the secondary potential integral (Equation 6.2) between 0 and some

finite upper limit. The effect of varying this limit of integration is shown in Figure 6.2, where an upper limit of 2 is seen to be sufficient for numerical calculation.

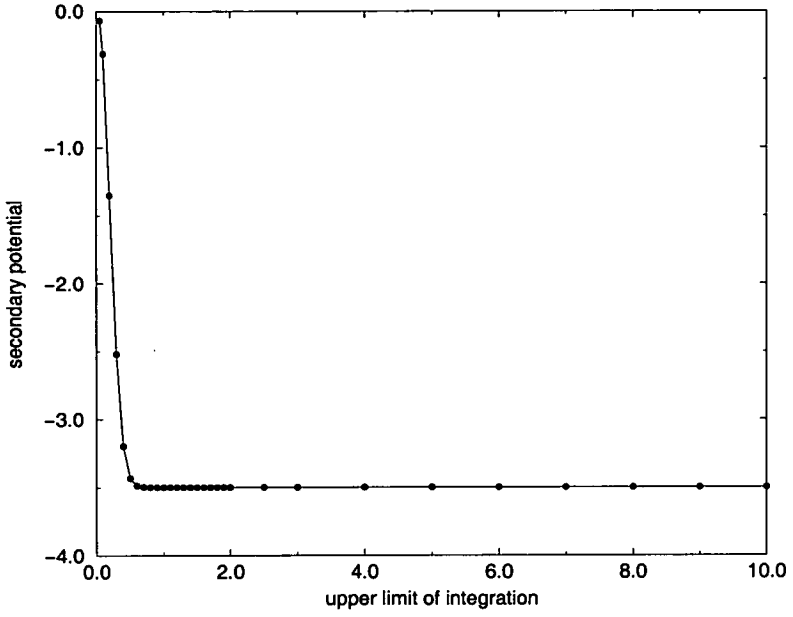

Figure 6.2: The effect of varying the upper limit of the integral in Equation 6.2. The value of the secondary potential with the centre of the electrode array 8m from a 0.15m diameter pipe, buried at a depth of 1m in a background resistivity of 100 Ωm (electrode spacing of 15m).

The method of integration is defined by the NAG FORTRAN library routine D01BDF which calculates the approximation to the integral of a function over a finite interval, input by the user. The user has no control over the integration method but it is possible to specify absolute or relative errors (relative errors used in this case) that the routine will attempt to satisfy. There is no guarantee that the errors will be achieved and so it is recommended that the interval is subdivided if increased accuracy is required. Consequently, the NAG FORTRAN library routine has been successfully tested, in two ways. 1) By checking the effect of varying the accuracy criterion. 2) By comparing the integral values obtained through subdividing the range. For example, $\int_0^2 f(x)\,dx = \int_0^1 f(x)\,dx + \int_1^2 f(x)\,dx$ for a chosen relative error of 0.1%.

The Effect of Parameter Variation on Apparent Resistivity Profiles

The user must input a number of variables; electrode spacing, starting point of profile with respect to the pipe, number of measurements, step distance between measurements, background resistivity, pipe depth, pipe diameter and orientation of electrode array with respect to the pipe. All these variables considerably alter the resulting apparent resistivity profile.

In a resistivity imaging survey, increased electrode spacings sample successively deeper into

the subsurface. As the electrode spacing increases, the pipe effect spreads. Figure 6.3 shows the characteristic double lobe signature of the pipe. A low resistivity lobe appears either side of the pipe location. In these lobes the measured apparent resistivity is reduced to a fixed percentage of the background resistivity, regardless of the background value. This was determined by calculating the apparent resistivity profile over a pipe buried within a halfspace which is assigned a different background resistivity value for each run. The background resistivities were varied over orders of magnitude.

Varying the pipe diameter, within reasonable constraints, does not alter the shape of the pipe anomaly but it does alter the amplitude of the anomaly. Reducing the pipe diameter reduces the pipe's effect on apparent resistivity measurements (Figure 6.4). Varying the depth of pipe alters both the shape and amplitude of the pipe anomaly. Deeper pipes produce a less detailed, lower amplitude anomaly (Figure 6.5).

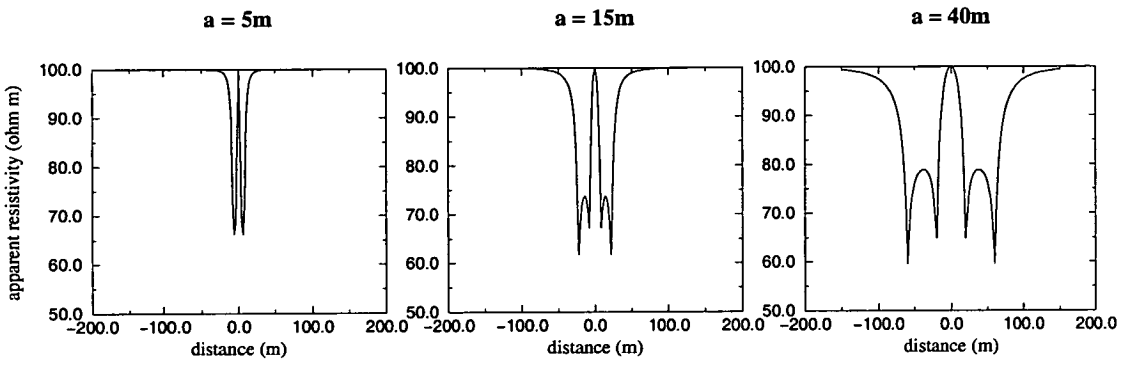

Figure 6.3: Apparent resistivity profiles to show the effect of varying electrode spacing a. Pipe diameter = 0.15m, depth = 1m. Background resistivity = 100Ωm. Electrode array is perpendicular to pipe.

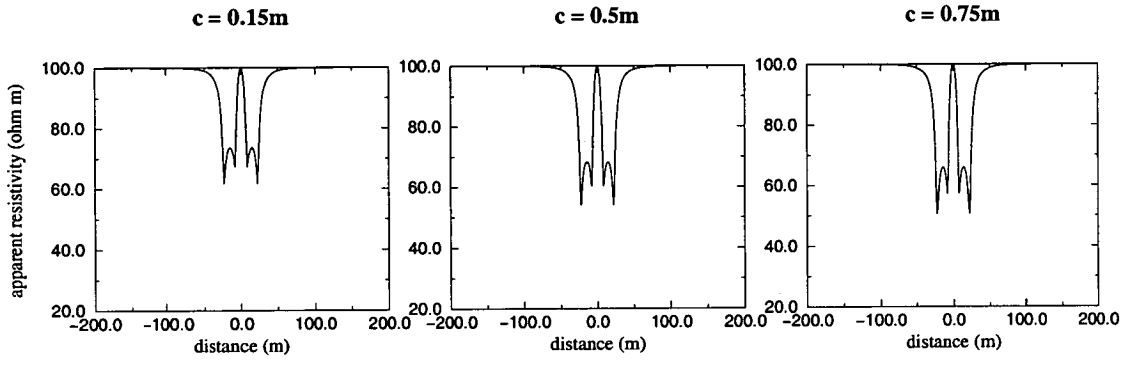

Figure 6.4: Apparent resistivity profiles to show the effect of varying pipe diameter c. Pipe depth = 1m. Background resistivity = 100Ωm. Electrode spacing = 15m. Electrode array is perpendicular to pipe.

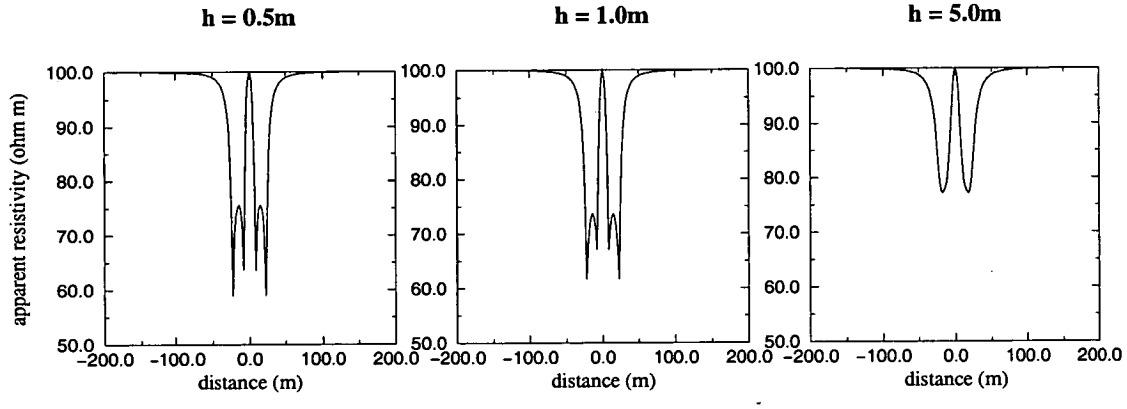

Figure 6.5: Apparent resistivity profiles to show the effect of varying pipe depth h. Pipe diameter = 0.15m. Background resistivity = 100 Ωm. Electrode spacing = 15m. Electrode array is perpendicular to pipe.

Varying the angle between the pipe and the electrode array again has a significant effect on both the amplitude and shape of the anomaly. When the pipe and electrode array are parallel, the resultant apparent resistivity measurements are a uniformly reduced value. Figure 6.6 shows a few of the intervening steps between the electrode array being perpendicular and parallel to the pipe.

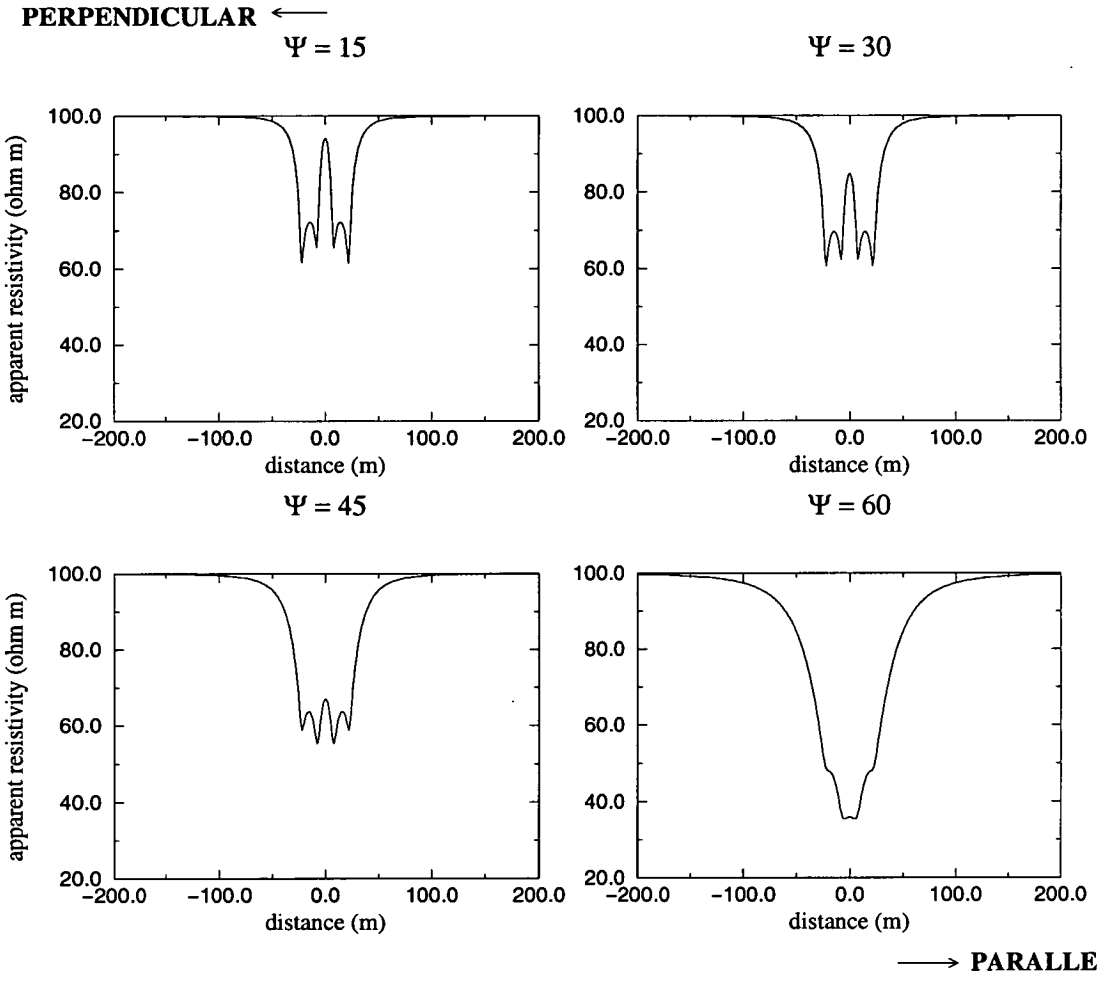

Figure 6.6: Apparent resistivity profiles to show the effect of varying angle Ψ between electrode array and the perpendicular to the pipe.
Pipe diameter = 0.15m, depth = 1m. Background resistivity = 100Ωm. Electrode spacing = 15m.

6.3 Recognising the Pipe Effect within Real Data by Cross Correlation

Figure 6.7 shows an apparent resistivity pseudosection obtained from across the Texaco site (R53 on Figure 5.5). The effect of a single pipe can clearly be seen due to the relatively uncomplicated background geology. The characteristic 'double lobe' signature spreads outwards, either side of the pipe location, with increasing depth. This example is clear but this is rarely the case particularly where the background geology is more complicated or where more than one pipe have interacting effects. Consequently, research has been conducted to automatically recognise the pipe signature within apparent resistivity data.

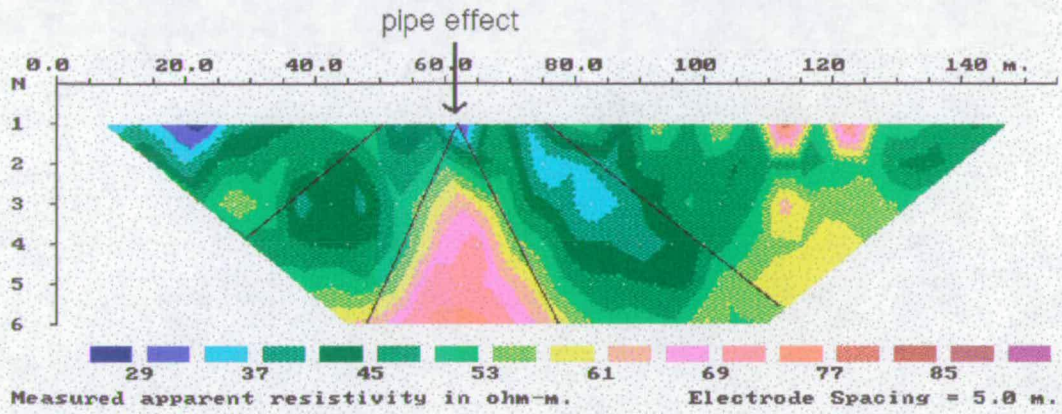

Figure 6.7: Apparent resistivity pseudosection of profile R53 showing the effect of a buried, conducting pipe.

The program developed utilises unbiased cross correlation techniques. The correlation r at lag k between the field apparent resistivity profile data x_i at one electrode spacing and the analytical apparent resistivity profile calculated in the presence of a pipe y_i at the same spacing, is given by

$$r_k = \frac{(\frac{1}{M}) \sum_1^M \tilde{x}_i \, \tilde{y}_{i+k}}{(\sum_1^N \tilde{x}_i{}^2 \sum_1^N \tilde{y}_i{}^2)^{1/2}} \tag{6.12}$$

where $\tilde{x}_i$ is the detrended value of x_i and $\tilde{y}_i$ is the value of y_i with the DC offset (background resistivity value) removed. Removing the DC and detrending the data ensures that the cross correlation of two background resistivity values is minimal.

The maximum r_k occurs at the pipe location along the profile for each electrode spacing. The locations given for a single profile may vary slightly for each electrode spacing depending on the complexity of the data. To establish an overall location, r_k values from all electrode

spacings are summed for each lag, to reveal the maximum correlation for the entire profile.

6.3.1 The Program Outline

The program searches primarily for the position of a pipe along a particular apparent resistivity traverse. The many variables which determine the shape of a pipe anomaly require a new pipe anomaly to be calculated for cross correlation with each apparent resistivity traverse collected in the field. From invasive trial surveys, the pipes have a known diameter of 0.15m. The angle of the electrode array with respect to the pipe can be extracted by combining information from the map of the pipe network (obtained with the EM31 survey (Chapter 4) and the resistivity profile locations (Figure 5.5). The final variable is the depth of the pipe. The approximate depths of the pipes under the Granton site are known from the invasive surveys. The effect of the pipe depth on the pipe anomaly is very small when only considering realistic pipe depths. Figure 6.8 shows the effect of varying the pipe depth on a calculated pipe profile. The graph plots only the profile minimum, i.e. the value of the low resistivity lobe, for each pipe depth. The variation, within the realistic pipe depth range, is too small to be recognisable within the background noise likely to be present within the field data, so a depth search is not performed.

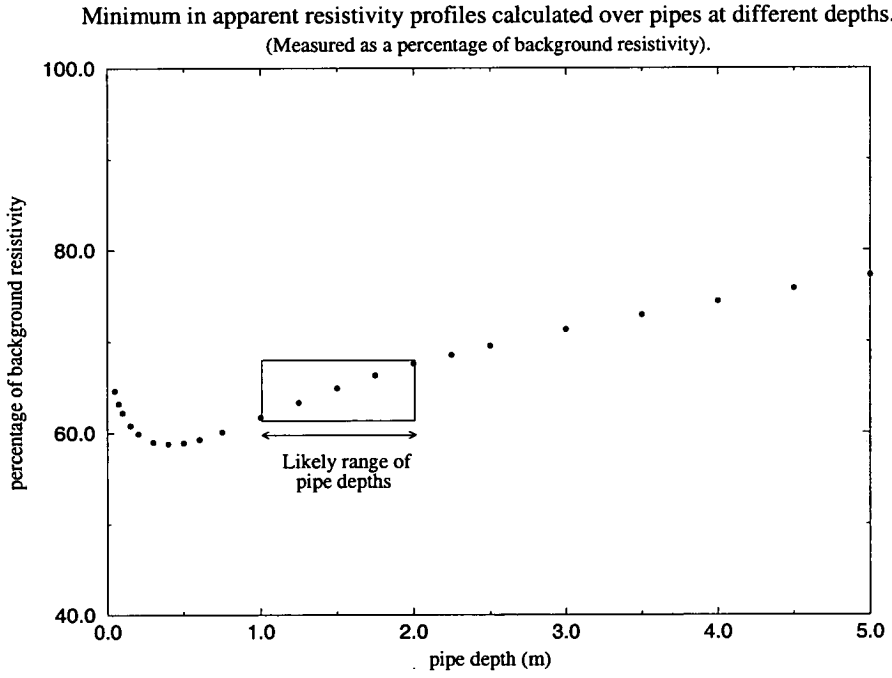

Figure 6.8: The effect of varying the depth of the pipe on the calculated apparent resistivity minimum (the low resistivity lobe) taken over the pipe. The minimum value of an apparent resistivity profile (taken with an electrode spacing of 15m, over a 0.15m diameter pipe) varies by only 5% between depths of 1m and 2m.

Two programs have been written as part of this research. PIPELOC searches the whole apparent resistivity pseudosection for the location of pipe effects. REMPIPE has a fixed search around estimated pipe location(s) to pinpoint their position(s) and remove the effects of the pipe(s). Outlines of these programs are detailed below:

PIPELOC

```
Read in GEOPULSE File.
.
Print out number of data points in each level (n=1-8).
Choose number of levels with a sufficient number of data points
for cross correlation.
.
Enter pipe diameter, depth and orientation,
.
For each level
      calculate the pipe anomaly,
      remove DC  offset (background apparent resistivity value)
      from pipe anomaly,
      detrend apparent resistivity profiles,
done.
.
For each level
      perform discrete cross-correlation of pipe anomaly
      with apparent resistivity profile,
done.
.
Sum cross correlation values for each position on all levels.
Locate maximum cross correlation value.
.
Print out the pipe location (position of maximum cross correlation).
...
```

REMPIPE

```
Read in GEOPULSE File.
.
Print out number of data points in each level (n=1-8).
Choose number of levels with a sufficient number of data points
for cross correlation.
```

```
Enter number of pipes affecting the profile data.
.
For each pipe
      enter pipe diameter, depth and orientation,
      enter estimated pipe location,
done.
.
For each pipe
      For each level
            calculate the pipe anomaly,
            remove DC offset (background apparent resistivity
            value) from pipe anomaly,
            detrend apparent resistivity profiles,
      done.
done.
.
For each pipe
      For each level
            For a fixed distance around estimated pipe location
                  discrete cross-correlation of pipe anomaly
                  with apparent resistivity profile,
            done.
      done.
done.
.
For each pipe
      sum cross correlation values for each position on all
      levels,
      locate maximum cross correlation value,
done.
.
For each pipe
      For each level
            construct a matrix to multiply out the effect of the
            pipe,
            multiply out the pipe effect,
      done.
done.
.
```

```
Write out the 'pipe-free' apparent resistivity data in GEOPULSE
format.
...
```

6.3.2 Limitations of the Pipe Removal Program

Present data analysis and inversion techniques do not perform well in regions of rapid lateral changes or sharp boundaries between extreme resistivity contrasts. These complexities are obviously apparent in the case of buried pipes. In an attempt to overcome these limitations of interpretation, apparent resistivity pseudosections have been decomposed, as described above, to approximately remove the effect of the pipes. The inverse of this method (model composition) has been investigated by Habberjam and Watkins (1974), highlighting the fact that the total electrical response to a number of sources is not a simple combination of individual responses. Habberjam and Watkins (1974) calculate the product of normalised models to estimate their combined apparent resistivity. The analysis recognises the increase in errors where high resistivity contrasts are encountered but limitations in the research are also evident due to the available models which only relate to simple features. The model used here for the removal of pipe effects is well defined and allows approximate decomposition to compensate for the percentage reduction of the background resistivity due to the pipe. The effects of pipes on resistivity pseudosections are so extreme that it is imperative that their removal is implemented, no matter how approximate, in order to interpret the background geology. Tests presented below (Section 6.3.3) show that, in practice, the chosen method of removing pipe effects is very successful. However, where the model is poor, decomposition will not be possible. For example solutions have not been calculated for situations where a pipe path is in close proximity to a profile without actually crossing it or where a profile is near to a bend in a pipe. In consideration of the problems involved in source combination, there may also be circumstances where multiple pipe and geological effects produce a pseudosection that is too complicated to decompose.

6.3.3 Testing the Program

RES2D is a 2-D resistivity forward modelling program written by Loke (1994). This package has been used to simulate a number of pipe affected field data. The possible model and survey designs are controlled by a number of restrictions imposed by the program. The user can choose either 2 or 4 nodes per unit electrode spacing which defines a maximum possible number of electrodes as 101 and 51 respectively. This limits the depth of penetration of the survey as well as restricting the size and shape of models. Consequently all models are made up of rectangles with a minimum horizontal width equal to one quarter of the electrode

spacing (or half the electrode spacing if the body is to be centred between electrodes). The rows are limited in number to 29 but are less restricted in the value of their thicknesses.

A 1.25m by 0.15m, 0.0001 Ωm conducting block represents a 0.69m diameter pipe in the testing models. The pipe radius is calculated to make the cross sectional area of the pipe directly comparable to the cross sectional area of the block. Figure 6.9 shows how the anomalies vary for profiles taken at 4 different electrode spacings over a pipe (in red) and over a block (in blue) with identical cross sectional areas.

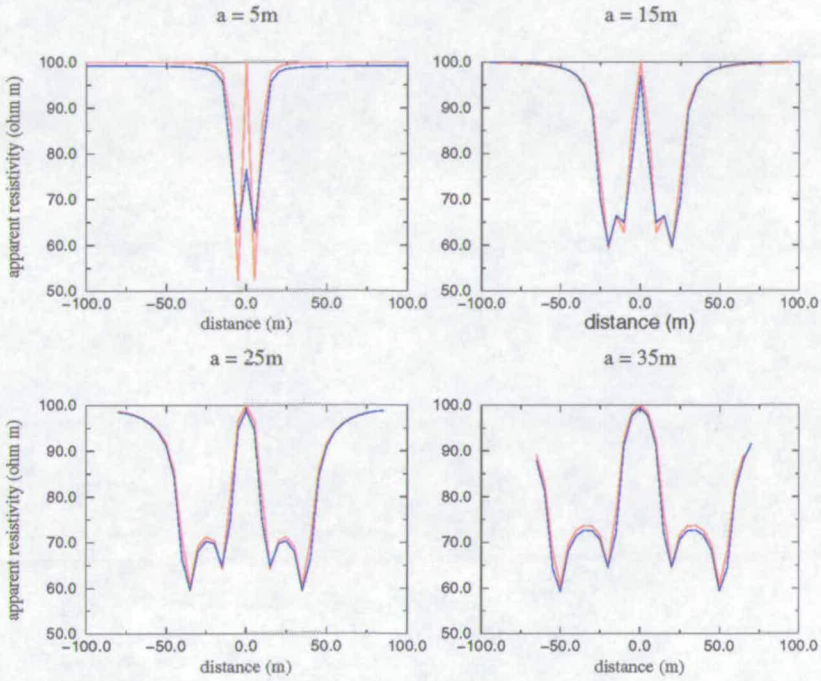

Figure 6.9: Comparison of apparent resistivity over a pipe (in red) with apparent resistivity over a block (in blue), at electrode spacings a of 5, 15, 25 and 35m.

The anomalies over a conducting pipe and a conducting block are extremely similar but not identical. The similarity is adequate for testing the pipe location program but inherently introduces errors when attempting to remove the effect of a pipe from an apparent resistivity profile affected by a conducting block. Figure 6.10 shows the apparent resistivity profiles over a buried conducting block in a resistive halfspace, before (solid line) and after (dashed line) the removal of a pipe effect. Removing the effect of a pipe is more successful at greater electrode spacings where the pipe and block anomalies become increasingly similar.

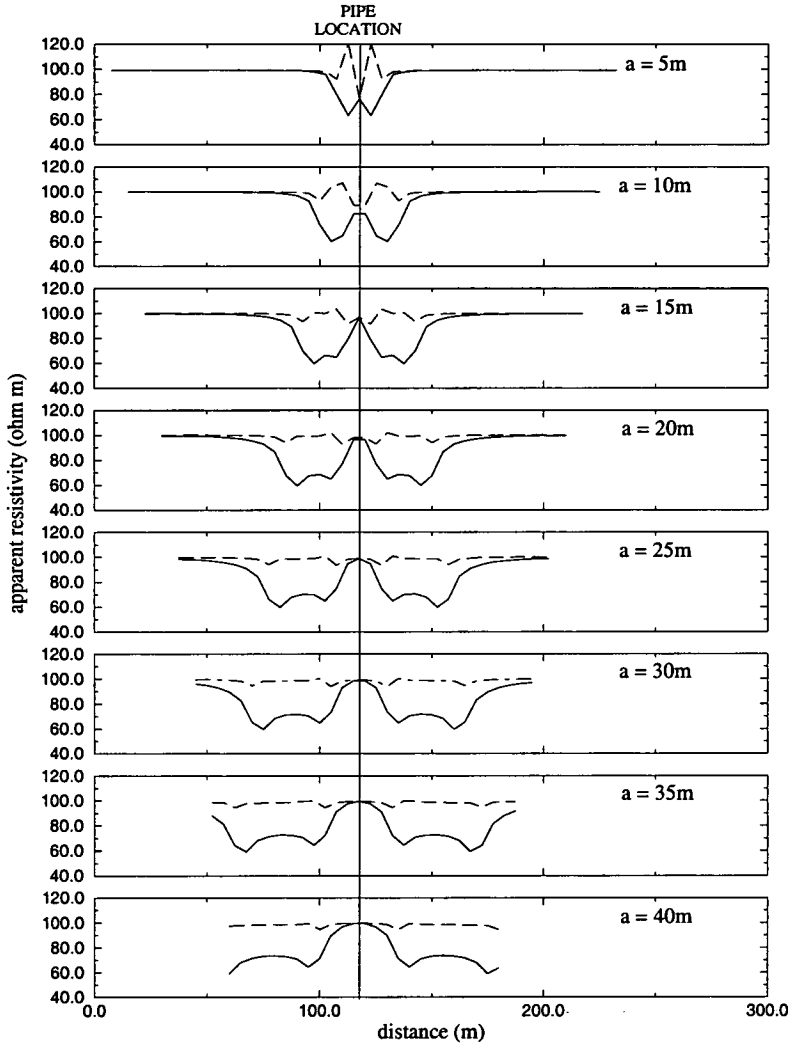

Figure 6.10: Apparent resistivity profiles, at increasing electrode spacings a, over a conducting block in a resistive halfspace, before (solid line) and after (dashed line) the removal of a pipe effect.

Figure 6.11 shows a 1.25m by 0.15m, 0.0001 Ωm conducting block (closest approximation to a conducting cylinder with a diameter of 0.69m) in a resistive quarter space. Figure 6.12 shows the resulting forward modelled, apparent resistivity profiles at increasing electrode spacings a. The pipe location program easily recognises and removes the anomaly due to the conducting block that can be seen within this data set.

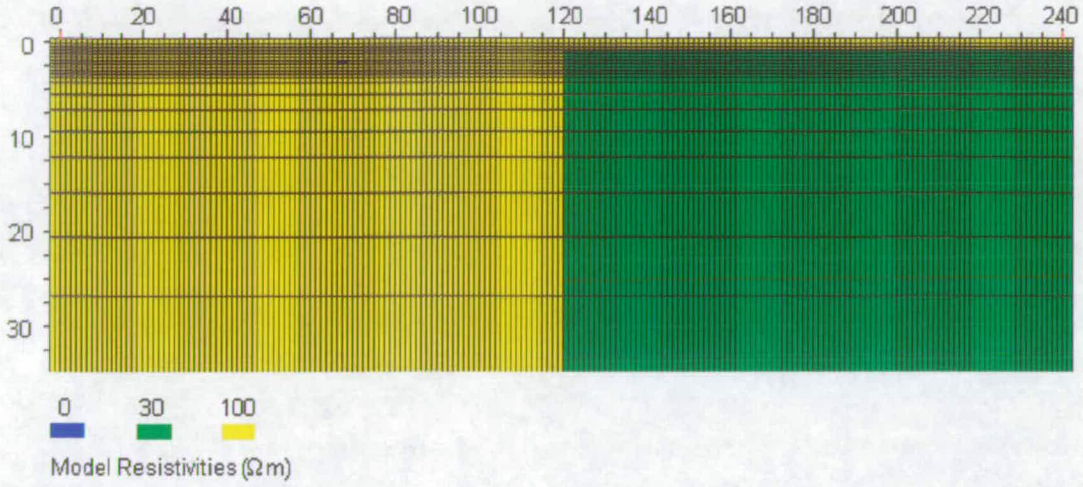

Figure 6.11: Model of the closest approximation to a conducting pipe in a resistive quarter space, constructed within the RES2D forward modelling package

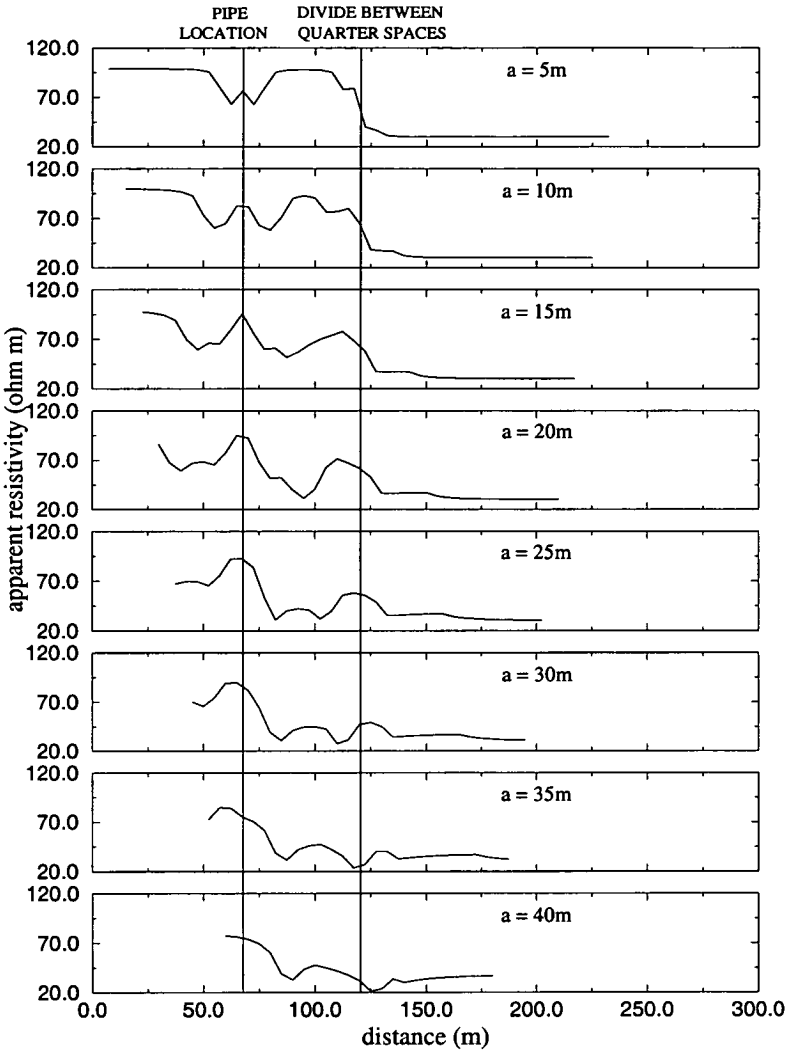

Figure 6.12: Forward modelled apparent resistivity profiles over a conducting block in a resistive quarter space. Measurements taken from increasing depths corresponding to the electrode spacing a.

In order to test the program with a more realistic problem, a quarter space model is used with 5% noise added. (The type of noise, which is added within the RES2D program, is undefined beyond choosing the percentage of noise required). Figure 6.13 shows (a) the apparent resistivity pseudosection of the noisy data and (b) a modelled resistivity section calculated by the RES2DECO inversion program. Inverse modelling is only partly successful at recognising the source of the anomaly. The effect of the conducting block prevents the inversion algorithm from accurately locating the division between the $100\Omega m$ and 30 Ωm quarter spaces.

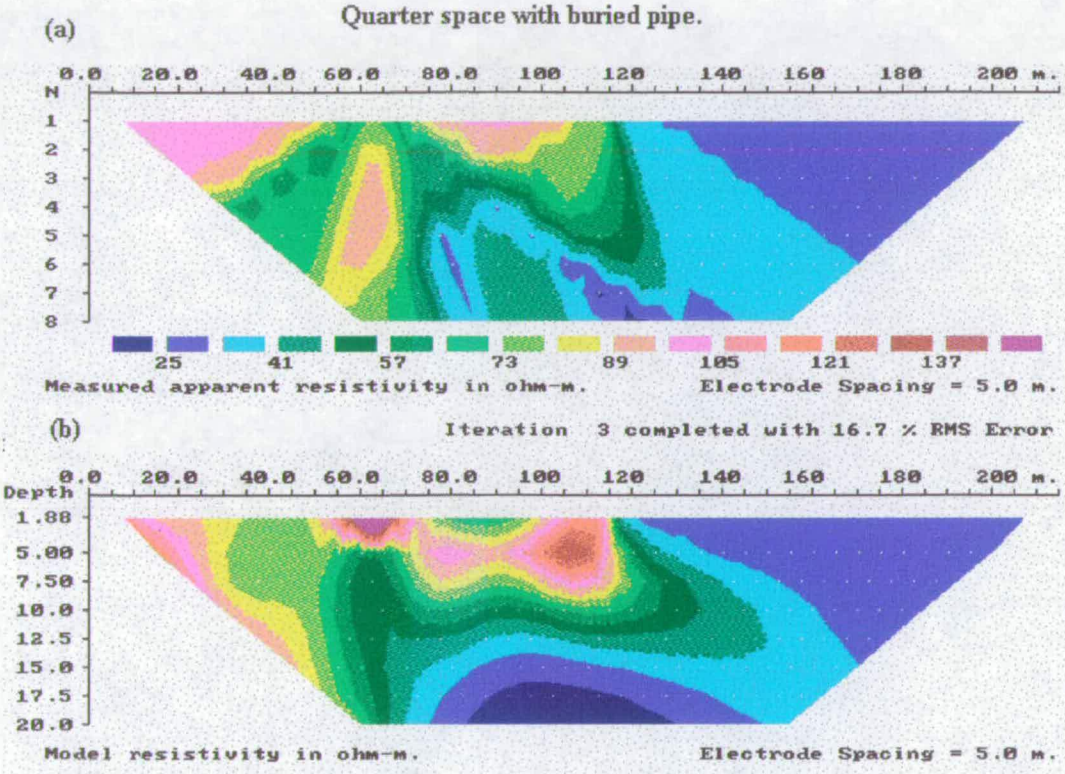

Figure 6.13: (a) Apparent resistivity pseudosection of a conducting block in a resistive quarter space and (b) the resulting true resistivity section modelled by the RES2DECO inversion program.

In an attempt to remove the effect of the conducting block from the pseudosection, the data are passed through PIPELOC , the pipe location program. The correct position of the conducting block is found (67.5m) and the effect of a pipe with comparable cross sectional area is removed. The original (solid line) and resultant 'pipe free' (dashed line) apparent resistivity profiles are shown in Figure 6.14.

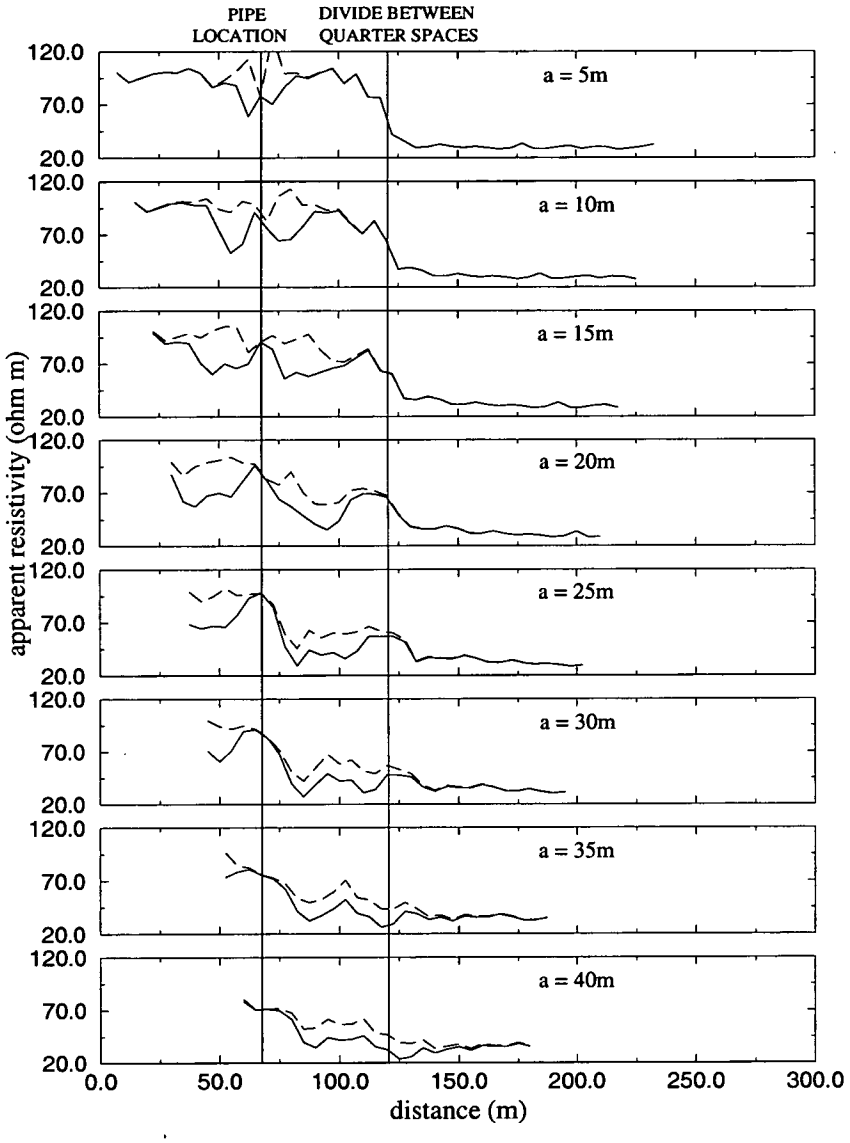

Figure 6.14: Forward modelled apparent resistivity profiles over a conducting block in a resistive quarter space before (solid line) and after (dashed line) the effect of a pipe is removed. 5% random noise added. Measurements taken from increasing depths corresponding to the electrode spacing a.

Some errors are evident beyond the 5% noise deliberately added, due to approximating the block to a pipe. However, despite these differences, the inverse model of this 'pipe free' data set (using RES2DECO) is more easily interpreted as 2 quarter spaces (Figure 6.15).

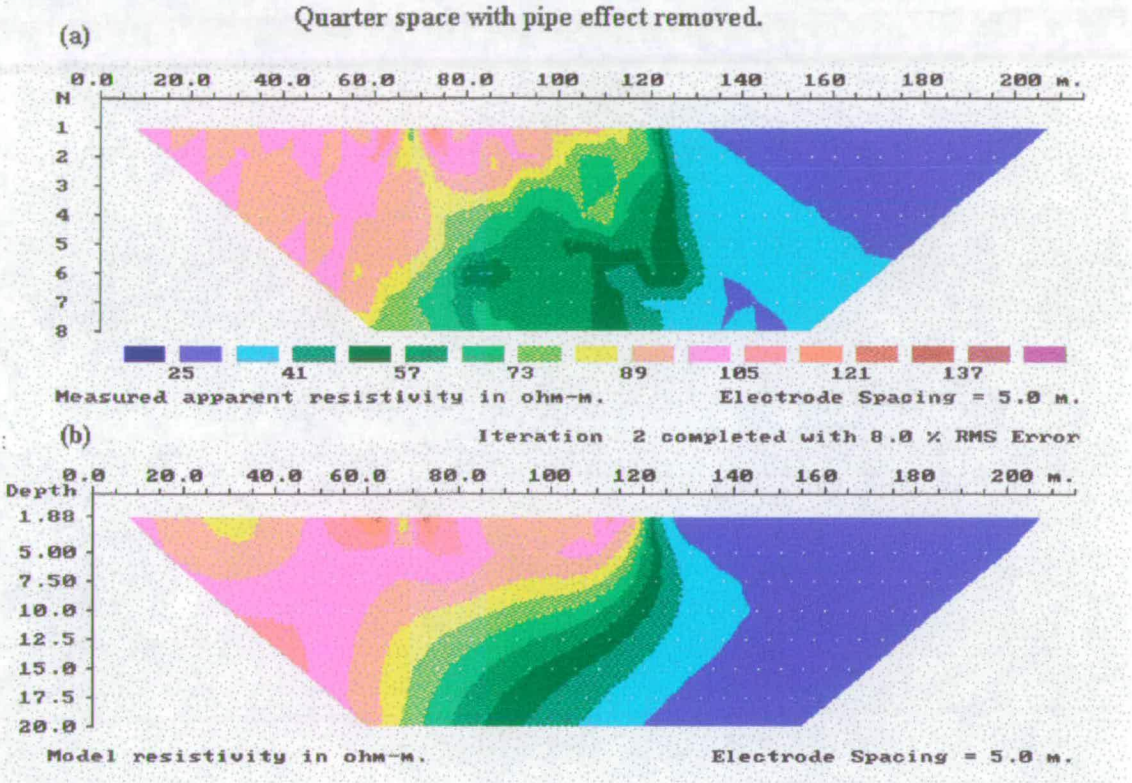

Figure 6.15: (a) Apparent resistivity pseudosection of a conducting block in a resistive quarter space with a pipe effect removed and (b) the resulting true resistivity pseudosection modelled by the RES2DECO inversion program.

The program has also been tested on a model of 2 pipes in a 100Ωm resistive half space. The interacting pipe effects completely disguise the background resistivity value (Figure 6.16).

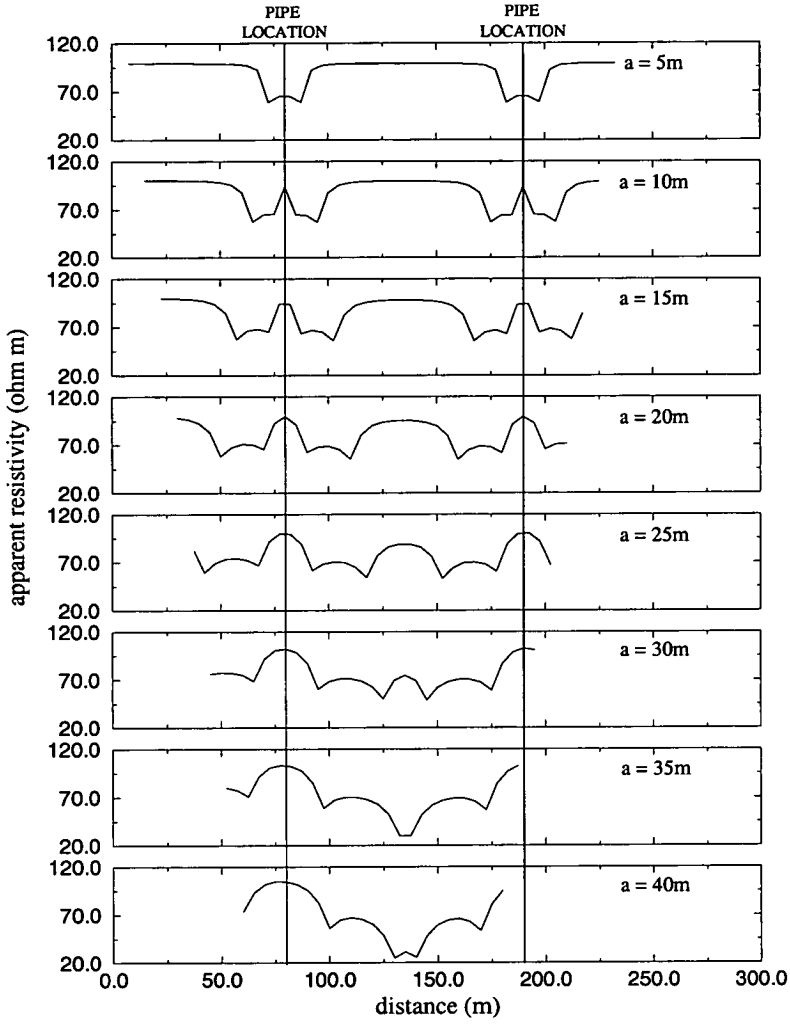

Figure 6.16: Apparent resistivity profiles, taken with increasing electrode spacings a, over two conducting blocks in a resistive half space.

After the addition of 5% random noise, even with this more complicated pipe anomaly, the pipes are accurately located and removed. The original (solid line) and resultant 'pipe free' (dashed line) apparent resistivity profiles are shown in Figure 6.17.

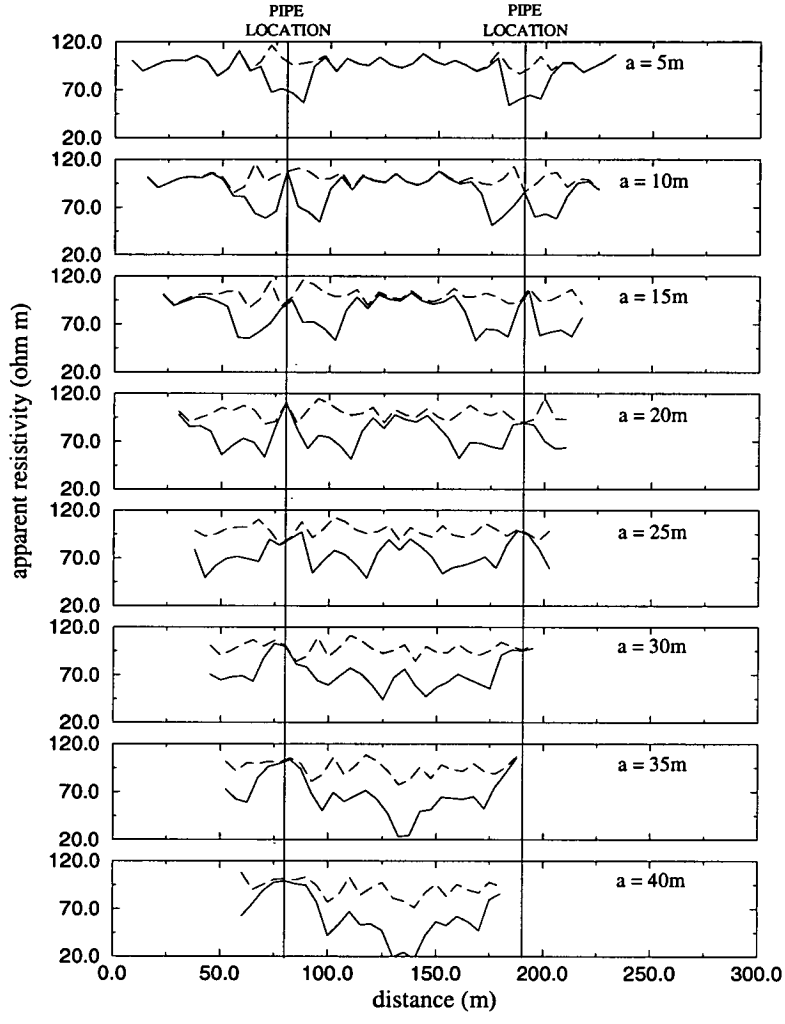

Figure 6.17: Apparent resistivity profiles, taken with increasing electrode spacings a, over two conducting blocks in a resistive half space with the effect of two pipes removed.

As a final test, the pipes are removed from profile R53 (Figure 6.7) where a single pipe anomaly is clearly evident and can be picked out by eye within the natural response of the background geology. By removing the effect of the pipe with the REMPIPE program, the apparent resistivity of the background geology alone is more clearly seen. The inverse model of the 'pipe free' data reveals a simple layered structure which is interpreted as ~8m of clay above rockhead (Figure 6.18).

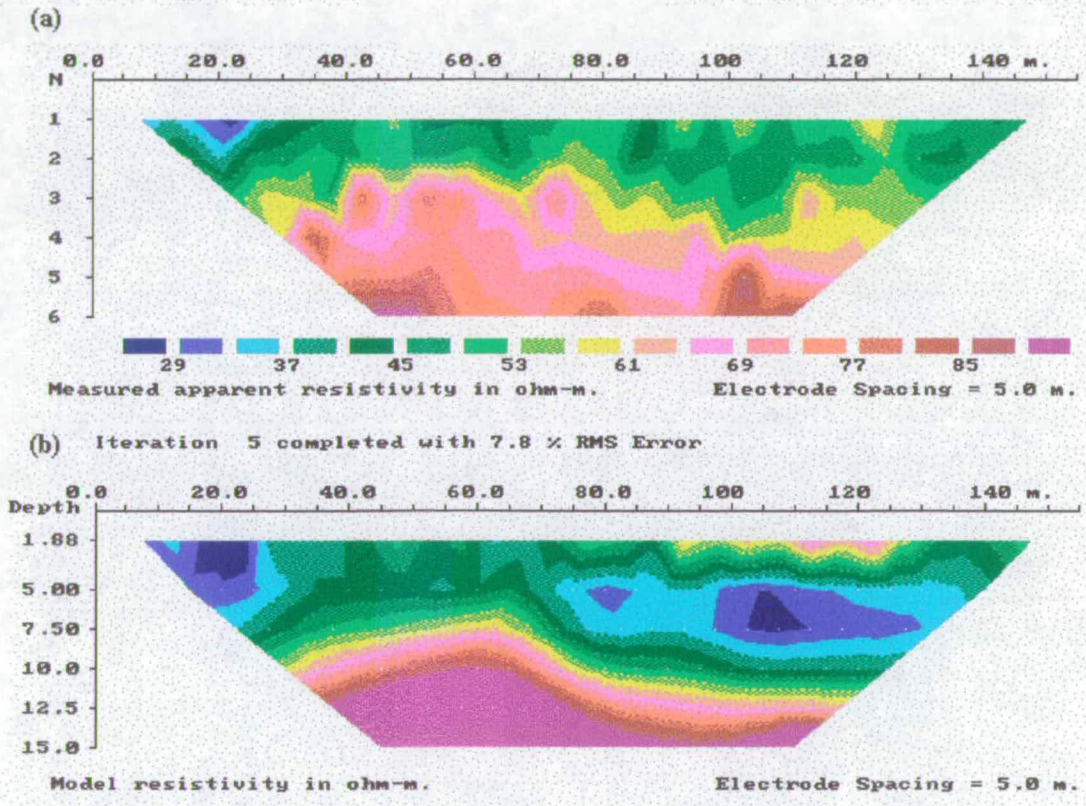

Figure 6.18: (a) Apparent resistivity pseudosection and (b) modelled resistivity pseudosection of profile R53 with pipe effect removed.

All 3 tests suggest that REMPIPE is successful at removing the effect of subsurface pipes from apparent resistivity data. Wherever possible, the pipe effects were removed from all apparent resistivity pseudosections from across the Granton site.

6.4 Conclusions

A program has been written to calculate the effect of an infinitely long conducting cylinder of variable diameter, depth and orientation with respect to the electrode array. This allows the user to calculate the effect of any pipe which may be corrupting resistivity measurements. A number of simple tests show that the second program to be written successfully locates and removes the effect of the calculated pipe from apparent resistivity pseudosections leaving a clearer image of the background resistivity variations.

7 INTERPRETATION OF RESISTIVITY SURVEY

7.1 Introduction

Once all the pipe effects have been removed from the pseudosections it is possible to continue with data interpretation. The 'pipe free' data are inverted using RES2DECO (Section 5.2.1) to obtain estimates of resistivity for each survey line. (Profile locations are shown on Figure 5.5). These models stand alone to provide valuable information while resistivity contour maps allow data from all modelled profiles to be viewed together. Although the models calculated from 2-D inversion assume that the model blocks are infinite in the y- direction, in reality the area of ground that contributes to an apparent resistivity measurement is very small. The current density decreases with distance from the source r as $\frac{1}{r^2}$ and, in the case of the Wenner array, the main signal contribution comes from the ground within half the electrode spacing of the array (Barker, 1979). Therefore, for the purpose of combining the model resistivity information from all profiles it is possible to assign each model resistivity data point to a finite rather than infinite block around that point. Consequently, it is possible to produce an overall contour plot of the resistivity distributions across the complete site by extracting data points at equivalent depths from each profile and assigning the correct x and y coordinates to construct a map (Vickery and Hobbs, 1998b). The resistivity distribution across the site is contoured using the default interpolation method (bilinear) in the UNIMAP visualisation package.

The combination of data presentation methods yields maximum information and successfully achieves the main aims of the survey introduced in Chapter 5:

- To evaluate the integrity of the the superficial clay deposit.
- To locate any potential rapid contaminant pathways.
- To delineate the saline/fresh water interface.

7.2 Clay Coverage

To examine the clay coverage, model data were extracted from a depth of 5m (which lies below the made ground surface and above rock head) (Figure 7.1). Clay is one of the most

electrically conductive geological units due to its cation exchange capacity. It is recorded as having resistivities within the range 10 to 100 Ωm but typically has a resistivity ranging between 35 and 60 Ωm in this case. Consequently, on the contour map, low resistivity signifies good clay coverage ranging through to the higher resistivity values (around 100 Ωm and above). For a more detailed interpretation four areas (marked **a**,**b**,**c** and **d** on Figure 7.1) are examined more closely with one dimensional (1-D) soundings.

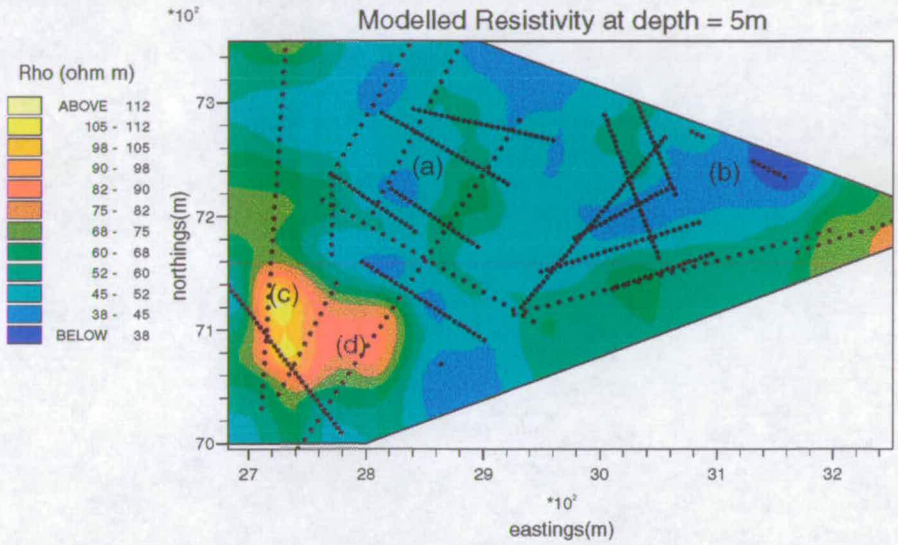

Figure 7.1: Contour plot of modelled resistivity at a depth of 5m. (Dots represent measurement points.)

By extracting single data points at the same position on each level from the complete pseudosection recorded by GEOPULSE it is possible to simulate the simpler VES survey. The extracted data define a sounding curve which is then inverted using an automatic interpretation method written by Zhody (1989). The number of layers in the resulting model equals the number of digitised points on the sounding curve. After a number of iterations the final layered models have been broadly packaged into units of similar resistivities giving estimations of depths to boundaries and thicknesses of units (Figure 7.2). However, care must be taken with these interpretations as a 3-D problem is being represented by a 1-D solution.

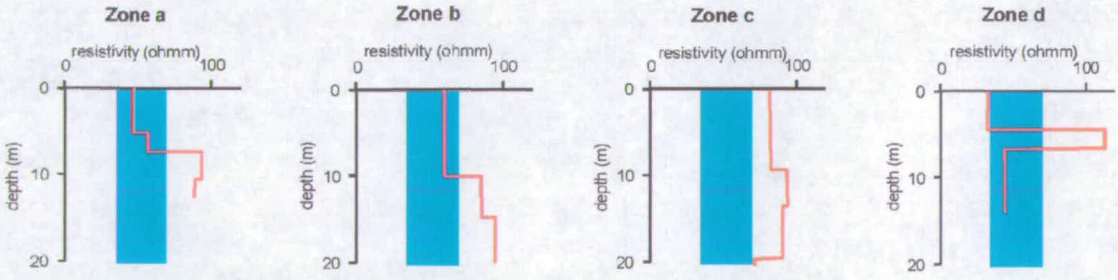

Figure 7.2: 1-D resistivity depth soundings over 4 zones with varying clay coverage. The blue strips mark the boundaries of the typical range of resistivities for clay.

Depth sounding **a** represents the clay coverage seen over the majority of the site. It has a resistivity typical of clay for approximately 7m lying above a higher resistivity unit. The low resistivity unit in sounding **b** extends to a greater depth of approximately 10m signifying good clay coverage.

The depth soundings from the zones with higher resistivities on the contour plot, show different characteristics. The sounding from zone **c** does not contain any units with resistivities that have been previously associated with clay whereas zone **d** does seem to contain clay but within which there is a higher resistivity unit. Trial pit and borehole information (Appendix C) have shown this unit to be a layer of fine sand and gravel with thin layers of clay either side.

For comparison, clay thicknesses were extracted from all the available borehole information (taking made ground and sand layers into account) and presented as an overlay to the resistivity map in Figure 7.3. The borehole data strongly agree with all the resistivity inversions. This combination of information allows a more quantitative interpretation of the resistivity contour plot presented in Figure 7.4. Attempts were made to compare the resistivity at an apparent depth of 5m with the EM31 ground conductivity data. The comparison was hindered by the masking effect of the pipes in the electromagnetic data but the pipe free area in the south of the site has a similar pattern and magnitude of ground conductivity to that measured in the resistivity survey.

In the main, the site is covered by over 4m of clay but a large window in the clay coverage is located in the southwest corner. This window is a likely area for the downward migration of surface contaminants.

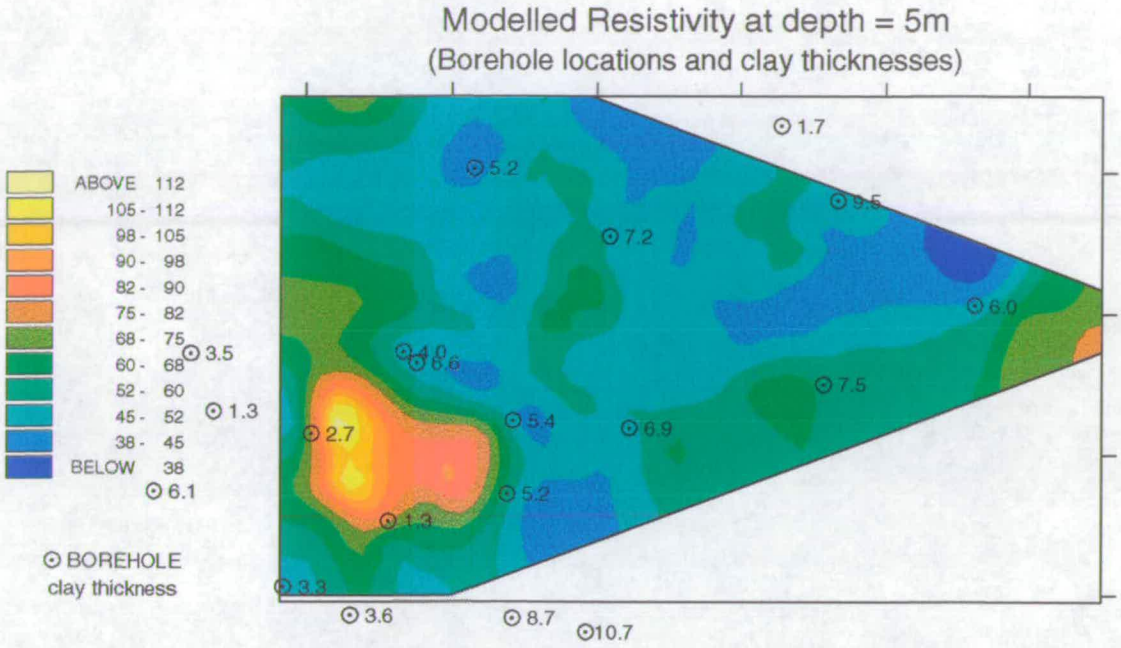

Figure 7.3: Comparison of clay thicknesses measured in boreholes and with resistivity.

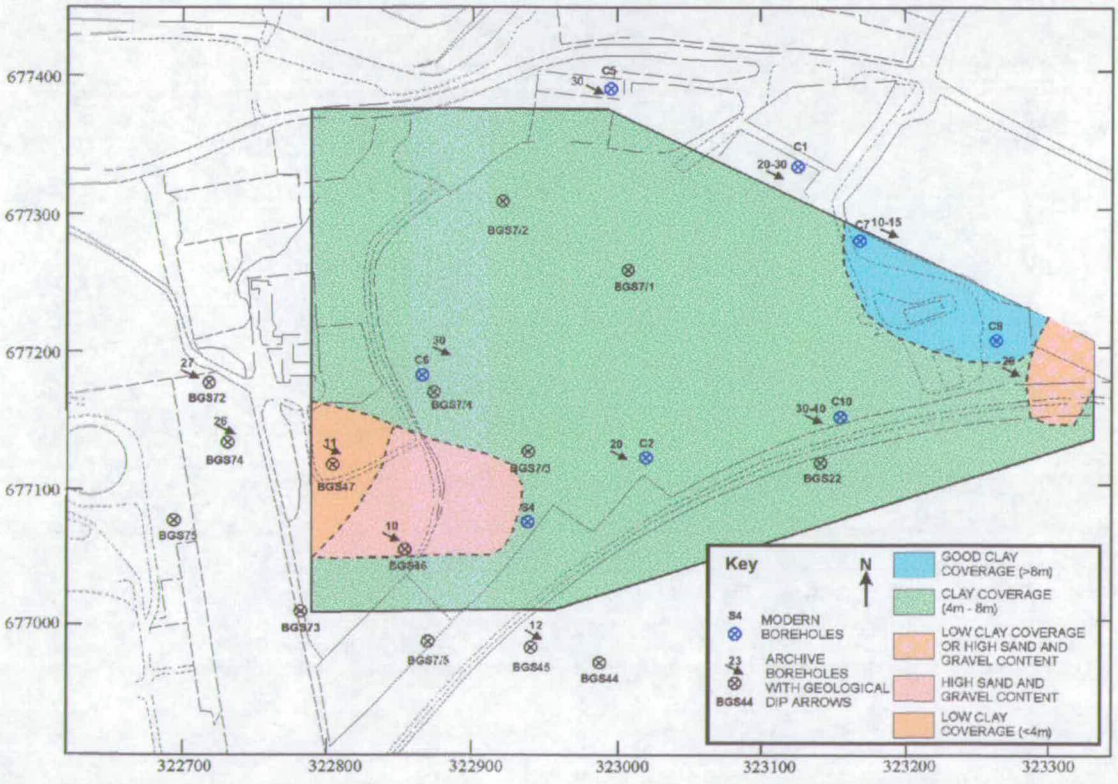

Figure 7.4: Representation of clay coverage from interpretation of resistivity and borehole data

7.3 Rapid Contaminant Pathways

Potential contaminant pathways include faults and connected high permeability units (Section 2.2.1). Below the former Shell and Texaco sites the sandstones are the only units with significant permeability (Section 3.3). Consequently, the aim of the deeper geophysical survey was to locate significant sandstone units and faults. The interpretation of the geophysics is aided by the use of borehole data from on and near the site. Appendix C contains the borehole logs grouped together to present cross sections running from west to east.

By comparison of 1-D soundings with borehole data it is clear that sandstone is the most electrically resistive unit in the sequence encountered at Granton.

Figure 7.5, 7.9 and 7.10 show contour plots of modelled resistivity at apparent depths of **(a)** 10, **(b)** 15 and **(c)** 20m. In these plots the reds, oranges and yellows pick out higher resistivities which are associated with sandstones.

7.3.1 Location of Faults

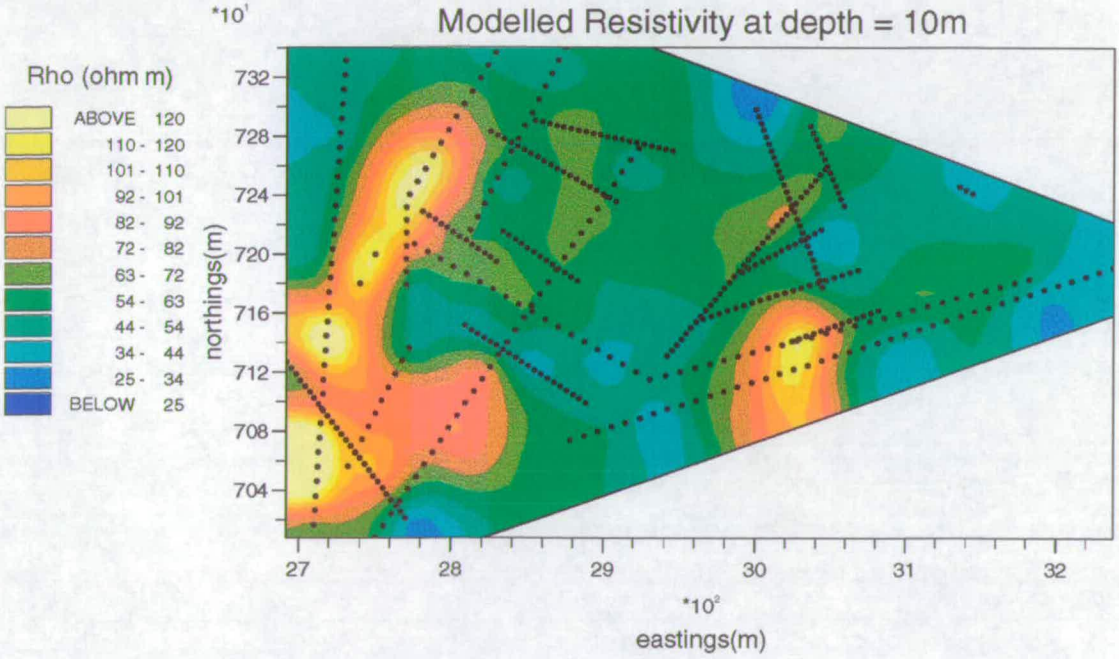

Figure 7.5: Contour plot of modelled resistivity at a depth of 10m

Figure 7.5 shows narrow high resistivity bands which terminate abruptly to the north. The termination point of the western band is located at the old sandstone quarry where a fault in the Ravelston sandstone was recorded (Section 3.3). Figure 7.6 shows a more detailed picture of the resistivities over the eastern band of sandstone which appears to subcrop across the Shell site. The change in scale of the resistivity contours on Figure 7.6 highlights the

northern band of the higher resistivity unit which is only sampled by a few data points and therefore does not produce a strong anomaly on the larger scale contour maps. The map indicates the presence of another fault and offset sandstone units. Profile **C10** shows the text book expression of the fault (Figure 7.7) and profile **R51** (Figure 7.8) clearly picks out the dipping sandstone to the north of the fault. For both the major sandstone units, the faults at their northern termination points have identical orientations thus suggesting the existence of one large fault running northwest-southeast across the two sites.

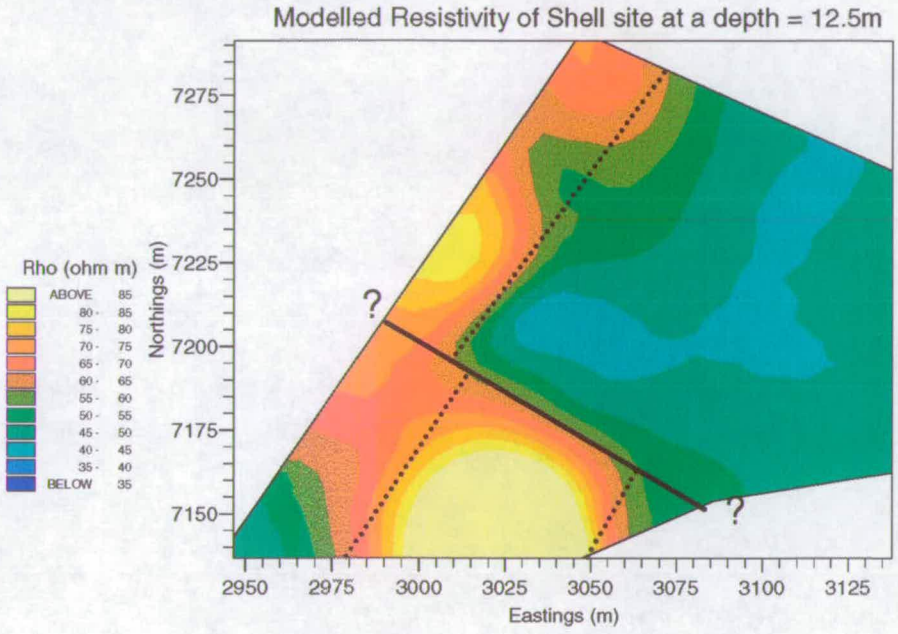

Figure 7.6: Contour plot of modelled resistivity at a depth of 12.5m below the Shell site.

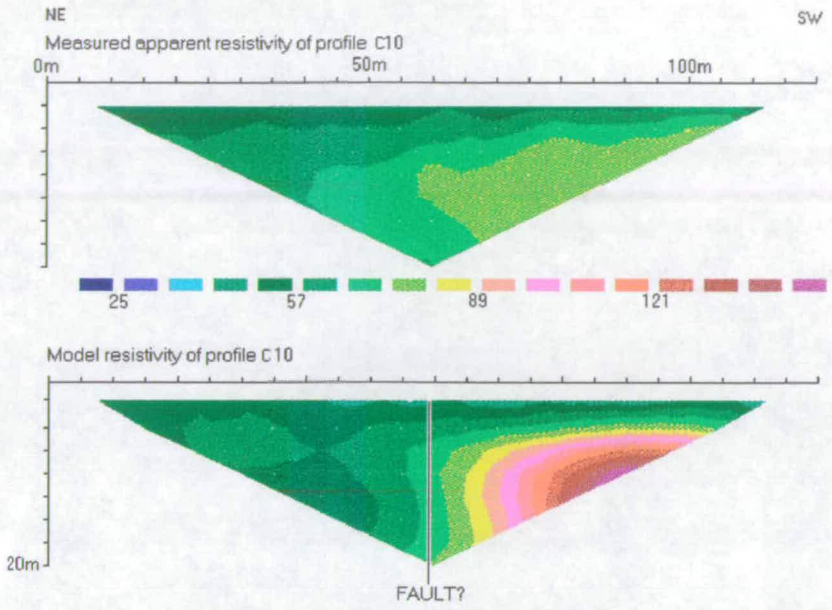

Figure 7.7: Apparent resistivity pseudosection and modelled resistivity section of profile C10 with interpretation.

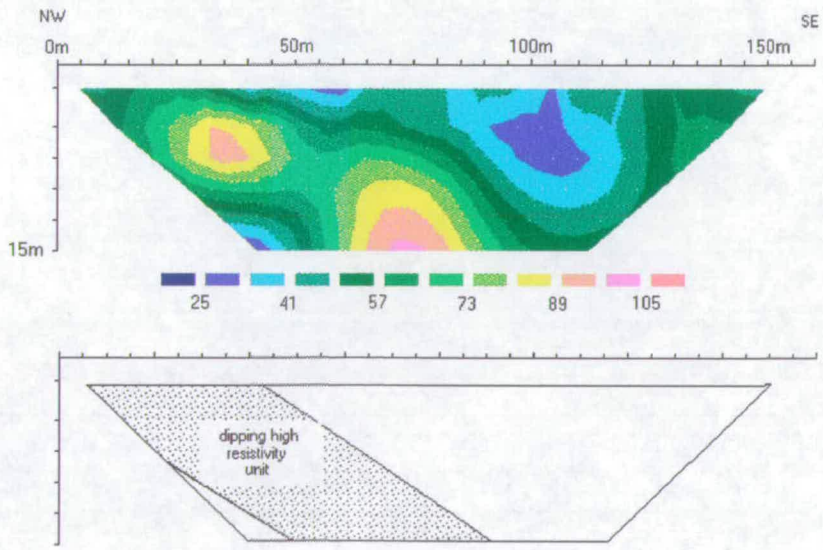

Figure 7.8: Modelled resistivity section of profile R51 with interpretation.

The 15m layer (Figure 7.9) shows a similar resistivity distribution to that of the 10m layer. There is still evidence for a major fault across the site but it is slightly further north suggesting that the fault is dipping to the north as was observed in the quarry.

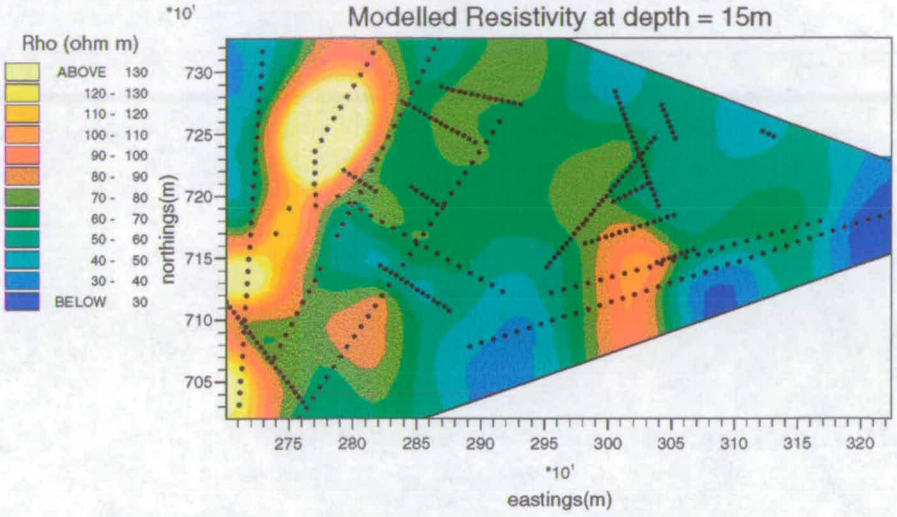

Figure 7.9: Contour plot of modelled resistivity at a depth of 15m

All three layers show further offsets to the southern end of the Ravelston sandstone (western high resistivity band) suggesting the existence of a second fault. This offset is least complicated in the 20m layer (Figure 7.10) which contains the least number of data points but still follows the trend of the shallower layers. The measurements to the south of the inferred fault show no evidence of the high resistivities related to the sandstone units. The 20m measurements are looking beneath the offset unit which the shallower measurements can still detect. Profile **R104** (Figure 7.11) provided these data points. The fault is represented as a definite break between two differently shaped high resistivity units.

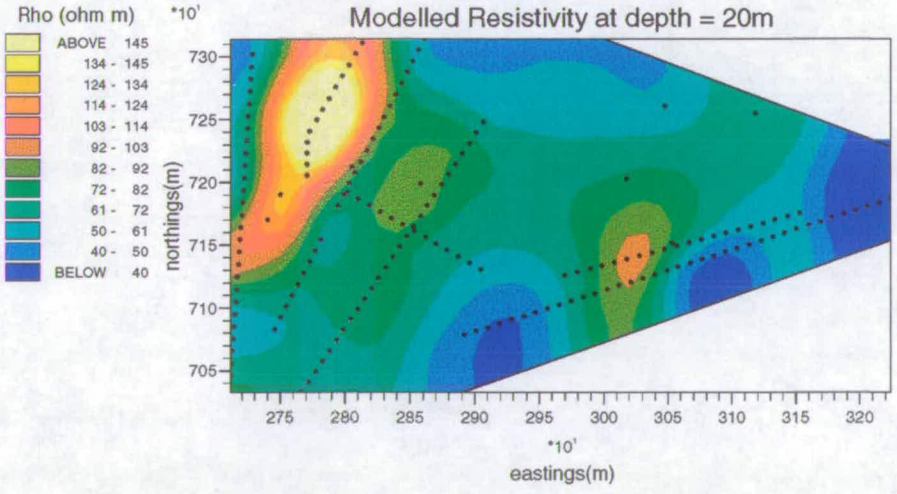

Figure 7.10: Contour plot of modelled resistivity at a depth of 20m.

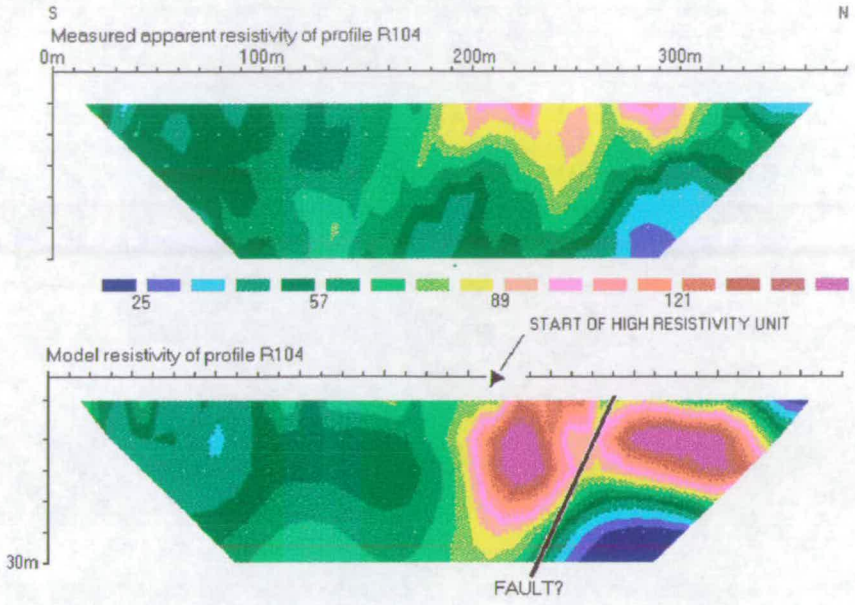

Figure 18. Profile R104 with interpretation.

Figure 7.11: Apparent resistivity pseudosection and modelled resistivity section of profile R104 with interpretation.

7.3.2 Mapping the Sandstone Boundaries

The bottom (western side) of the sandstone bands are frequently easy to locate where the shallow measurements first register high resistivity values. The tops of the units are invariably more difficult to define. The borehole information can be used to aid these interpretations. The depths to the sandstone units in the boreholes have been overlain on top of the resistivity contour plots (Figure 7.12) for direct comparison. An '**X**' signifies that no sandstone was detected but this may simply be due to a shallow borehole so the interpretation should be conducted with reference to the full borehole records in Appendix C.

The outcrop of the bottom of the Ravelston sandstone is clear on all three contour plots. This boundary is slightly displaced from that inferred by the original geological map. Evidence for this is clear in profile **R104** which runs from north to south across this boundary pinpointing its location.

The location of the outcrop for the top of the unit is less well defined but its position can be calculated using the dip values of the bedding and knowing the depth below rockhead of the sandstone in borehole C6. Although BGS7/2 is only a shallow borehole, it shows that sandstone is not at rock head at that point either, therefore the top outcrop lies to the west of both C6 and BGS7/2. At the southern end of the unit, sandstone is detected at rock head in BGS47.

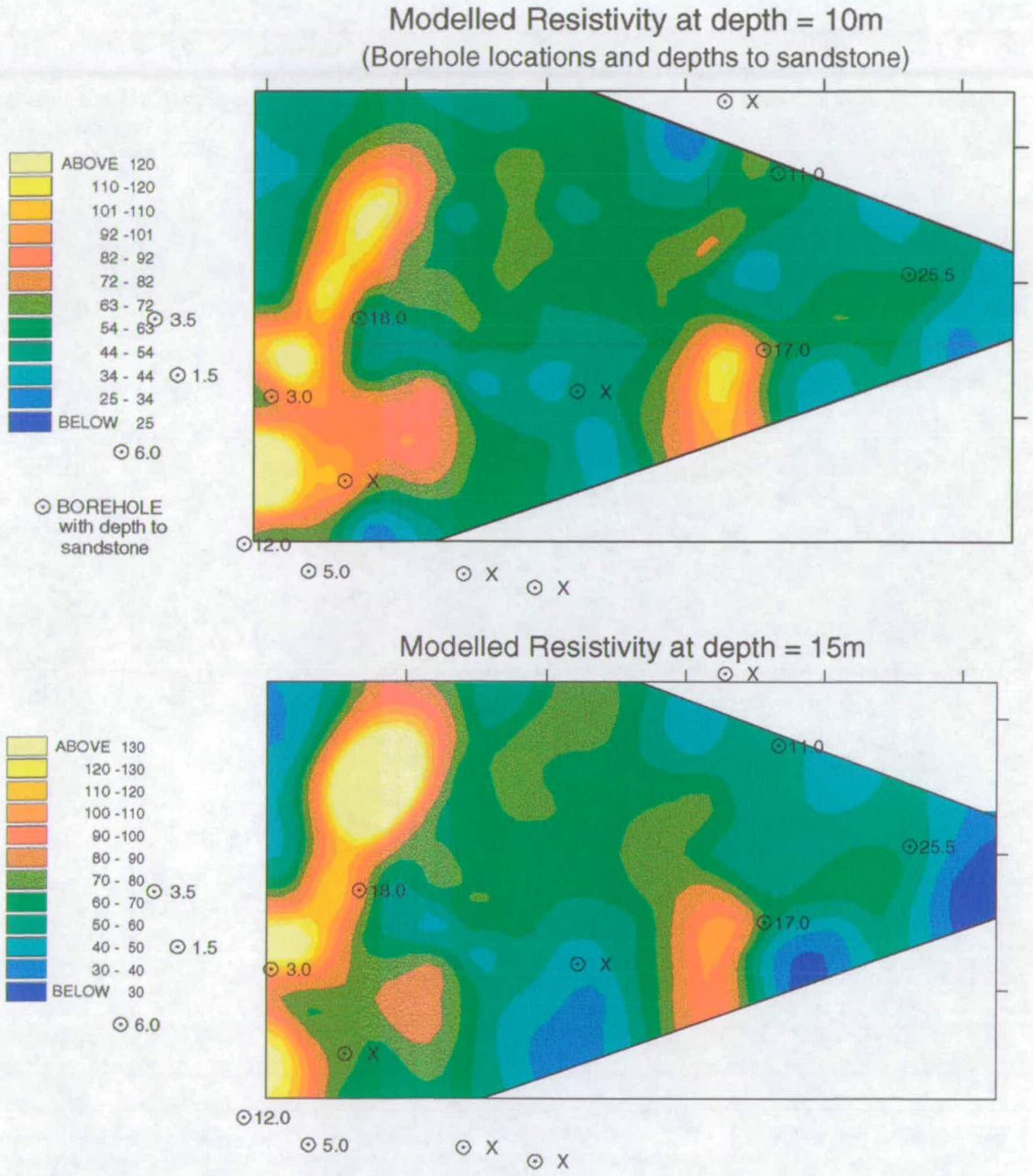

Figure 7.12: Comparison of resistivity distributions, at a depth of (a) 10m and (b) 15m, with depth to sandstone measured in boreholes.

The boreholes outwith the southwest corner of the survey area cannot be easily tied into one another without the aid of the geophysics but they imply structurally complex geology.

The eastern sandstone unit is detected in C7, north of the fault. The unit has a relatively shallow dip of 10° and so it is perhaps the top of this sandstone that is identified at the bottom of C9. To the south of the fault, sandstone appears at rock head in borehole BGS 22. The fault is shown to exist at the centre of the profile **C10** very close to the borehole. Consequently this borehole may contain important information if logged in more detail.

The eastern sandstone unit was also investigated with seismic techniques. A seismic refraction line was shot coincident with resistivity profile **AL**. The results were difficult to model due to the structural complexity but they did yield three different rock velocities increasing with depth (Gardiner, 1997). Layer 1 = 0.51kms^{-1} (expected value for made ground), layer 2 = 2.18kms^{-1} (average compressional wave velocity of clay = 1.1 - 2.5kms^{-1}) and layer 3 = 2.63kms^{-1} (average compressional wave velocity of sandstone = 2.0 - 4.5kms^{-1}).

A complete interpretation is summarised in Figure 7.13.

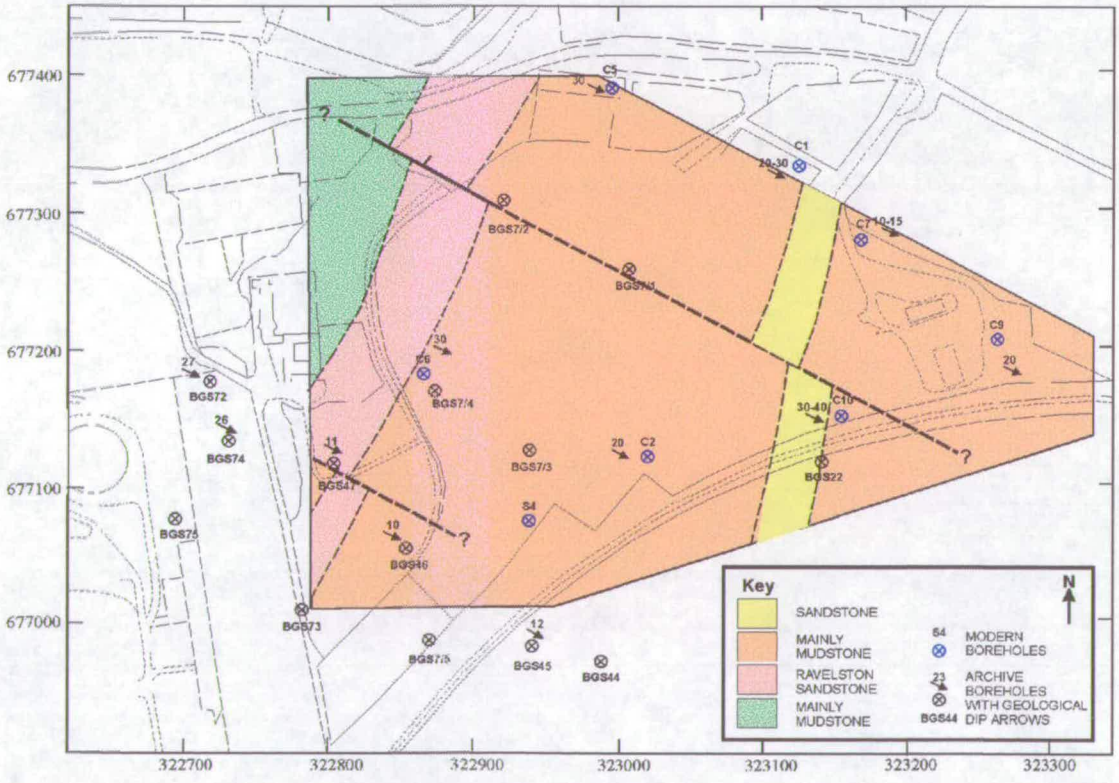

Figure 7.13: New geological map constructed with resistivity and borehole data.

The survey was continued to investigate whether or not the major northwest-southeast trending fault extends to the foreshore northwest of the site. Several attempts were made to take measurements along the foreshore itself but, save for one site, the low tide was never low for

a long enough period to complete a profile. The only completed shore line profile (**R58** on Figure 7.15) detects the change from unconsolidated sand saturated with sea water at the east end to the sandstone which can be seen in outcrop to the west.

Away from the shore, access was limited to a small field which could only accommodate electrode arrays with 5m spacings. These parallel profiles do not see the change into sandstone but this could be attributed to the shallow depth of penetration of the survey or an increased quantity of man made materials.

7.4 Fresh / Saline Water Interface

At the coast, the encroachment of the saline water is limited by the flow of fresh groundwater towards the sea. This results in the existence of a subsurface saline / fresh water interface. When the two groundwater types are in hydrostatic equilibrium the lighter fresh groundwater forms a lens shaped wedge and 'floats' on the heavier saline groundwater (Section 3.4). This density variation may cause the fresh groundwater to be discharged at the surface. It is unrealistic to assume a sharp interface between the fresh and saline groundwater. Due to tides and variations in recharge and discharge, the interface is more likely to fluctuate resulting in the production of a mixing or transition zone. Consequently, with geophysical surveys one expects to see a gradual change in the physical properties of the subsurface rather than a well defined boundary.

Figure 7.14 shows the location of the profiles that have been examined for the investigation of the saline interface. Again, the majority of measurements along the shoreline were unsuccessful. Large quantities of building materials have been dumped along the shore so consequently, even at low tide, there is only a very small region of open sand suitable for surveying. Unfortunately this region of sand was never above water for long enough for a complete profile to be measured. The one successful shoreline measurement (**T58**) was used to assign a value of resistivity to unconsolidated sediments saturated with salt water ($<14\Omega$m).

Further inland, measurements were taken wherever possible and were examined for resistivities close to those detected along the shore itself. Figure 7.15 shows all the pseudosections which contain information about the saline/fresh water interface.

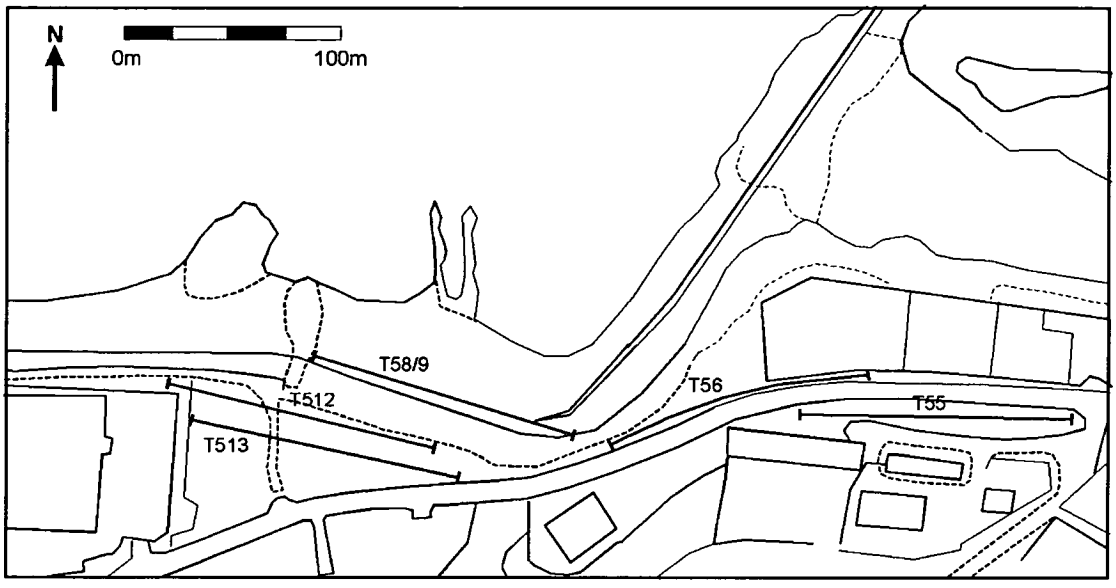

Figure 7.14: Location of profiles measured for the detection of the saline interface.

Resistivities of $<14\Omega$m are shaded dark blue. These values can be seen at depth in profile **T55** and slightly increased resistivities (less/deeper salt water) in **T513**, **T56** and **T512** respectively. Due to the steep gradient of the interface shown in hydrological models, it is considered that when salt water is detected near to the surface this should be close to the interface. This leads to the interpretation shown in Figure 7.16. This interpretation should be considered only as a guideline due to the limited data set.

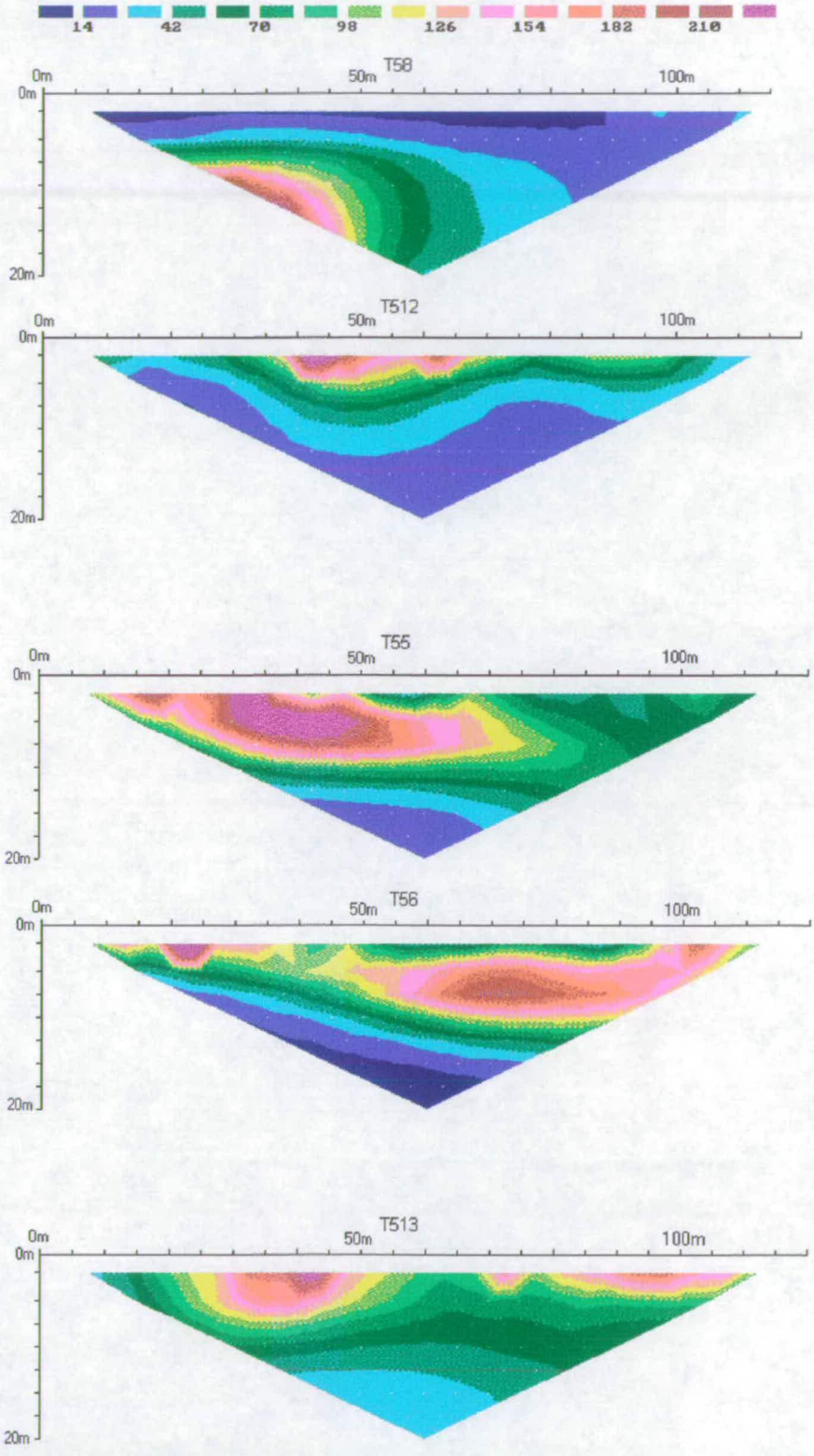

Figure 7.15: Resistivity pseudosections measured to locate the saline/fresh water interface.

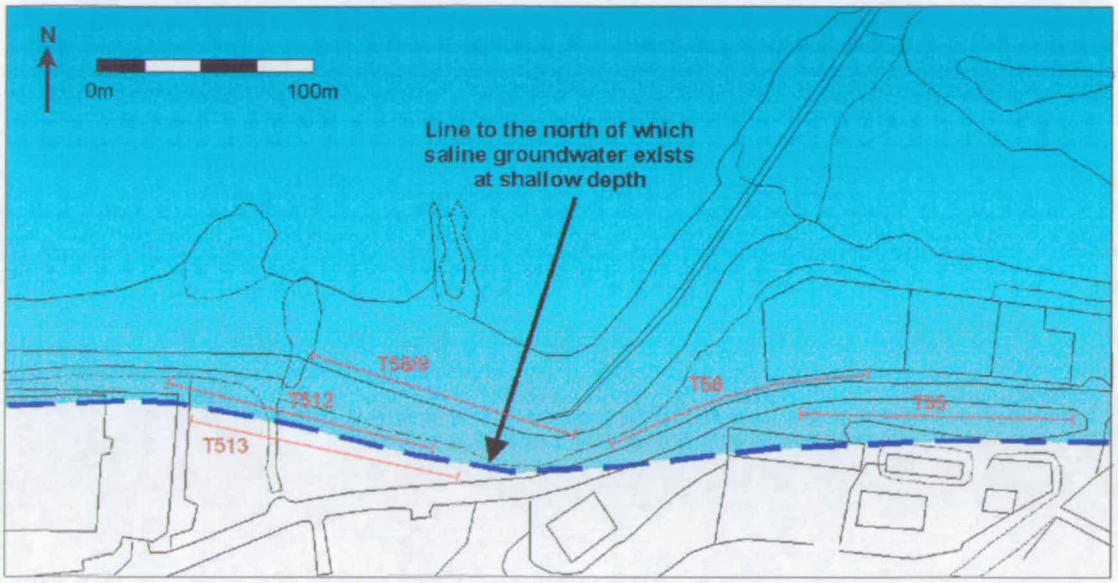

Figure 7.16: Location of shallow saline groundwater.

7.5 Conclusions

Resistivity has proven to be the correct geophysical tool for the various targets explored beneath the former Shell and Texaco sites. Resistivity could easily be tied into borehole logs and was also the parameter of interest where no invasive information was available. The clay coverage, contaminant pathways and, to some extent, the saline interface have all been successfully evaluated.

Whilst the clay coverage is adequate in most places, the survey has highlighted zones that require further investigation.

A major fault has been detected and the suggestion of a further smaller fault has also been presented. The high permeability units have been located beneath the site which, together with the fault locations, provide a map of potential contaminant pathways.

The saline interface is not a sharp boundary and can therefore not be pinpointed but there is sufficient evidence to infer the location of the transition zone where fresh water may rise and discharge at the surface.

8 TESTING PSEUDO THREE-DIMENSIONAL (3-D) MODELS

8.1 Introduction

The construction of resistivity contour maps for each depth (Chapter 7) effectively produces a pseudo 3-D model of the subsurface. It is necessary to test this model for two reasons: Firstly the 2-D models produced by inversion are non-unique and therefore carry uncertainty forward into the 3-D model. Secondly, the complex geology beneath the Granton site is definitely a 3-D problem.

Although 3-D inversion of resistivity data has been achieved (Park and Van, 1991; Li and Oldenburg, 1994; Zhang *et al.*, 1995) the process requires enormous quantities of computer power and time. Furthermore, inversion schemes are less applicable when a complete, even coverage of data points is unavailable. However, low data densities yield highly ill-posed problems for both forward and inverse modelling increasing the problems of non-uniqueness. Instability usually arises when observations (in this case, apparent resistivity measurements) are a smoothed version of the real earth model. Each measurement is an average of all the resistivities sampled and could therefore have an infinite number of possible causative real earth resistivity distributions. To reduce the problems of non-uniqueness, a smoothly varying earth is assumed on a fine scale. As a consequence of this assumption, data interpretation methods (e.g. interpolation, forward and inverse modelling) have the effect of smoothing out high frequency inhomogeneities and highlighting the larger scale variations with more significant causative bodies.

Forward modelling is a flexible means of investigating complex structures by producing a synthetic response and comparing it with the observed data. By inputting data from the Granton pseudo 3-D resistivity model it is possible to forward model the apparent resistivity measurements from any chosen electrode array at the surface to compare to the pseudosection measured in the field. The first test of the model is therefore satisfied by the comparison of the measured 2-D pseudosection with the pseudosection calculated in response to the 3-D model. Secondly, if the 3-D model is a good representation of the resistivity distribution across the site, then the forward modelled pseudosection in response to the 3-D model should match the measured data more closely than the calculated response to the 2-D model in RES2DECO

(Section 5.2.1).

The forward modelling algorithm used for this work was developed by Spitzer (1995).

8.2 Spitzer's 3-D Forward Modelling Algorithm

Spitzer's algorithm is suitable for a wide range of complex models. Resistivity values can be distributed arbitrarily throughout the half space and the grid spacing, within the half space, is variable. The resistivity values are calculated at grid nodes using a volume-weighted arithmetic average of the resistivity values assigned to individual cells. This discretization scheme was proposed by Brewitt-Taylor and Weaver (1976). The scheme results in a non-symmetric set of linear equations. After transforming the matrix equations into a symmetric form, Spitzer (1995) uses the preconditioned conjugate gradient method (Hestenes and Stiefel, 1952) which provides rapid convergence.

There is no limit on the number and configuration of the source electrodes, so many DC resistivity surveys can be simulated including the Wenner arrays utilised in the Granton survey.

8.3 3-D Investigation of Granton Resistivity Data

8.3.1 The Input File

In order to forward model a resistivity pseudosection it is necessary to define the electrode array location and the resistivity model in the correct language for the program. The input file for Spitzer's program must include a full description of the grid, the source and receiver locations and the resistivity model. There are very few restrictions to any of these parameters but each one must be considered carefully to best represent the Granton resistivity model.

Grid Spacing

The grid spacing must be fine enough to incorporate electrode locations and adequately define the detail of the model. However, a very fine grid will not only expend greater computer power and time but also conveys unrealistic confidence in the entered model. The model is subject to errors from the original field measurements and then from the inversion modelling that was performed to construct the resistivity contour plots. As a compromise, the x and y grid spacing, within the zone of interest surrounding the chosen profile, is equal to half the electrode spacing. Outside of the zone of interest, the spacing increases by a factor of 1.3 until a significant area of background resistivity is represented (minimum background size is twice the dimensions of the zone of interest). The z grid spacing is set at 1m for the calculated region of current penetration and increases beyond this depth by a factor of 1.3.

Source and Receiver Locations

There are no restrictions on the source and receiver locations (except that they are placed at grid nodes) but for the case of a long electrode array it is convenient to rotate the grid to coincide with the orientation of the profile. All the source electrode pairs which are utilised in the measurement of the apparent resistivity pseudosection must be defined i.e. 1-4, 2-5..., 1-7, 2-8... etc (Section 5.2). The apparent resistivity is calculated at each receiver location for every source electrode pair.

Resistivity Model

Although resistivity values may be arbitrarily distributed within the half space for forward modelling, the preliminary program which creates the input file, is not as flexible. The program reads in a background resistivity value and further resistivity values are assigned in blocks e.g. a block with dimensions x_1-x_2, y_1-y_2, z_1-z_2 has one resistivity value. This method

of inputting data is not suited to the smoothly varying resistivity contour plots obtained for the Granton data (Section 7). To get round this problem a new set of programs (written in MATLAB and FORTRAN languages) have been written to bypass Spitzer's preliminary program to create an input file by an alternative process. The file can now include all the Granton data from the area surrounding the chosen 2-D profile under investigation.

8.3.2 Creating an Input File

(i) Choose a profile for comparison.
For the best results, it is prudent to choose a profile which is surrounded by a reasonable density of data points from other profiles. Figure 8.1 shows all the data points at an apparent depth of 15m. The arrangement of these data points can easily be related to the map of profile locations in Figure 5.5.

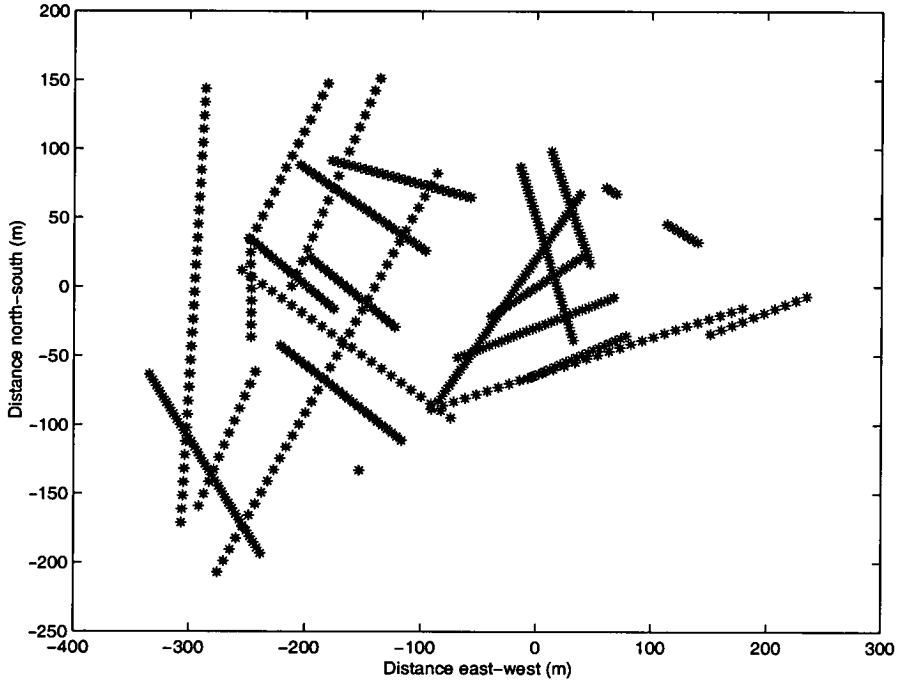

Figure 8.1: Spatial arrangement of all modelled resistivity data points at a depth of 15m.

The data are rotated to align the model grid with the line of the chosen profile. The user must define the region to be extracted for forward modelling i.e. define the required number of grid points to be extracted away from the profile in both the x and y directions. The number of extracted grid points must be large enough to cover the expected area likely to contribute to the signal. Sections of signal contribution for given electrode arrays are given in Barker (1979) which describes a boxed region containing both the profile data points and data from surrounding profiles (Figure 8.2). For this example profile **T52** is chosen.

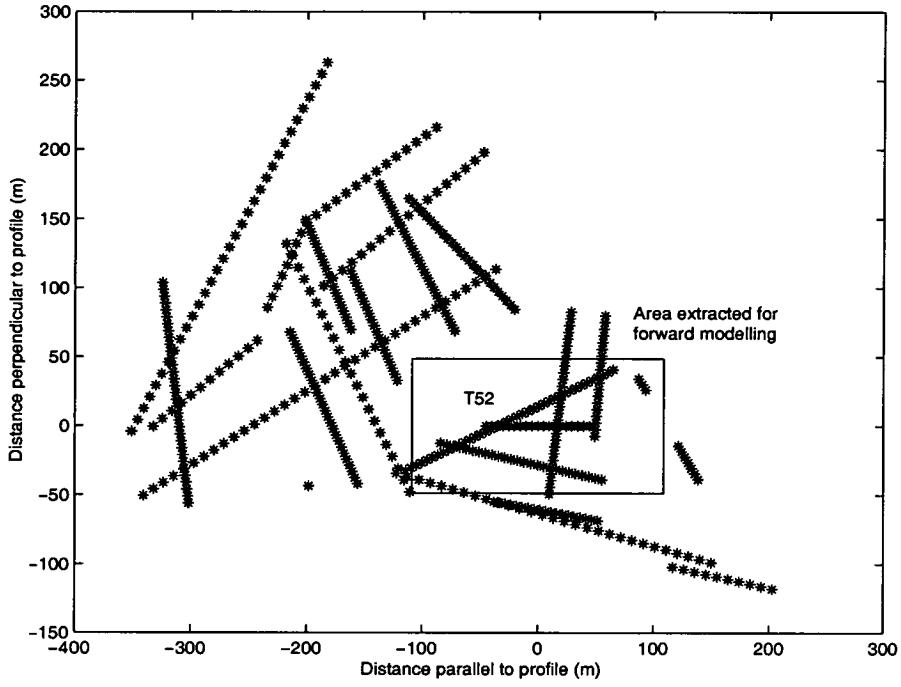

Figure 8.2: Data rotated to align the chosen profile (**T52**) to the model grid lines. Boxed region highlights data points extracted for forward modelling.

The grid spacing and the source / receiver locations are automatically calculated from details of the chosen profile (i.e. number of electrodes, electrode spacing) and written into the input file.

(ii) Interpolate data within boxed region.

The data from the boxed region are extracted from each layer (apparent depth) and interpolated (using the default linear method of interpolation in MATLAB) onto a finer grid (Figure 8.3). The grid spacing is equal to half the electrode spacing. This interpolated data must now be translated into a language to be read into Spitzer's program. Spitzer's program will accept a maximum of 62 resistivity values that can be labelled by the numbers 1-0 and the letters a-z in upper and lower case. The user must define the number and size of resistivity classes to which each resistivity data point will be allocated and labelled accordingly as a number or letter corresponding to the average resistivity of that class (Figure 8.4).

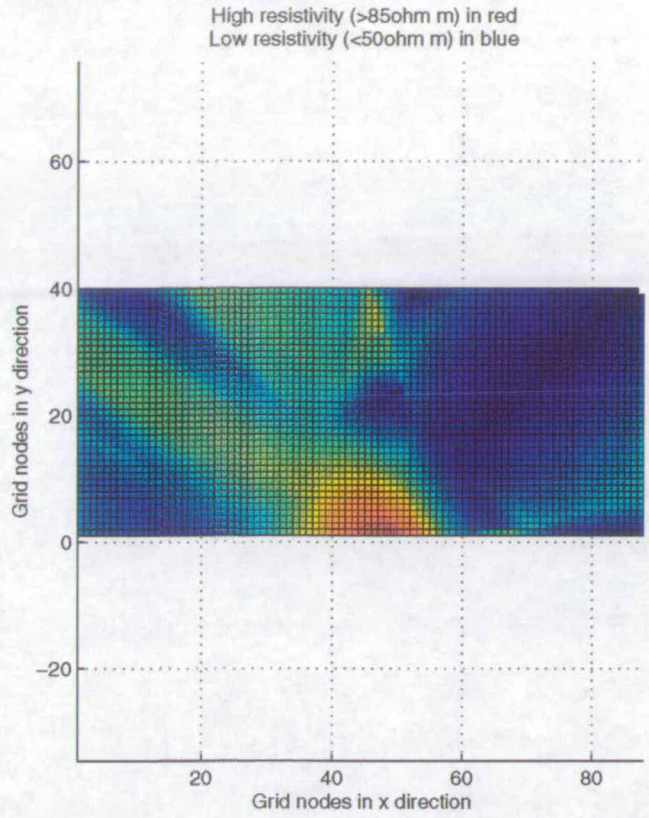

Figure 8.3: Extracted data points (from around the chosen profile (**T52**)) interpolated onto a grid with spacing equal to half the electrode spacing in both the x and y directions.

```
554444444555667777777777777777777777666666776554444445555555555544444444444444444334
555554444445556677777777777777777777776666677765444444455555555555444444444444433344
655555544445566677777777777777777777766666777665543444455555555555444444444444433344
665555555545556667777777777777777777766666777765544555555555555544444444444444344444
666655555555555666777777777777777777766777876655555555555555554444444444444434444444
776666555555555566677777777777777777766777876655555555555555554444444444444434444445
777666655555555566677777777777777777766777876655556665555555554444444444444444444445
777776666555555555666777777777777777766777866666666555555554444444444444444444445
777777766665555555566677777777777777767777766666655555555544444444444444444444445
777777776666555555556667777777777777776666655555555444444444444444444444444455
777777777666655555556667777777777777776666655555555444444444444444444444444455
777777777766666665566677777777777777776666655555555444444444444444444444444455
777777777776666666556667777777777777766666555555544444444444444444444444444455
777777777777666666665667777777777777666665555555444444444444444444444444444555
777777777777766666666667777777777776665555665555554444444444444444444444445555
777777777777776666666666777777777766555556555555544444444444444444444444455556
677777777777777766666666677766667666555443465555554444444444444444444444455555556
666777777777777777166666666677666666655544445555555444444444444444444444455555555556
666677777777777777716666666676666666555444455555555444444444444444444444455555555566
666667777777777777777166666666666666555555555555554444444444444444444455555555566
666666777777777777777716666666666666555555555555554444444444444444444455555555566
666666677777777777777771666666666666555555555555554444444444444444444555555555566
666666667777777777777777166666666666555555555555554444444444444444455555555555566
666666666777777777777777716666666655555555555555444444444444444445555555555555666
666666666677777777777777771666666655544444444444455555555555555555566666666666
666666666667777777777777777166666655444444444445555555555555555566666666666
666666666666777777777777777716666655444444444455555555555555555566666666666
666666666666677777777777777777166666554444444444555555555555555566666666666
666666666666667777777777777777716666554444444444555555555555555566666666666
666666666666666777777777777777771666554444444444555555555555555566666666666
666666666666666777777777777777777166554444444444555555555555555566666666666
666666666666666677777777777777777716554444444444555555555555555566666666666
666666666666666667777777777777777771554444444444555555555555555566666666666
665555555566666666667777777777778788888888888887776665554455555555555555566666666666
655555555556666666666777777777778888888888888887776665554455555555555555566666666666
655555555555666666666677777777778888888888888887776665554455555555555555566666666666
655555555555566666666667777777777888888999999888776665555445555555555556666666666666
665555555555555566666666677777777788889999999998887766655555455566555566666666666666
665555555555555555666666667777777788899999999099988776655555556666666666666666666666
665555555555555555566666666677777778889999990000009998877665555555566666666666666666666
665555555555555555556666666667777888899990000000999887766555555556666666666555555555555
666555555555555555555566666667777888899990000000a000998776665555555666666666555555555555
666555555555555555555566666667777888899900000aaaaa000988776665667777766655555444444444456
```

Figure 8.4: Extracted data points translated into the input file language for 3-D forward modelling.
3=35Ωm, 4=45Ωm, 5=55Ωm, 6=65Ωm, 7=75Ωm, 8=85Ωm, 9=95Ωm, 0=105Ωm, a=115Ωm.

(iii) Assigning z (depth) values to resistivity layers.

Each resistivity layer is extracted from a resistivity contour map at a particular depth. The resistivity between each contour plot is unknown so each layer is considered to have a thickness comparable to the distance between each contour plot. For example, resistivity contour plots at depths of 5, 10, 15 and 20m will yield layers 5m thick which lie between 2-7m, 7-12m, 12-17m, 17-22m. The layer between 0-2m will be assigned a surface resistivity value (Figure 8.5). Below the last layer, the grid is assigned a user defined background resistivity value equal to that which is assigned to all grid cells outside the region of interest.

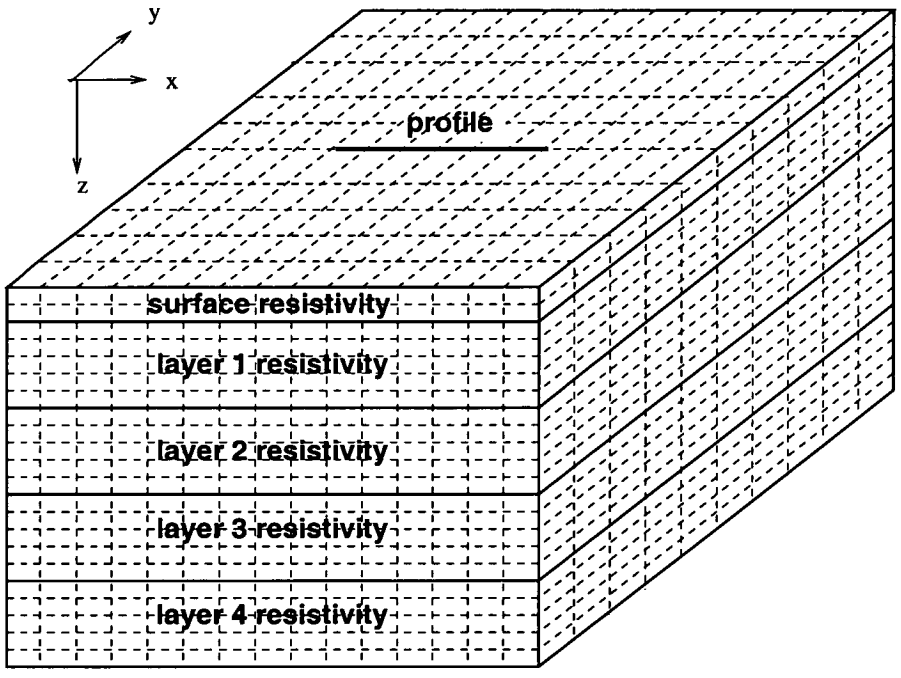

Figure 8.5: The arrangement of resistivity layers within the 3-D forward modelling grid.

Finally all the information (grid spacing, electrode location and resistivity model) is written into an input file to be entered into Spitzer's program.

8.4 Comparing Forward Modelled and Field Data

Four profiles were chosen for comparison **T51, T52, R53** and **R101**. These profiles are labelled on Figure 8.6 which shows the locations of all the available resistivity data points from the Granton site. The measured resistivity pseudosections and the resistivity pseudosections calculated using Spitzer's forward modelling algorithm are shown in Figures 8.7, 8.8, 8.9, 8.10.

The first test of the 3-D model is done qualitatively by the comparison of the measured pseudosection with the pseudosection calculated in response to the 3-D model. The second test is carried out quantitatively to evaluate whether or not the 3-D model represents the Granton site more accurately than the 2-D models. If the 3-D model is a good representation of the resistivity distribution across the site, then the forward modelled pseudosection in response to the 3-D model should fit the measured data more closely than the calculated response to the 2-D model in RES2DECO (Section 5.2.1).

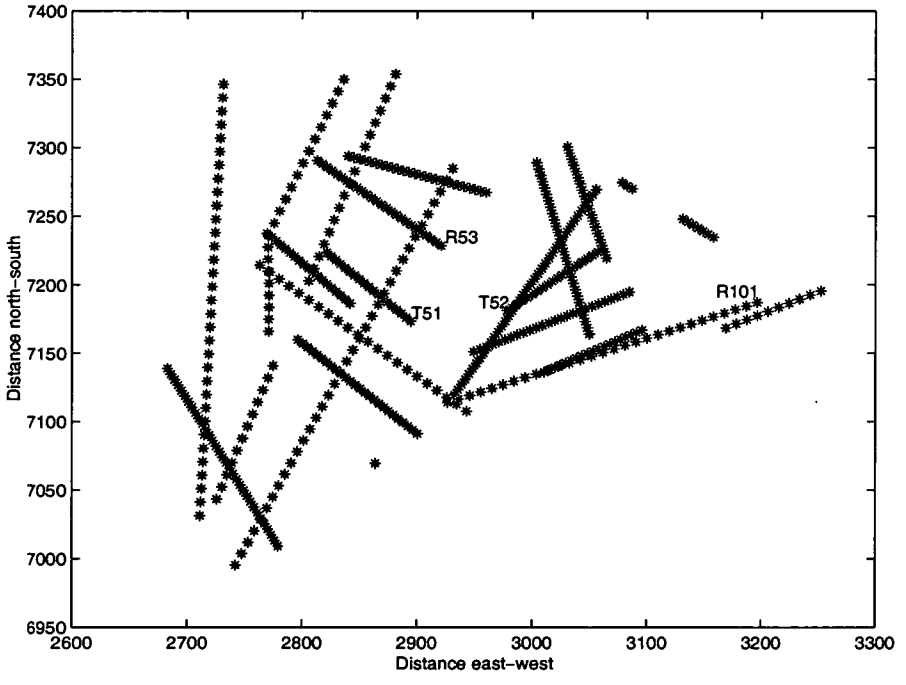

Figure 8.6: Location of data points defining profiles **T51, T52, R53** and **R101** with respect to all other data points collected at Granton site.

8.4.1 Qualitative Comparison

Profile T51

The measured pseudosection of profile **T51** (Figure 8.7.a.) shows an example of a very detailed image. The complexity of the pseudosection makes it hard to model with the inversion routine, RES2DECO (Section 5.2.1). The 2-D model obtained with RES2DECO is inevitably far smoother and less detailed than any model that would be required to produce a response identical to the measured data. Because the smooth 2-D model has been used to construct the 3-D model, the pseudosection calculated from forward modelling of the 3-D model (Figure 8.7.b.) also exhibits a much smoother appearance. The overall trend of the two pseudosections is, however, very similar.

Profile T52

Profile **T52** is in close proximity to many other profiles (Figure 8.6) so the 3-D model of the surrounding area has been constructed with a good density of data points. The measured resistivity pseudosection is relatively smooth (Figure 8.8.a.). As a consequence of both these factors, the pseudosection calculated from forward modelling of the 3-D model (Figure 8.8.b.) appears to be a very close fit to the image measured in the field.

Profile R53

The measured pseudosection of profile **R53** (Figure 8.9.a.) has complexities that are predominantly a response to the geology but also a result of removing the effect of a pipe (Section 6.3). These complexities lead to a repeat of the problems described in the comparison of the measured and calculated response of profile **T51**. The general trend of the **R53** pseudosection calculated from forward modelling of the 3-D model (Figure 8.9.b.) follows the measured data except for the right hand edge where the deeper, high resistivity layer rises to a shallower depth than is evident in the measured data. This behaviour is due to the lack of data points surrounding the east end of profile **R53** where a steep embankment prevented the measurement of resistivity (Section 5.3).

Profile R101

Profile **R101** has a very poor density of data points to the south east. The 3-D model describing the resistivity distribution in the area surrounding the profile is therefore quite poor. The high resistivity patch in the measured pseudosection (Figure 8.10.a.) (the response to a sig-

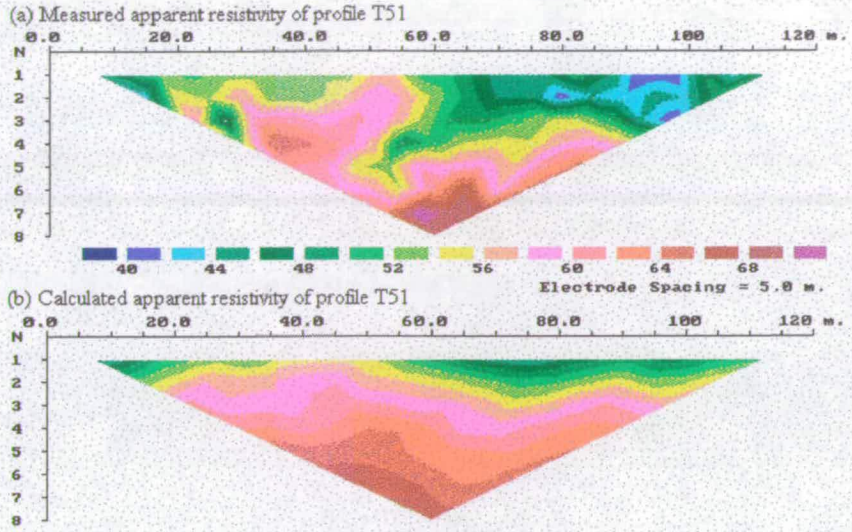

Figure 8.7: Profile **T51**: (a) Measured apparent resistivity pseudosection and (b) apparent resistivity pseudosection calculated from forward modelling using Spitzer's program.

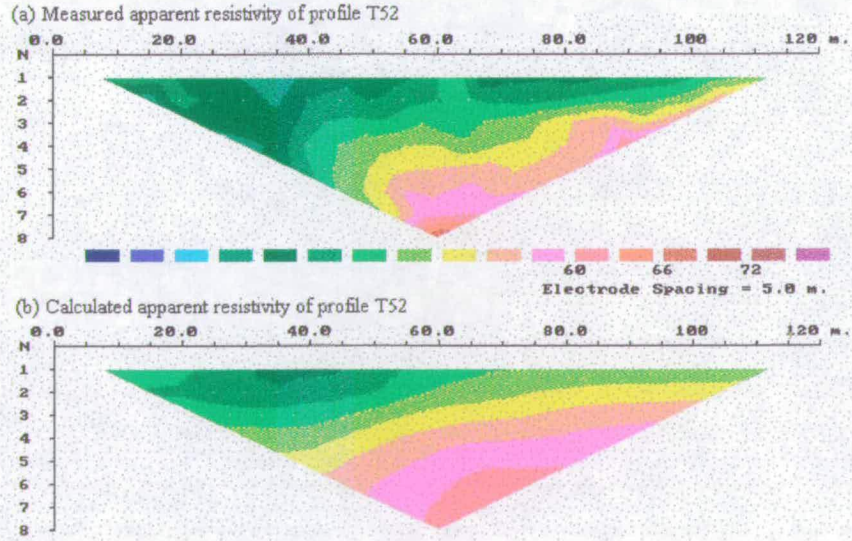

Figure 8.8: Profile **T52**: (a) Measured apparent resistivity pseudosection and (b) apparent resistivity pseudosection calculated from forward modelling using Spitzer's program.

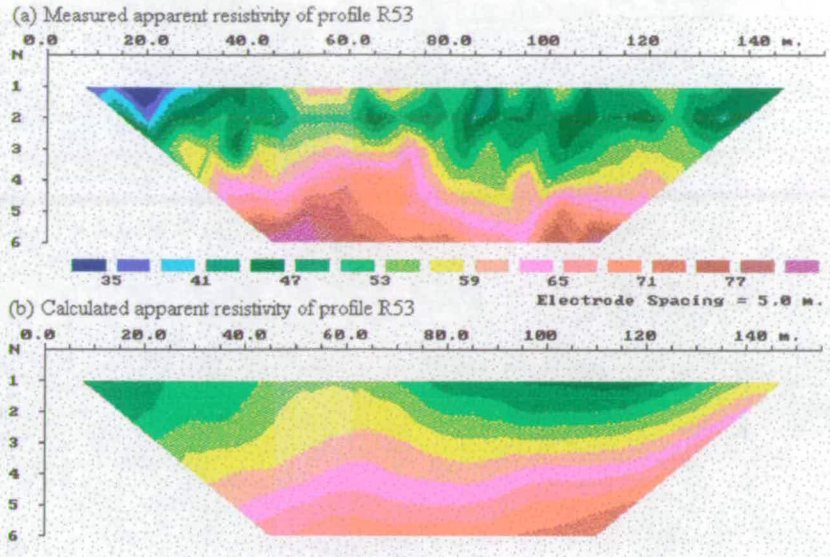

Figure 8.9: Profile **R53**: (a) Measured apparent resistivity pseudosection and (b) apparent resistivity pseudosection calculated from forward modelling using Spitzer's program.

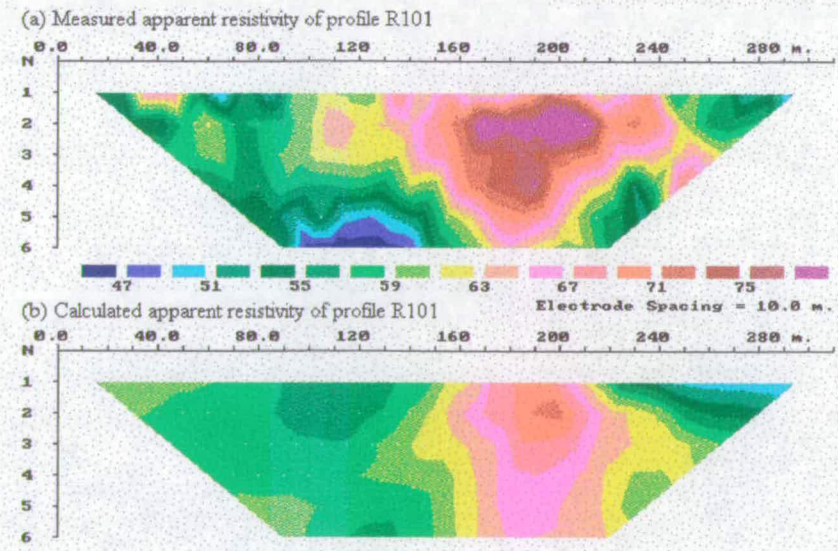

Figure 8.10: Profile **R101**: (a) Measured apparent resistivity pseudosection and (b) apparent resistivity pseudosection calculated from forward modelling using Spitzer's program.

nificant sandstone unit) is inevitably much weaker in the calculated response (Figure 8.10.b.) which is affected by the background resistivity value input by the user which is also used to substitute for missing data points (Section 8.3).

8.4.2 Quantitative Comparison

Chi-Square Fitting

Chi-square fitting can be used to evaluate how well the dependent data (calculated response) c_i fits N independent data points (measured response) m_i, $i = 1, ...N$. Each measured data point has an associated standard deviation which, in this case, is a percentage error to represent how repeatable the resistivity measurement would be in the field (i.e. δm_i). The Chi-square misfit χ^2 is given by:

$$\chi^2 = \sum_{i=1}^{N} \left(\frac{c_i - m_i}{\delta m_i} \right)^2 \tag{8.1}$$

For N data, the expected value of χ^2 is N. A value below N symbolises over-fitting whilst a value far in excess of N can either be due to a poor model or to unrealistically small errors δm_i. A more detailed explanation of chi-square fitting is given by Press *et al.* (1986).

In order to use the chi-square misfit for resistivity data an alteration is made. Resistivity responses are usually displayed as graphs of apparent resistivity against electrode spacing, with logarithmic scales for apparent resistivity and electrode spacing. The logarithm scales are employed to allow the display of the extensive range of possible resistivities. Resistivity varies by orders of magnitude so that detecting a boundary between units with resistivities of 1 and 100 Ωm has very different implications to a boundary between units with resistivities of 700 and 800 Ωm. To compensate for this in the chi-square fit, logarithms are taken of the measured and calculated resistivities;

$$\chi^2 = \sum_{i=1}^{N} \left(\frac{\log c_i - \log m_i}{\delta \log m_i} \right)^2 \Longrightarrow \chi^2 = \sum_{i=1}^{N} \left(\frac{\log(c_i/m_i)}{\delta \log m_i} \right)^2 \tag{8.2}$$

where $\delta \log m_i = \frac{1}{m_i} \delta m_i$. The use of logarithms is an approach adopted by Weaver and Agarwal (1993) to test the fit of modelled 1-D magnetotelluric data.

The errors for each measured data point δm_i are automatically recorded by GEOPULSE and can be used in the evaluation of chi-square. Chi-square values are used to measure the misfit between the measured resistivity pseudosection and the resistivity pseudosections calculated in response to both the 2-D and 3-D models. If the 3-D model is a good representation of the resistivity distribution across the Granton site, then the forward modelled pseudosection in response to the 3-D model should fit the measured data more closely than the calculated response to the 2-D model constructed by RES2DECO .

The chi-square misfit values for the chosen profiles **T51, T52, R53** and **R101** are given in Table 8.1. The table also presents the minimum and maximum percentage errors recorded by GEOPULSE representing the repeatability of the resistivity measurements m_i.

Table 8.1: Chi-squared misfit between the measured resistivity pseudosection and the resistivity pseudosections calculated in response to the 2-D and 3-D models.

Profile	N	**min** δm_i **(%)**	**max** δm_i **(%)**	χ^2 **misfit 2-D response**	χ^2 **misfit 3-D response**
T51	92	4.02×10^{-2}	2.98	1.24×10^5	7.38×10^4
T52	92	4.35×10^{-2}	3.43	5.92×10^4	5.46×10^4
R53	129	2.97×10^{-4}	3.87	1.66×10^9	1.64×10^9
R101	129	9.99×10^{-3}	3.75	2.36×10^5	2.74×10^5

The chi-squared misfit of both the 2-D and 3-D responses are far greater than N indicating either poor models or unrealistically small errors. To test the size of the errors the chi-squared fit calculation has been repeated to find the average percentage error of the measured response δm_i which gives a fit equal to N. The results of this search are given in Table 8.2

Table 8.2: Average error of measured data points required to yield a chi-squared misfit equal to N

Profile	N	δm_i **(%) 2-D response**	δm_i **(%) 3-D response**
T51	92	6.79	5.08
T52	92	4.35	4.32
R53	129	6.11	6.09
R101	129	4.38	4.41

The errors required for the measured data points vary between 4.32 and 6.06%. These errors seem reasonable for the complex resistivity distributions that one would expect to find at an old industrial site. As expected, the model is too smooth. The errors recorded by GEOPULSE may be a realistic measure of the repeatability of the exact same measurement point but do not represent the short wavelength detail which effects the variability of the resistivity images.

A new chi-square misfit has been calculated using the smallest derived data point error (4.32%)

for all profiles. The new values for the chi-square misfit are presented in Table 8.3

Table 8.3: Chi-square misfit between the measured resistivity pseudosection and the resistivity pseudosections calculated in response to the 2-D and 3-D models using an average measured data point error of 4.32%.

Profile	N	χ^2 **error 2-D response**	χ^2/N	χ^2 **misfit 3-D response**	χ^2/N
T51	92	228.9	2.49	127.9	1.39
T52	92	93.6	1.02	92.0	1.00
R53	129	258.6	2.00	256.4	1.99
R101	129	132.3	1.01	134.6	1.03

In general the fit of the calculated responses is best for the smooth measured pseudosections (profile **T52** and **R101**) whereas the fit is poorer for the more complex measured pseudosections (profile **T51** and **R53**). The fit of the 3-D response is better than the fit of the 2-D response for 3 out of the 4 profiles. The responses at profiles **T51** and **R53** favour the 3-D model but the differences between the 2-D and 3-D responses are small demonstrating the 2-D nature of the geology in that region. Whereas the fit of the 3-D response over a truly 3-D structure (the dipping sandstone at profile **T52**) is particularly good. The fit is also increased due to the high density of data points that were used to build the model. Conversely, the fit of the 3-D response to profile **R101** is not quite as good as the 2-D response. This is probably due to the poor density of data points available for the construction of the model to the southeast of the profile.

8.5 Conclusions

Forward modelling provided a valuable tool for the testing of the pseudo 3-D model of the Granton site. The 3-D forward modelling takes into account the resistivity distributions across the entire site rather than in a 2-D vertical plane.

The calculated responses to the 3-D model compare favourably with the measured responses. Moreover the responses to the 3-D model generally have better (lower) chi-square misfits to the measured data than the responses to the 2-D models. From this, it is possible to conclude that the 3-D model is a more accurate representation of the resistivity distribution which exists beneath the Granton site thus adding weight to the geological interpretations of the resistivity contour plots presented in Chapter 7.

9 DISCUSSIONS AND CONCLUSIONS

The ultimate aim of this research has been to present the invaluable role of shallow, non-invasive geophysical surveying for the evaluation of contaminated sites. An extensive desk study has been carried out to appraise the contributions that a particular geophysical technique could make to the investigation of a contaminated site (Section 2.3). The desk study, along side trial surveys, prompted the use of electrical and electromagnetic techniques to address a number of problems relating to 2 ex-oil distribution terminals. The terminals form part of some 100 hectares of industrial land in West Granton, Edinburgh, which the City of Edinburgh Council aim to acquire for remediation and redevelopment. As part of a complete assessment of the surface pollution, the University of Edinburgh were consulted and a rapid reconnaissance electromagnetic survey was conducted employing a Geonics EM31 conductivity meter. This method was chosen to address the particular contaminants likely to reside at the site. Early trial pit information confirmed the predominant contaminants to be diesel related organics which effect the electrical resistivities of the subsurface. Other possible targets included man made structures. After the completion of this survey, a second non-invasive geophysical survey was designed to locate potential contaminant pathways. The 2-D resistivity imaging technique was used to determine the complex geology of the ground beneath the 2 ex-oil distribution terminals and the immediate surroundings. Both the electrical and electromagnetic techniques were extremely successful at imaging complicated subsurface structures and geological features with far greater resolution than boreholes and trial pits could ever hope to achieve restrained with the same budget.

The EM31 survey proved the Granton site to be contaminated with shallow diesel related organics and a labyrinth of subsurface pipes which require remediation before site development can continue. The second resistivity survey did not detect any obvious denser-than-water phase liquid plumes. DNAPL plumes are considered to be resistive targets because they are more resistive than water and, due to their physical properties, they displace pore water (Monier-Williams, 1995). However, this is only a guide because firstly, at a contaminated site, DNAPLs and LNAPLs may be composed of several components. It will be possible, for example, to find LNAPL as part of a DNAPL phase and vice versa. The behaviour of the contaminant will therefore depend on the relative proportions of the various components. Secondly, it should be noted that the properties of any liquid could change as its composition changes due to subsurface reactions with other groundwater contaminants and NAPL biodegradation (Sauck *et al.*, 1998). However, although LNAPLs have been associated with

conductive groundwater due to biodegradation, the same has not been proven for DNAPLs. Therefore, the lack of electrically resistive plumes may indicate that the DNAPL contaminants have already migrated away from the site along one of the many contaminant pathways. These comprise: connected high permeability sandstones; minor faults; and a major fault which, if open, provides a rapid pathway directly to the Forth estuary.

During the interpretation and presentation of the Granton data, a number of conclusions were drawn. These conclusions are detailed below:

- The electromagnetic technique, involving a Geonics EM31 soil conductivity meter, was capable of detecting subsurface metal pipes and contaminant concentrations resulting from the oil terminal works.

  Electromagnetic methods, like electrical methods, are sensitive to the changes in resistivity caused by the introduction of diesel related organics. The EM31 survey detected shallow oil plumes emanating from the ends of buried, broken pipes. The pipes formed part of a labyrinth of underground pipes which turned out to be a major unexpected discovery. These interpretations were ground truthed with trial pits confirming the locations of both pipes and contaminant pools.

- Use of the second derivative of unidirectional EM31 measurements eliminates the directional dependence of the survey.

  The EM31 is directionally dependent and yields results that depend on the orientation of the boom with respect to subsurface linear anomalies. The directionality is confusing for a non-geophysicist to interpret. Rather than undertake a more time-consuming survey with orthogonal measurements at each location, use of the second derivative of unidirectional measurements is shown to reveal all the pipes clearly and similarly, whatever their direction relative to the EM31 boom.

- The 2-D Resistivity Imaging method proved to be a profitable choice for a secondary, deeper geophysical investigation of the Granton site.

  The computer controlled resistivity imaging method provided rapid coverage of the Granton site returning a large number of 2-D apparent resistivity pseudosections. The technique was chosen because resistivity methods are responsive to complex geology including faults.

- A conducting subsurface pipe has a significant effect on resistivity measurements. This effect can be quantified using an analytical solution (Wait, 1982).

A program has been written, as part of this research, which utilises Wait's analytical solution to calculate the expected apparent resistivity anomaly due to an infinitely long conducting cylinder of variable diameter, depth and orientation with respect to the electrode array. It has not been possible to calculate the exact effect of multiple pipes but the addition of more than one normalised pipe effect has proved, in tests, to be a good approximation.

- The effect of subsurface pipes can be located and removed from within apparent resistivity pseudosections.

  The resistivity profile over a particular pipe, relevant to a chosen resistivity pseudosection, can be calculated. The pipe effect can then be located within the resistivity pseudosection by cross correlation of the pipe profile with the resistivity pseudosection (the point of maximum cross correlation locates the pipe). The effect of the pipe is removed by matrix multiplication. The pseudosection is now 'pipe free' and ready for inversion to model the resistivity relating to the background geology.

- Resistivity contour maps allow data from all modelled profiles to be viewed together.

  Contour plots (plan views) of the resistivity distributions across a complete site can be constructed by extracting resistivity data points from all modelled profiles at equivalent depths.

- The resistivity survey proved invaluable for the evaluation of the integrity of the superficial clay coverage, for the location of faults and for resolving complex geology across the Granton site.

  The clay coverage is adequate across the majority of the site but the survey has highlighted windows in the coverage which may allow the downward migration of contaminants into the subsurface geology.

  The signature of a major fault and the suggestion of a further smaller fault have been detected. High permeability sandstone units have also been located beneath the site which, together with the fault locations, provide a map of potential contaminant pathways.

  The saline interface is not a sharp boundary and can therefore not be pinpointed but there is sufficient evidence to infer the location of the transition zone where fresh water may rise and discharge at the surface.

- The pseudo 3-D model, constructed using the resistivity contour plots, is a good representation of the resistivity distribution across the site.

The forward modelled 2-D pseudosection in response to the 3-D model matches the measured data more closely than the calculated response to the 2-D model using RES2DECO . This demonstrates the increased accuracy of the 3-D rather than 2-D representation.

The overall outcome of this work has been to promote geophysics as a powerful tool for the rapid investigation of contaminated sites. The geophysical investigation of the 2 ex-oil distribution terminals at Granton proved invaluable to Edinburgh City Council. As a result of the work, the Granton site remediation plans have been substantially redesigned and, in return, Edinburgh City Council have begun to recommend the use of geophysics to the contaminated land community.

10 FUTURE WORK

The value and effectiveness of geophysical surveying, prior to invasive site investigation, has been clearly demonstrated. There are, however, a number of improvements that could be made to the survey design and the data processing techniques if time and access to equipment and computer power were available. The improvements would increase confidence in data interpretation.

Survey Design

- The 2-D resistivity imaging survey suffered limitations mainly due to access problems. The triangular nature of the resistivity pseudosections give rise to large zones which contain no information. The profiles cannot be extended to sample these regions due to access restrictions. This is likely to be a common problem for investigations of this type because derelict sites will often be surrounded by industrialised or built up areas. For future surveys it is proposed that time domain electromagnetic (TDEM) techniques be employed in these situations to supplement the resistivity results. Although they will contain less detail than resistivity pseudosections, they do not require the same areas of open space and can thus be employed at the ends of resistivity profile lines and in tight corners.
- If a fault is detected, the role of the fault can be investigated with azimuthal studies. The major fault that runs across the Granton site could provide a pathway from the site straight to the foreshore if the fault is open. The rapid azimuthal electromagnetic technique (Appendix A) may, with further development and understanding of the theory, detect whether or not the fault is conducting.

Data Processing

- With an increased quantity of data (due to the addition of TDEM data) 3-D inversion (and joint inversion of resistivity and electromagnetic data) will become more profitable thus providing a 3-D solution to a 3-D problem. However, model non-uniqueness will inherently be a restriction.
- The main interpretations of the resistivity survey at Granton have, on a fine scale, assumed a smoothly varying earth concentrating more closely on the major resistivity

anomalies caused by larger scale geological features (e.g. faults and varying geological units). The fine scale heterogeneities of the real earth are smoothed out by inversion, interpolation and forward modelling. In order to accommodate these heterogeneities it may be possible to complete all data processing using a logarithmic scale for resistivity to focus on the order of magnitude resistivity variations which are more representative of varying geological units.

REFERENCES

Abramowitz, M. and Stegun, I. A., editors (1973). *Handbook of Mathematical Functions*. Dover (New York).

Archie, G. E. (1942). The electrical resistivity log as an aid in determining some reservoir characteristics. Trans. AIME.

Barker, R. D. (1979). Signal contribution sections and their use in resistivity studies. *Geophys. J. R. astr. Soc.*, **59**, 123–129.

Barker, R. D. (1980). Applications of geophysics in groundwater investigations. *Water Serv.*, **84**, 489–492.

Barker, R. D. (1981). The offset system of electrical resistivity sounding and its use with a multicore cable. *Geophysical Prospecting*, **29**, 128–143.

Barker, R. D. (1992). A simple algorithm for electrical imaging of the subsurface. *First Break*, **10**(2), 53–62.

Bauman, P. D., Lockhard, M., Sharma, A., and Kellett, R. (1997). Case studies of 2-D resistivity surveying for soils, waste management, geotechnical, and groundwater contaminant investigations. In *Proceedings of the Symposium on the Applications of Geophysics to Engineering and Environmental Problems, Reno, Nevada.*, volume 1, pages 261–270.

Benson, R. C. (1993). *Geotechnical Practice for Waste Disposal*, chapter Geophysical Techniques for Subsurface Site Characterisation. Chapman and Hall, London.

Berkowitz, B. and Scher, H. (1996). Influence of embedded fractures on contaminant diffusion in geological formations. *Geophysical Research Letters*, **23**(9), 925–928.

Bernard, J. and Valla, P. (1991). Groundwater exploration in fissured media with electrical and VLF methods. *Geoexploration*, **27**, 81–91.

Brace, W. F. (1980). Permeability of crystalline and argillaceous rocks. *Int. J. Rock Mech.Min. Sci. Geomech. Abs.*,, **17**, 241–251.

Brewitt-Taylor, C. R. and Weaver, J. T. (1976). On the finite difference solution of two-dimensional induction problems. *Geophysical Journal of the Royal Astronomical Society*, **47**, 375–396.

Brown, S. (1989). Transport of fluid and electric current through a single fracture. *Journal of Geophysical Research*, **94**(B7), 9429–9438.

Brown, S. and Sholtz, C. H. (1985). Closure of random elastic surfaces in contact. *Journal of Geophysical Research*, **90**, 5531–5545.

Buselli, G., Barber, G., Davis, G. B., and Salama, R. B. (1990). *Geotechnical and Environmental Geophysics*, volume II, chapter Detection of groundwater contamination near waste disposal sites with transient electromagnetic and electrical methods. Society of Exploration Geophysics.

Campus Geophysical Instruments Ltd. (1994a). *Electrical tomography with the GEOPULSE, IMAGER25 and IMAGER50 modules*. Campus Geophysical Instruments Ltd, England.

Campus Geophysical Instruments Ltd. (1994b). *GEOPULSE*. Campus Geophysical Instruments Ltd, England.

Campus Geophysical Instruments Ltd. (1994c). *RES2DECO user's manual*. Campus Geophysical Instruments Ltd, England.

Carpenter, P. J., Kelley, M. C., and Kaufman, R. S. (1994). Azimuthal resistivity surveys over a fractured landfill cover. *Bulletin of the Association of Engineering Geology*, **XXXI**(1).

Couper, A. S. (1998). North Edinburgh project. In *Contaminated Soil Conference Proceedings, Edinburgh, U.K.*, page 495.

Darayan, S., Liu, C., Shen, L. C., and Shattuck, D. (1998). Measurement of electrical properties of contaminated soil. *Geophysical Prospecting*, **46**, 447–488.

Darcy, H. (1856). Les fontaines publiques de la vile de Dijon. V. Dalmont, Paris.

David, C. (1993). Geometry of flow paths for fluid transport in rocks. *Journal of Geophysical Research*, **98**(B7), 12,267–12,278.

deGroot Hedlin, C. and Constable, S. (1990). Occam's inversion to generate smooth, two-dimensional models from magnetotelluric data. *Geophysics*, **42**, 1020–1036.

Earth Science News (1993). Newsletter. Earth Science Systems Ltd, Harpenden, U.K.

Environment Act (1995). *Statutory guidance and regulations on contaminated land*. Department of the Environment.

Gardiner, A. B. (1997). Comparison of 2-D resistivity sections and seismic refraction data over an industrial site. Undergraduate report for the University of Edinburgh.

Geonics Ltd (1991). *EM31 Operating Manual.* Geonics Ltd, Canada.

Ghatge, S. L. (1993). Microgravity methods for the detection of abandoned shafts of the Schuyler copper mine in northeastern New Jersey. In *Proceedings of the Symposium on the Applications of Geophysics to Engineering and Environmental Problems, Orlando, Florida.*, pages 195–208.

Goldstein, N. E., Benson, S. M., and Alumbaugh, D. (1990). *Geotechnical and Environmental Geophysics*, volume II, chapter Saline groundwater plume mapping with electromagnetics. Society of Exploration Geophysics.

Grant, F. S. and West, G. F. (1965). *Interpretation Theory in Applied Geophysics.* McGraw Hill, New York.

Griffiths, D. H. and Barker, R. D. (1993). Two dimensional resistivity imaging and modelling in areas of complex geology. *Applied Geophysics*, **29**, 211–226.

Habberjam, G. M. and Watkins, A. A. (1974). Aapoximate rules for the composition of apparent resistivity sections. *Geophysical Prospecting*, **22**, 393–420.

Habberjam, G. M. and Watkins, G. E. (1967). The use of a square array configuration in resistivity prospecting. *Geophysical Prospecting*, **15**, 445–467.

Heigold, P. C., Gilkeson, R. H., Cartwright, K., and Reed, P. C. (1979). Aquifer transmissivity from surficial electrical methods. *Ground Water*, **17**(4), 338–344.

Hestenes, M. R. and Stiefel, E. (1952). Method of conjugate gradients for solving linear systems. *J. Res. Nat. Bur. Standards*, **49**, 409–436.

Hobbs, B. A. and Reading, A. M. (1994). Shallow fault location in coal measures using offset Wenner resistivity profiling. *Geophysical Prospecting*, **42**, 343–356.

Imperial Chemical Industries plc (1992). *Assessing Soil and Groundwater Contamination.* ICI International Soil and Groundwater Panel.

Jansen, J., Pencak, M., Gnat, R., and Haddad, B. (1993). Some applications of frequency domain electromagnetic induction surveys for landfill characterization studies. In *Proceedings of the Symposium on the Applications of Geophysics to Engineering and Environmental Problems, San Diego, California.*, volume 1, pages 259–271.

Kelly, W. E. and Frohlich, R. K. (1985). Relations between aquifer electrical and hydraulic properties. *Ground Water*, **23**(2), 182–189.

Kelly, W. E. and Reiter, P. F. (1984). Influence of anisotropy on relations between aquifer hydraulic and electrical properties. *Journal of Hydrology*, **3/4**.

Knipe, R. J., Jones, G., and Fisher, Q. J. (1998). Faulting, fault sealing and fluid flow in hydrocarbon reservoirs: an introduction. In G. Jones, Q. J. Fisher, and R. J. Knipe, editors, *Faulting, Fault Sealing and Fluid Flow in Hydrocarbon Reservoirs. Geological Society Special Publication*, number 147. The Geological Society.

Larson, T. H., Krapac, I. G., Dey, W. S., and Suchomski, C. J. (1997). Electromagnetic terrain conductivity surveys used to screen swine confinement facilities for groundwater contamination. In *Proceedings of the Symposium on the Applications of Geophysics to Engineering and Environmental Problems, Reno, Nevada.*, volume 1, pages 271–279.

Li, Y. and Oldenburg, D. W. (1994). Inversion of 3-D DC resistivity data using an approximate inverse mapping. *Geophysical Journal International*, **116**, 527–537.

Loke, M. H. (1994). *The inversion of two-dimensional apparent resistivity data.* Ph.D. thesis, University of Birmingham.

Loke, M. H. and Barker, R. D. (1996). Rapid least squares inversion of apparent resistivity pseudosections by a quasi-Newton method. *Geophysical Prospecting*, **44**, 131–152.

Lunn, R. L., Browne, M. B., and Ball, D. B. (1997). A scoping study to determine the hydrogeological conditions for contaminant transport beneath West Granton. Report prepared by the University of Edinburgh for Edinburgh City Council.

McCann, D. M. (1994). Geophysical methods for the assessment of landfill and waste disposal sites: a review. *Land Contamination and Reclamation*, **2**(2), 73–83.

Mills, T., Hoekstra, P., Blohm, M., and Evans, L. (1988). Time domain electromagnetic soundings for mapping sea water intrusion in Monterey County, CA. *Ground Water*, **26**, 771–782.

Mitchell, G. H. and Mykura, W. (1962). The geology of the neighbourhood of Edinburgh. One-inch geological sheet 32 53, British Geological Survey.

Monier-Williams, M. (1995). Properties of Light Non-Aqueous Phase Liquids and detection using commonly applied shallow sensing geophysical techniques. In *Proceedings of the Symposium on the Applications of Geophysics to Engineering and Environmental Problems, Orlando, Florida.*, pages 1–14.

Nash, M. S., Atekwana, E., and Sauck, W. A. (1997). Geophysical investigation of anomalous conductivity at a hydrocarbon contaminated site. In *Proceedings of the Symposium on the Applications of Geophysics to Engineering and Environmental Problems, Reno, Nevada.*, volume 2, pages 261–270.

Ngwenya, N. T. (1998). Laboratory determination of flow and contaminant transport parameters for lithologies beneath the west granton site. Report prepared by the University of Edinburgh for Edinburgh City Council.

Park, S. K. and Van, G. P. (1991). Inversion of pole-pole data for 3-D resistivity structure beneath arrays of electrodes. *Geophysics*, **56**, 951–960.

Pierce, D. and DeReamer, J. (1993). Geophysical investigation for buried drums. In *Proceedings of the Symposium on the Applications of Geophysics to Engineering and Environmental Problems, Orlando, Florida.*, pages 229–244.

Pittman, E. D. (1984). The pore geometry of reservoir rocks, in physics and chemistry of porous media. In *American Institute of Physics Conference Proceedings*, volume 107, pages 1–19.

Press, W. H., Flannery, B. P., Teukolsky, S. A., and Vetterling, W. T. (1986). *Numerical Recipes*. Cambridge University Press.

Reynolds, J. M. (1997). *An Introduction to Applied and Environmental Geophysics*. John Wiley and Sons Ltd, Chichester and London.

Ritzi, R. W. and Andolsek, R. H. (1992). Relation between anisotropic transmissivity and azimuthal resistivity surveys in shallow fractured carbonate flow systems. *Groundwater*, **30**(5), 774–780.

Roberts, R. L., Hinze, W. J., and Leap, D. I. (1990). *Geotechnical and Environmental Geophysics*, volume II, chapter Data enhancement procedures on magnetic data from landfill investigations. Society of Exploration Geophysics.

Sasaki, Y. (1992). Resolution of resistivity tomography inferred from numerical simulation. *Geophysical Prospecting*, **40**, 453–464.

Sauck, W. A. and Zabik, S. M. (1992). Azimuthal resistivity and the directional variations of hydraulic conductivity in glacial sediments. In *Proceedings of the Symposium on the Applications of Geophysics to Engineering and Environmental Problems*, pages 197 – 222.

Sauck, W. A., Atekwana, E. A., and Nash, M. S. (1998). High conductivities associated with an lnapl plume imaged by integrated geophysical techniques. *J. Environmental and Engineering Geoph.*, **2**(3), 203–212.

Schneider, G. W., Ryck, S. M. D., and Ferre, P. A. (1993). The application of automated high resolution DC resistivity in monitoring hydrogeological field experiments. In *Proceedings of the Symposium on the Applications of Geophysics to Engineering and Environmental Problems, Orlando, Florida.*, pages 39–50.

Schwarz, S. D. (1990). Application of geophysical methods to groundwater exploration in the Tolt River Basin, Washington State. In S. H. Ward, editor, *Geotechnical and Environmental Geophysics*. Society of Exploration Geophysicists.

Scottish Office (1996). Scottish vacant and derelict land survey.

Sibbit, A. M. and Faivre, O. (1985). The dual laterolog response in fractured rocks. In *SPWLA Annual Logging Symposium*, pages T1–T34.

Spitzer, K. (1995). A 3-D finite-difference algorithm for DC resistivity modelling using conjugate gradient methods. *Geophysical Journal International*, **123**, 903–914.

Vickery, A. C. (1996). The development of non-invasive geophysical techniques for the detection of electrically conducting pollutants. Transfer Report prepared for the University of Edinburgh.

Vickery, A. C. and Hobbs, B. A. (1997a). Electromagnetic (EM31) geophysical survey over the former Texaco site. Report prepared by the University of Edinburgh for Edinburgh City Council.

Vickery, A. C. and Hobbs, B. A. (1997b). Using azimuthal electromagnetic methods to detect leachate pathways. In *Proceedings of the European Geophysics Society Conference, Vienna, Austria*, page C96.

Vickery, A. C. and Hobbs, B. A. (1998a). Contributions of surface geophysics to the site investigation of former oil distribution terminals. *J. Environmental and Engineering Geoph.*, **3**(3), 1–10.

Vickery, A. C. and Hobbs, B. A. (1998b). Resistivity geophysical survey over the West Granton site. Report prepared for Edinburgh City Council.

Vickery, A. C. and Hobbs, B. A. (1999). Removing the effects of subsurface conducting pipes from apparent resistivity pseudosections. In preparation.

Wait, J. R. (1982). *Geo-electromagnetism*. Academic Press.

Watson, K. and Barker, R. (1998). Discriminating between true and pseudo-anisotropic ground using azimuthal resistivity soundings. In *Proceedings of the Environmental and Engineering Geophysical Society, Barcelona, Spain.*, pages 849–852.

Weaver, J. T. and Agarwal, A. K. (1993). Automatic 1-D inversion of magnetotelluric data by the method of modelling. *Geophysical Journal International*, **112**, 115–123.

Zhang, J., Mackie, R. L., and Madden, T. R. (1995). 3-D resistivity forward modelling and inversion using conjugate gradients. *Geophysics*, **60**, 1313–1325.

Zhody, A. A. R. (1989). A new method for the automatic interpretation of Schlumberger and Wenner sounding curves. *Geophysics*, **54**(2), 245–253.

A AZIMUTHAL ELECTRICAL AND ELECTROMAGNETIC SURVEYS

A.1 Introduction

The original aim of this work was to assess and ultimately develop a method for the detection of contaminants and their pathways. The relative success of azimuthal resistivity techniques for the assessment of fracture systems lead to the investigation of azimuthal electromagnetic techniques for the evaluation of preferred contaminant flow directions.

Direct comparisons are made between azimuthal resistivity and electromagnetic measurements and a new method of presentation for the data is proposed.

A.2 Azimuthal Resistivity

Faults and fractures have greater electrical conductivity along the orientation of the fracture. As a result of this relationship between electrical and hydraulic resistivity (Section 2.5.2), azimuthal surveys are frequently employed to infer the direction of preferred groundwater flow. An azimuthal resistivity survey measures ground resistivity as a function of azimuth to determine the level of electrical anisotropy of the earth (Figure A.1).

Under ideal conditions, the major axis of elongation on plots of apparent resistivity as a function of azimuth will parallel the trend of preferred flow, a phenomenon known as the paradox of anisotropy (Keller and Frischknecht, 1966). The phenomenon is termed paradoxical because intuitively one expects the apparent resistivity to be lower in the orientation of preferred current flow but the converse is true. This is a consequence of apparent resistivity values being calculated assuming an isotropic medium where current lines can diverge freely. In an anisotropic medium, current flow is concentrated in a particular direction. Therefore, when an electrode array is aligned with the direction of concentrated current flow, the potential drop increases due to the increased current density along that pathway thus producing a higher measure of apparent resistivity. This is represented in Figure A.2.

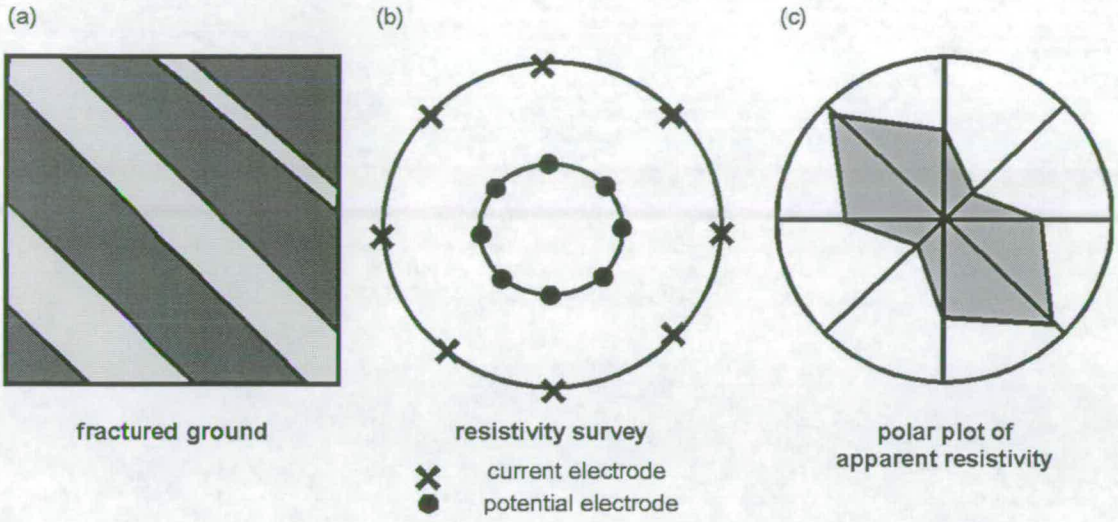

Figure A.1: The azimuthal resistivity technique.

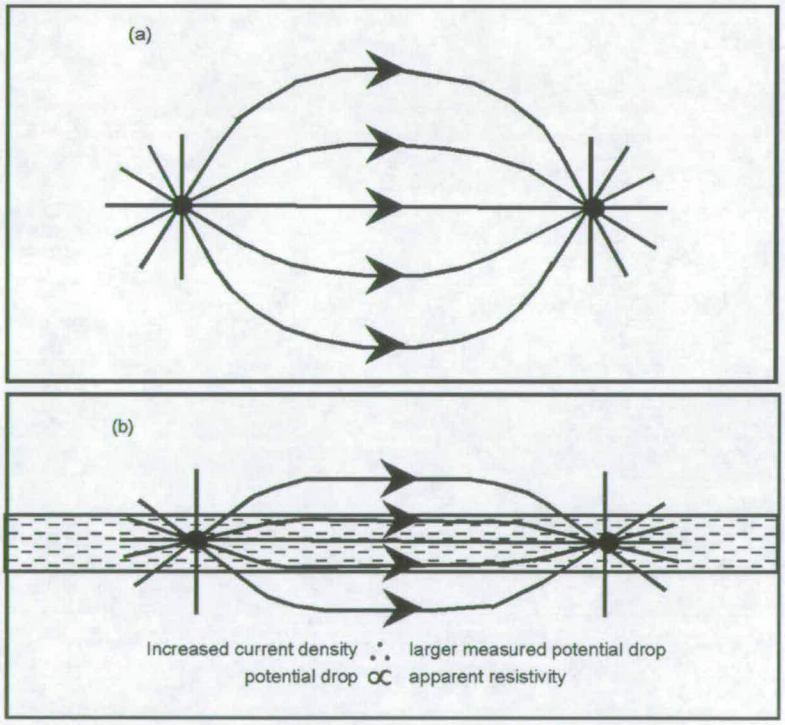

Figure A.2: The paradox of anisotropy. (a) Current lines diverge freely in an isotropic medium but (b) current lines become concentrated along the line of the electrode array when the array is aligned in the direction of layering or foliation.

A.3 Azimuthal Electromagnetics

The azimuthal electromagnetic surveying follows the same principles as the resistivity method (Figure A.3) but it should be noted that the results are displayed as a polar plot of conductivity rather than resistivity. This switch occurs because, for vertical dipole electromagnetic measurements, the electric current flow between transmitter and receiver is orthogonal to that in a resistivity measurement (Figure A.4) so the paradox does not hold. Consequently, for the comparison of the data presented in this section, azimuthal resistivity results are shown as apparent resistivity polar plots and azimuthal electromagnetic results are shown as apparent conductivity polar plots.

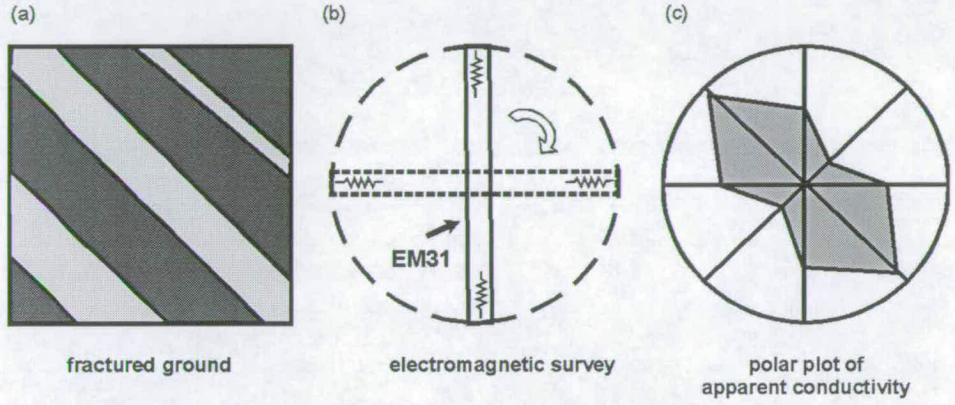

Figure A.3: The azimuthal electromagnetic technique.

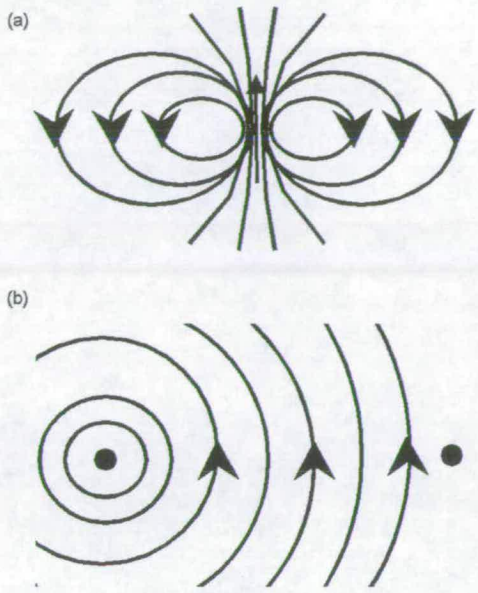

Figure A.4: (a) Magnetic and (b) electric field lines a vertical dipole electromagnetic technique.

A.4 Azimuthal studies at Niddrie

The Niddrie site, 5 miles east of Edinburgh, was chosen for testing azimuthal techniques because of the obvious directional dependence in the subsurface geology. The geology of the area consists of steeply dipping interbedded limestones and coals (Figure A.5).

The azimuthal surveys were completed within a large flat field. Three techniques were chosen for comparison: traditional azimuthal resistivity soundings, azimuthal EM31 and Max-Min (frequency domain electromagnetic technique with separate loops and adjustable frequencies). The relative locations of the surveys for each technique are shown in Figure A.6.

A.4.1 Comparison of Azimuthal Resistivity and Electromagnetic Surveys

EM31

For the comparison of the EM31 data with the resistivity data, the 9 electromagnetic azimuthal data sets positioned within the area covered by the resistivity survey, were used (A - C, 1 - 3). In order to distinguish between directional dependence and noise, the results are 'normalised' i.e. a percentage of directional dependence is calculated for each azimuthal survey $\frac{(max-min)}{average}$ and the maximum diameter of the polar plot is proportional to the percentage of directional

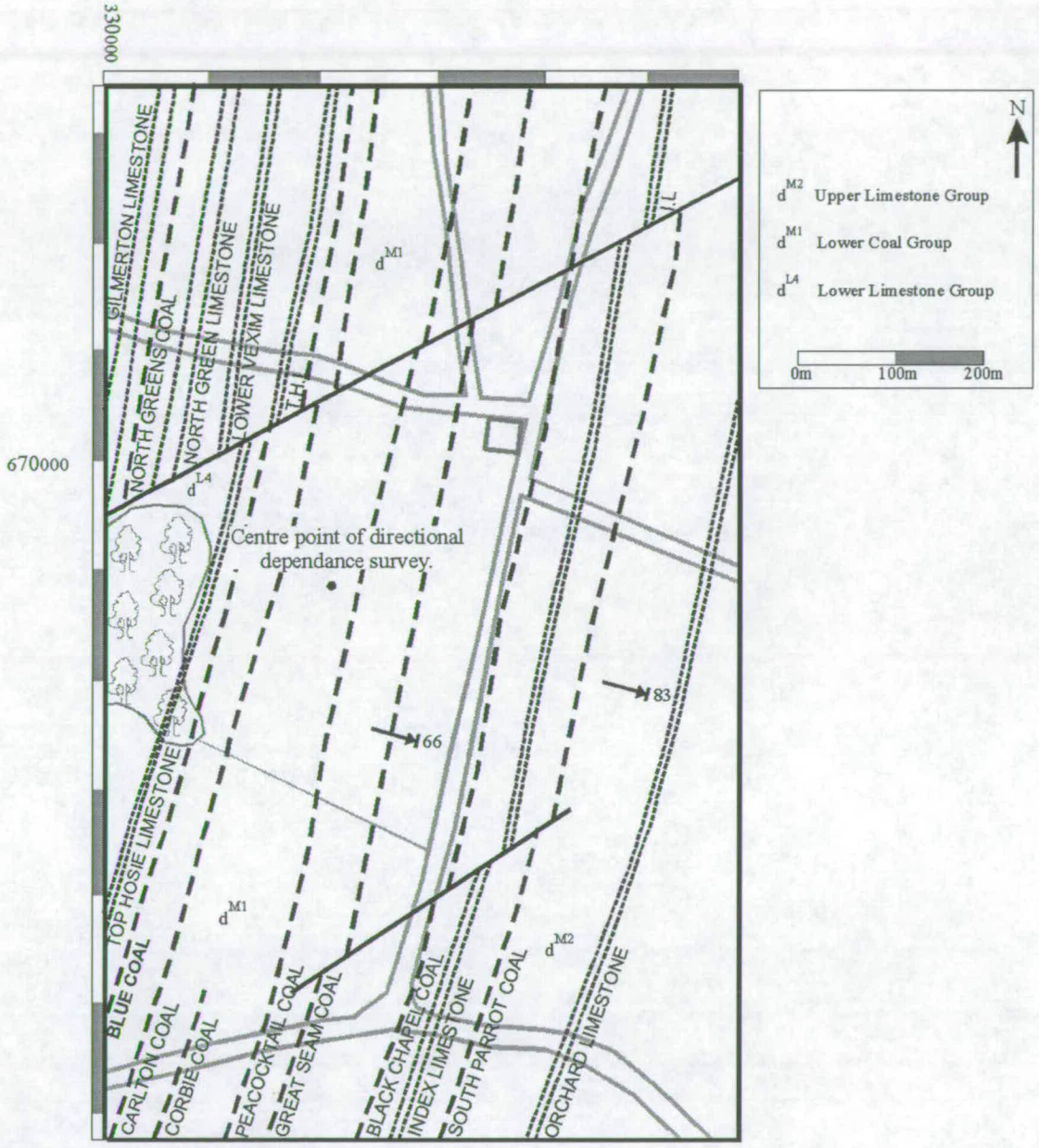

Figure A.5: Map of the geology in the Niddrie survey area.

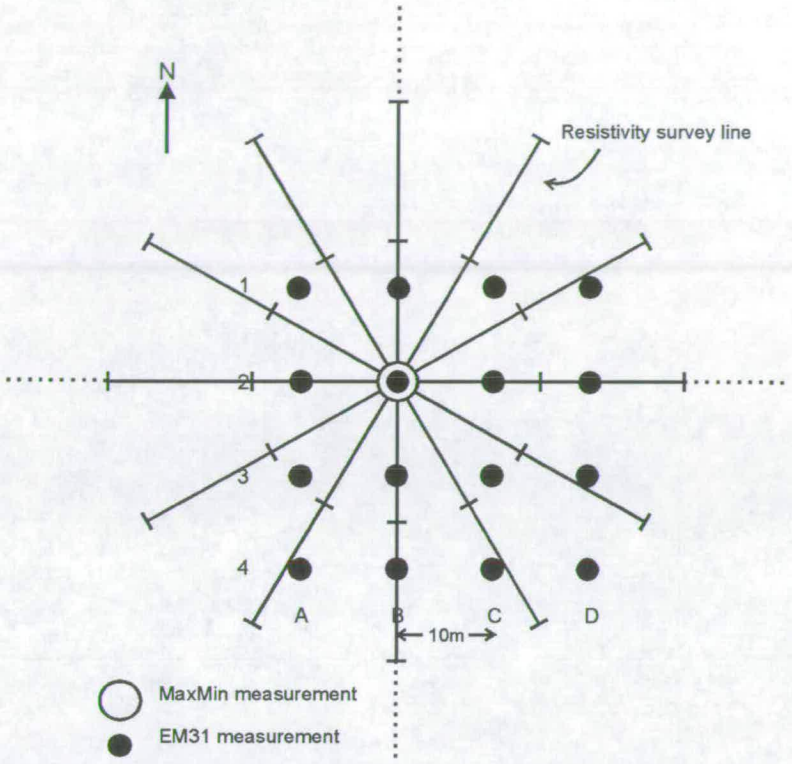

Figure A.6: Relative location of the azimuthal resistivity, EM31 and Max-Min surveys.

dependence shown. The minimum diameter of the polar plot is fixed at one third of the full plot diameter. The resulting polar plots of the EM31 data are shown in Figure A.7. The polar plots show very similar azimuths of maximum conductivity. The 9 azimuthal electromagnetic data sets were averaged for comparison with the azimuthal resistivity data.

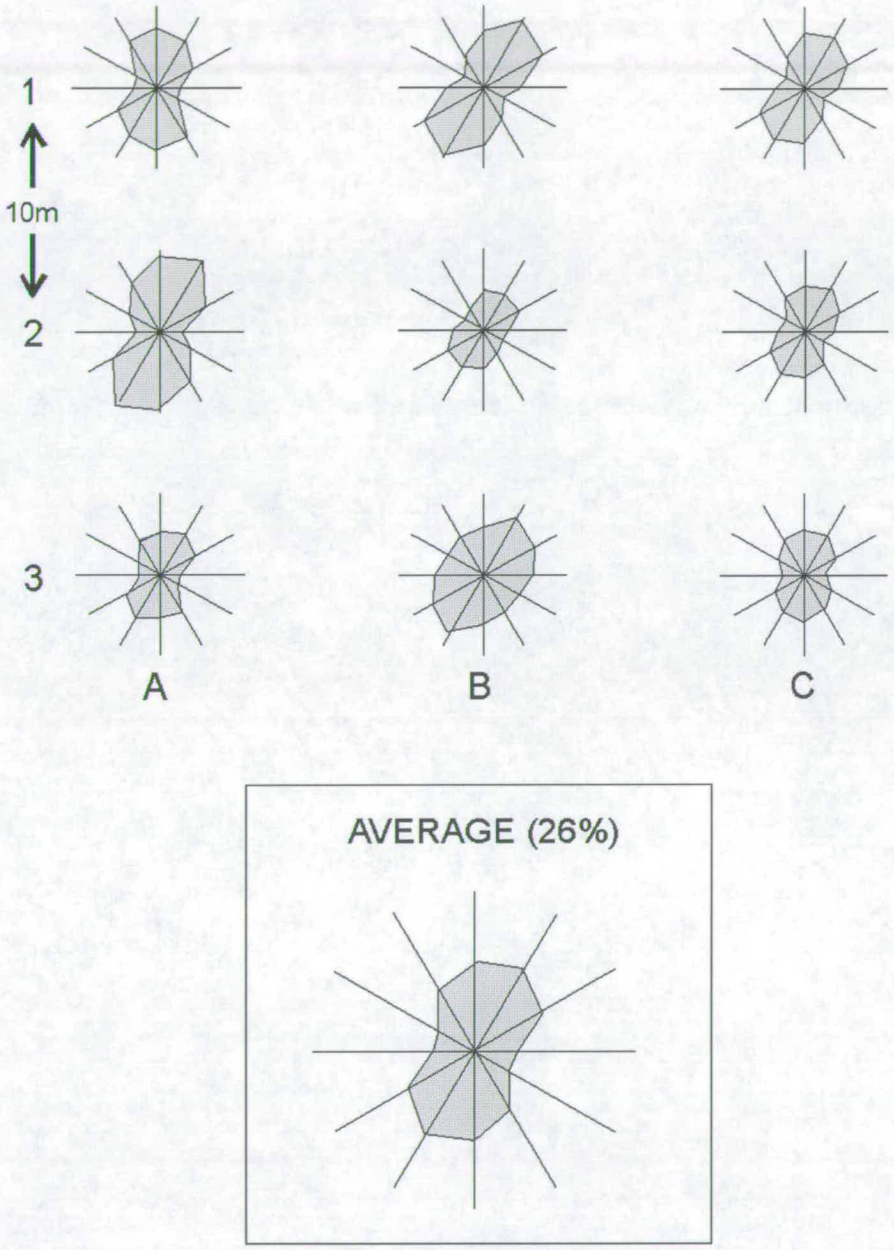

Figure A.7: Normalised polar plots representing the results of 9 azimuthal EM31 surveys.

Resistivity

The azimuthal resistivity sounding yields several polar plots corresponding to each electrode spacing i.e. different depths of investigation. Electrode spacings of 2, 4, 8, 16 and 32m were used for this survey.

The azimuthal resistivity results show that there is little directional dependence in the shallow subsurface ($\leq$ 2m) where the survey is probably sampling the soils but at greater depths (around 6m, comparable to depth of penetration of the EM31), the directional dependence becomes significantly greater (Figure A.1). The average polar plot from the EM31 survey has an almost identical form to that of the resistivity data at comparable depths.

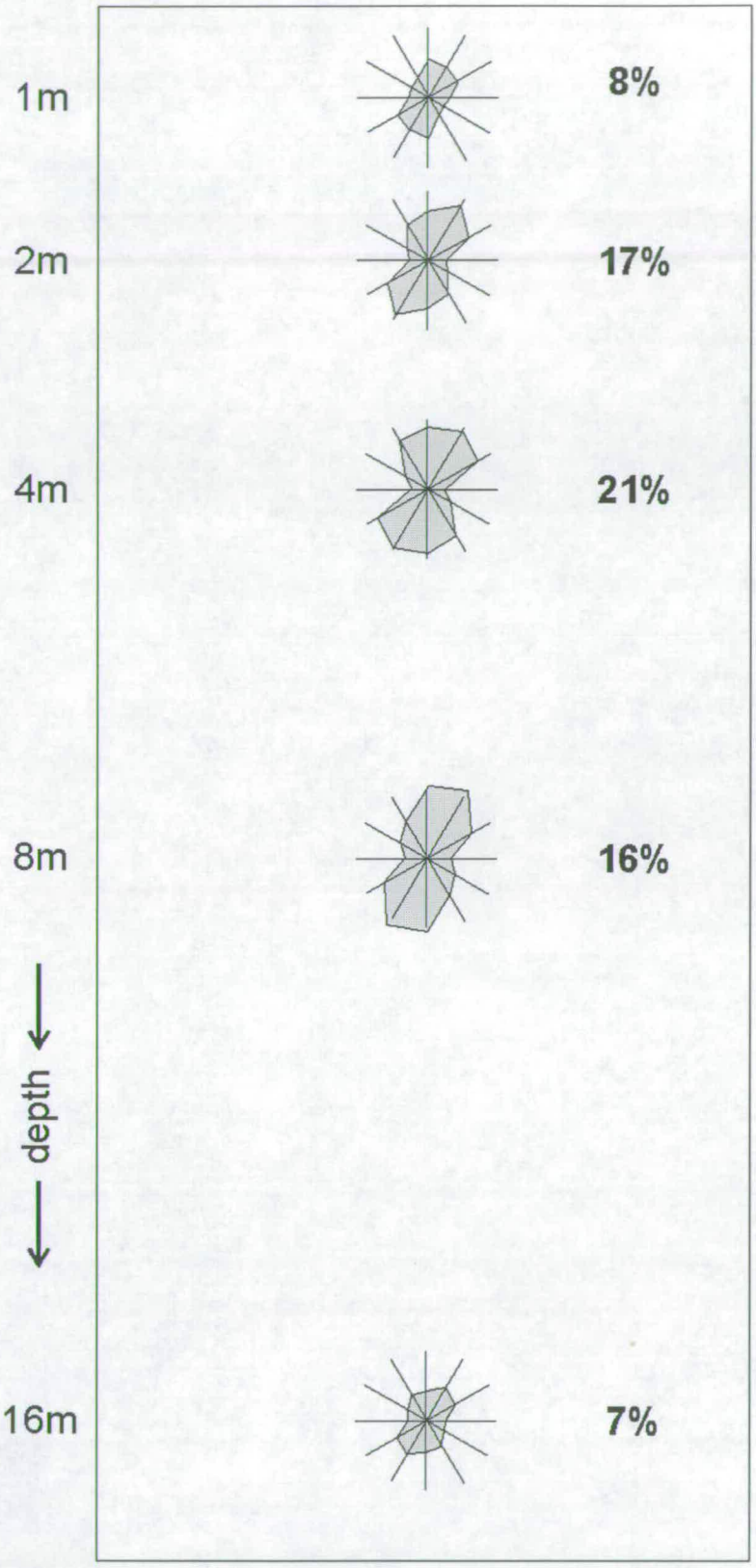

Figure A.8: Normalised polar plots representing the results of an azimuthal resistivity sounding. (Percentages denote the strength of the directional dependence).

Max-Min

The Max-Min survey was completed with a coil separation of 25m. The depth of penetration is predominantly controlled by the coil separation (depth of penetration ≈ half the coil separation) but the frequency also effects the penetration depth. The lower the frequency the greater the depth of penetration. The Max-Min results (Figure A.9) are also displayed as 'normalised' polar plots. The azimuth of maximum conductivity (out of phase component) matches those calculated from both the EM31 and resistivity data. The percentage (strength) of directional dependence shown in the Max-Min results is far greater than those detected by either of the other survey techniques. This could either show the sensitivity of the technique or represent an increased directional dependence at that depth.

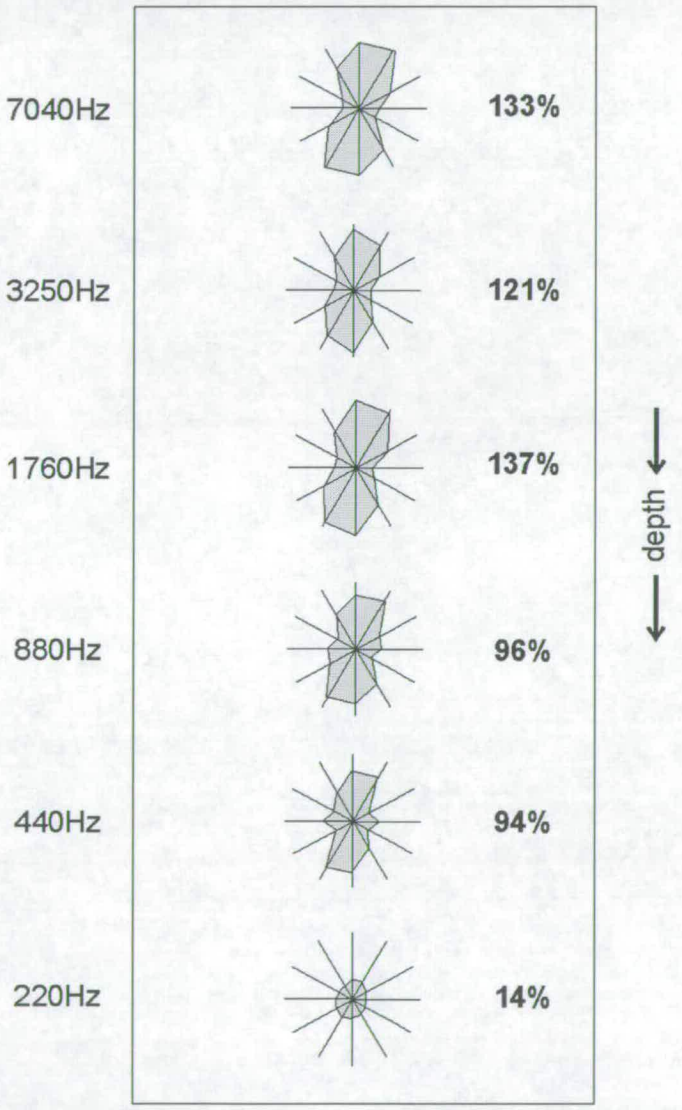

Figure A.9: Normalised polar plots representing the results of an azimuthal electromagnetic (Max-Min) sounding. (Percentages denote the strength of the directional dependence).

A.4.2 Presentation of Azimuthal Survey Results

As a final method of presentation for azimuthal data, the polar plots are replaced by double headed arrows. The arrow lies in the direction of maximum directional dependence with a length proportional to percentage strength of the dependence. An example is given in Figure A.10. This represents all 12 azimuthal EM31 surveys measured at Niddrie.

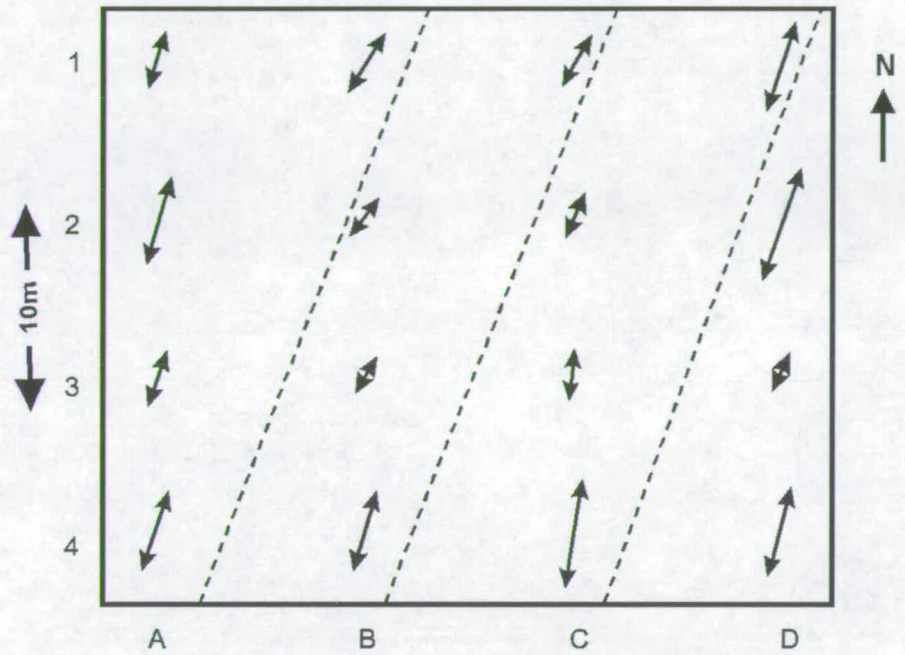

Rose diagram of polar plot orientations

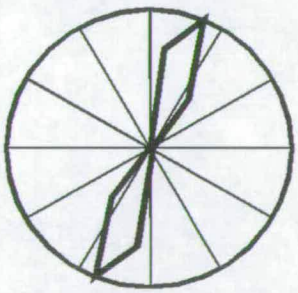

Figure A.10: Normalised double headed arrows representing the results of 12 azimuthal EM31 measurements.

The direction of maximum conductivity is clearly similar in all polar plots. In order to quantify the similarity in direction, a rose diagram was constructed. The complete 180^o was split into 15^o bins and the azimuth of maximum conductivity was measured for each survey and put into the appropriate bin. The rose diagram for the azimuthal EM31 survey (bottom of Figure A.10) clearly indicates a preferred orientation of current flow within the subsurface.

A.5 Conclusions

The azimuthal electromagnetic technique has distinct advantages over the azimuthal resistivity technique. These advantages are presented in the Table A.1 below.

Table A.1: Advantages of the azimuthal electromagnetic technique

Requirements	**Azimuthal Resistivity**	**Azimuthal Electromagnetics**
No. of field members	≥ 3	2
Area of open ground	6 x depth of investigation	2 x depth of investigation
Terrain	suitable for good electrode contact	
Time to complete measurement	$\approx$2 hours	$\approx$30 mins

This azimuthal technique produces very specific information and could prove useful in a final survey to locate particular contaminant pathways especially with improved, easily interpretable methods of data presentation. However, it is not suitable as a rapid survey tool to assess the degree of contamination on a site.

B METHODOLOGY OF THE EM31

Electro-magnetic ground conductivity mapping has been in use since the early 1960s and is perhaps one of the most frequently used geophysical methods in environmental and engineering applications today.

B.1 Principle of EM31 Operation

A transmitting coil of wire is separated from a receiving coil by a fixed distance of 1.66m. The coils are housed within a plastic boom. The transmitter generates an electromagnetic (EM) field by passing an alternating current through the coil. In the case of the EM31, the frequency of the generated field is 9.6kHz. The field is made up of two orthogonal vector components, an electrical intensity (E) and a magnetising force (H) in a plane perpendicular to the direction of propogation (Figure B.1). The field generated by the transmitter coil is the primary EM field, which propagates above and below the ground. If a conductive medium is present within the ground the magnetic component of the EM field induces eddy currents (alternating currents) within the conductor. These eddy currents then generate their own, secondary, EM field, which is detected by a receiver. The receiver also detects the primary field which travels through the air so the overall response of the receiver is the combined (resultant) effect of both the primary and secondary fields (Figure B.2). Consequently, the measured response will differ in both phase and amplitude relative to the transmitted primary field. The measuring system compensates for the primary field so that it can measure the amplitude of the secondary field. Within the linear regime of the EM31 (for conductivites around 'expected' soil conductivties) the ratio of the two fields is in direct proportion to the apparent conductivity of the ground through which the EM radiation has passed.

Eddy currents within a conductor take a finite time to generate. This generation time is manifest as the phase lag. Good conductors can yield large phase lags and in poor conductors the phase lag is small. The generated secondary magnetic field interacts with the primary to form a resultant magnetic field, which has a total phase lag behind the primary magnetic field. The resultant field can be represented by the real (in-phase) and imaginary (quadrature) components. The maximum effective depth of penetration (defined primarily by the frequency of the transmitted EM field and the intercoil spacing) is 6m.

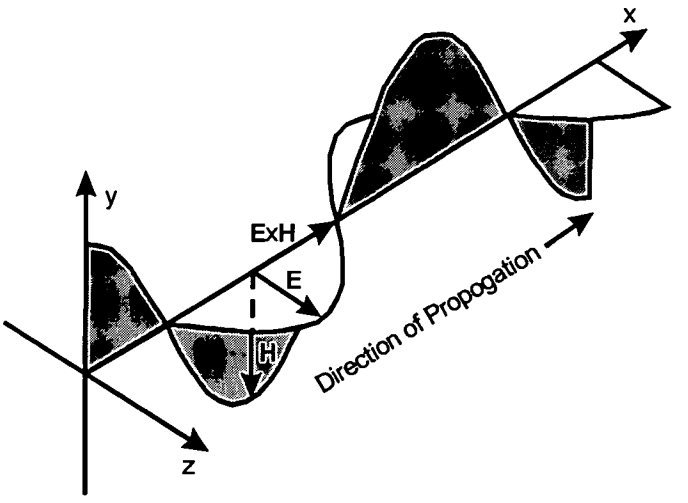

Figure B.1: The principal electric (**E**) and magnetic (**H**) components of an electromagnetic wave.

B.2 Modes of Deployment

The orientation of the transmitter and receiver coils influences the depths of penetration achievable. When the plane of the coils lies parallel to the ground surface, the Magnetic Dipole orientation is said to be vertical, hence the term Vertical Magnetic Dipole (VMD). When the coils are at right angles to the ground surface, this is known as the Horizontal Magnetic Dipole (HMD) orientation. Effective depths of penetration are typically 0.75 and 1.5 times the inter-coil separation in the HMD and VMD orientations respectively.

For EM31 surveys, measurements can also be taken in orthogonal directions at each point for each dipole orientation. The EM31 boom is rotated throughout 90^o about a vertical axis. Differences in readings are attributed to lateral inhomogeneities in the conductivity of the subsurface.

The EM31 is capable of recording both the in-phase and the quadrature components. The quadrature component is measured in terms of the apparent conductivity in milli-Siemens per metre (mS/m) while the in-phase component is read as parts per thousand (ppt). The apparent conductivity measured is the weighted average of all the true conductivities present within a volume of material sampled at the time of measurement.

B.3 Interpretation

Great care must be taken in the interpretation of EM data with particular consideration given to the coil locations and the range of conductivities for which the EM31 is within its linear

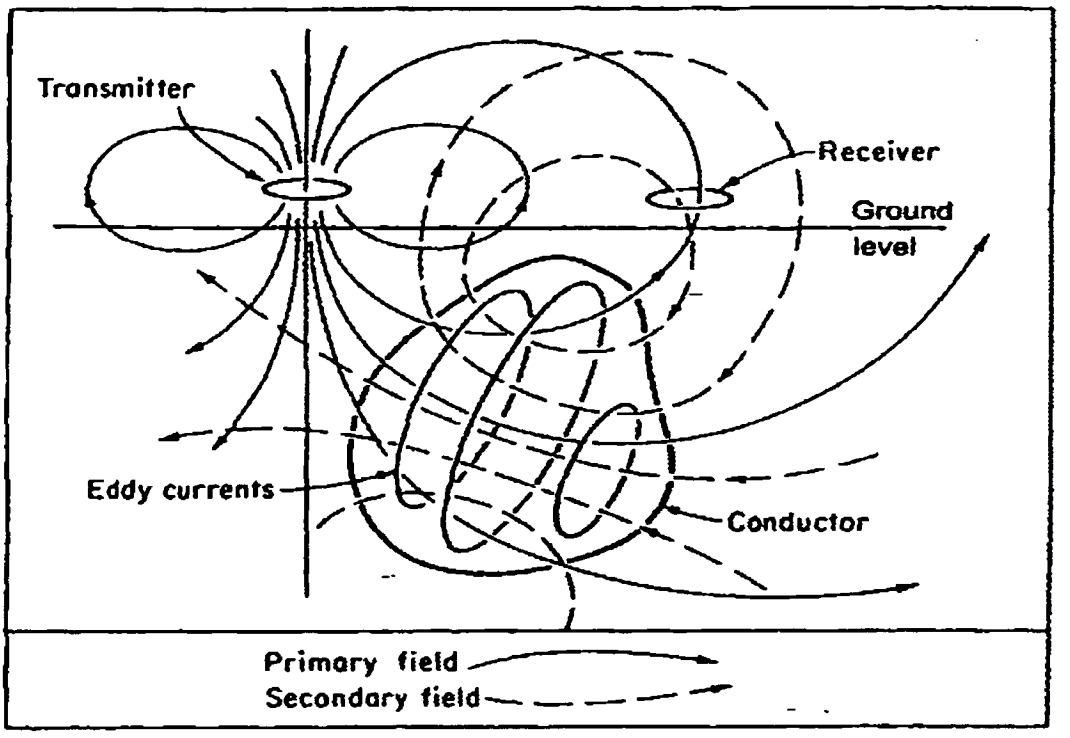

Figure B.2: Generalised schematic of the EM surveying method. Reproduced from Grant and West (1965)

response regime. It is usual to imagine that it is always the anomalous high or low values that correlate with buried targets. This is not necessarily true with EM ground conductivity mapping. The anomaly of a particular causative body can vary depending on the position of the transmitter and receiver coils relative to the body. A linear conductive target, for example a metal pipe whose width is much shorter than the inter-coil separation, may generate an 'M' shaped anomaly. That is it consists of two high values separated by a low (sometimes negative) in between, where the horizontal distance between the high peaks is of the order of the inter-coil separation. The low occurs when the two coils straddle the pipe. When the two coils remain on the same side of the pipe, the pipe is seen as a conductive body.

A comprehensive description of further EM surveying methods is given by Reynolds (1997).

C DESCRIPTION OF BOREHOLES IN GRANTON AREA

The borehole logs used in the geological desk study of the Granton Area were constructed from British Geological Survey archive data. The descriptions of the logs were written by Mike Browne.

Five dip-orientated lines of borehole graphic sections (Figures C.1 - C.5) have been collated to augment the geophysical profiles. The combination of the shallow depth of each borehole and the generally steep apparent dip (20-30^o) observed in the cores means that there is almost certainly no overlap of the stratigraphical record between bore sites along the transects (assuming no intervening faults). The direction of apparent dip is inferred based on current knowledge of the geological structure.

Transect 1: the stratal gap between the top of Borehole C5 and the base of C1 is likely to be $>22m$; similarly the gap between C1 and C7 and between C7 and C9 is $>6m$ in both cases. All the succession is above the Ravelston Sandstone of the infilled quarry and local shore section. The un-named sandstone in C7 is likely to be the same as that in BGS 22 and C10 in Transect 2. The small dolerite intrusions in C1 are probably two of those seen in the shore section to the north.

Transect 2: The record of BGS 22 is likely to be unreliable but the sandstone in it is probably to be correlated with that in the lower part of C10. The sandstone is un-named and lies well above the Ravelston Sandstone. This transect is cut by a fault between the sites of BGS 7/1 and C10.

Transect 3: The sandstone at the base of C6 is likely to be the top of the Ravelston Sandstone.

Transect 4: The transect may be unfaulted. The stratal gaps between the tops and bottoms of adjacent boreholes are estimated to be as follows;- BGS 72 and 74 is $>14m$; BGS 74 and 47 is $>9m$; BGS 47 and 46 is $>7m$; 46 and 45 is $>18m$; BGS 45 and 44 is $>7m$. BGS 47 may be located on the basal part of the Ravelston Sandstone.

Transect 5: The stratal gap between the top of the un-correlated sandstone in BGS 75 and the sandstone forming the base of BGS 73 is $>16m$. The geology of the SW corner of the site is obscure without further work (e.g. in the gasworks site).

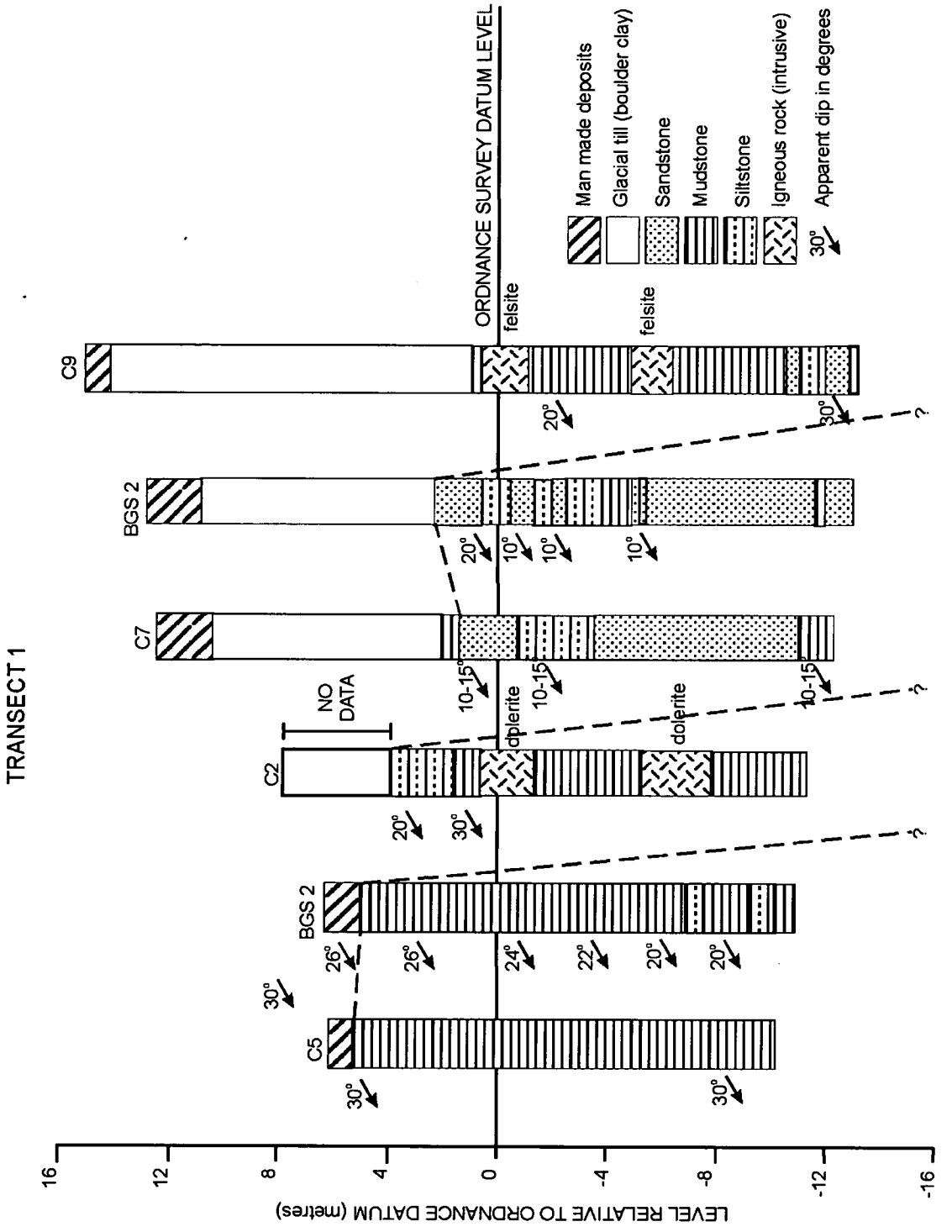

Figure C.1: Borehole logs from Transect 1

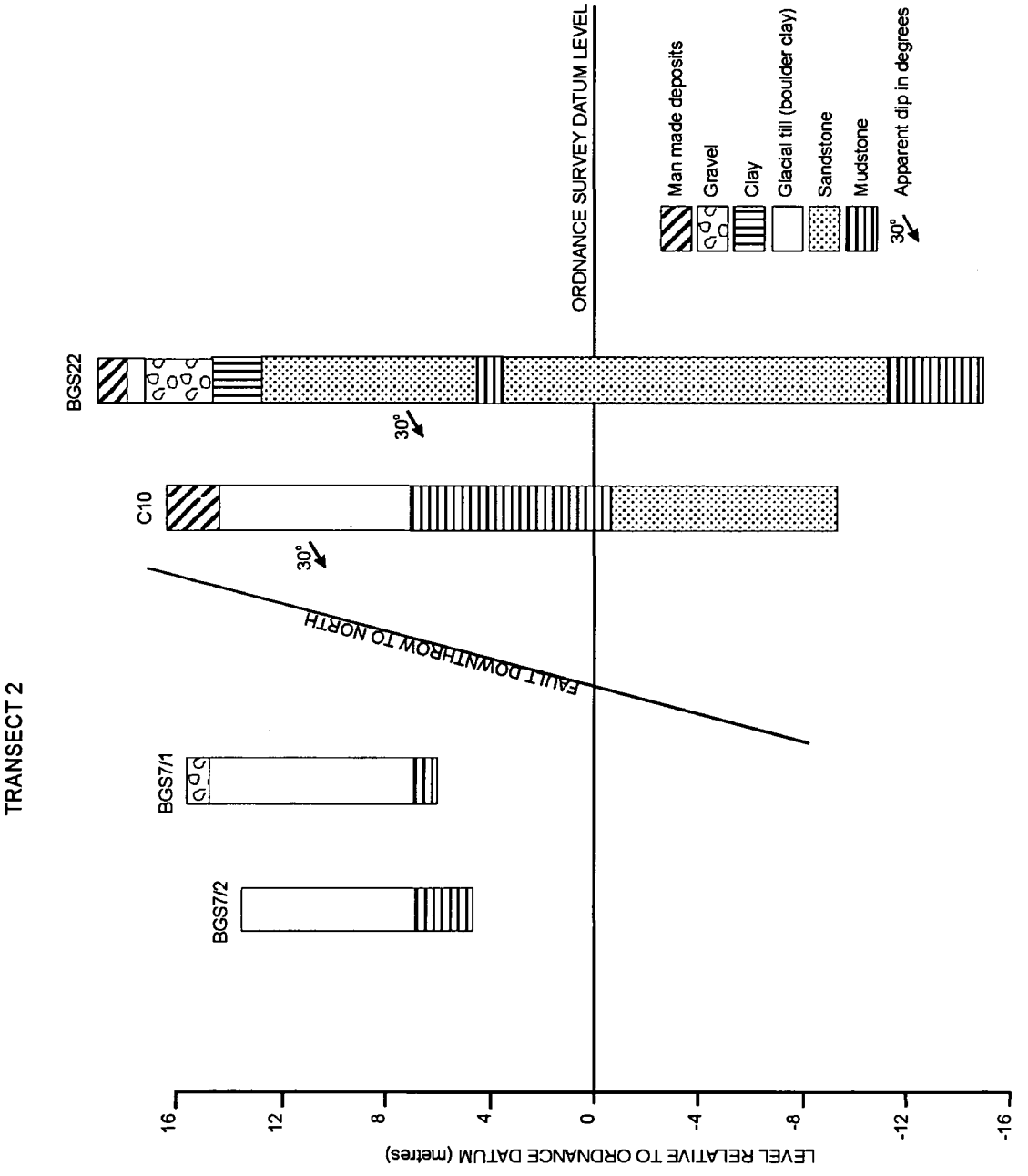

Figure C.2: Borehole logs from Transect 2

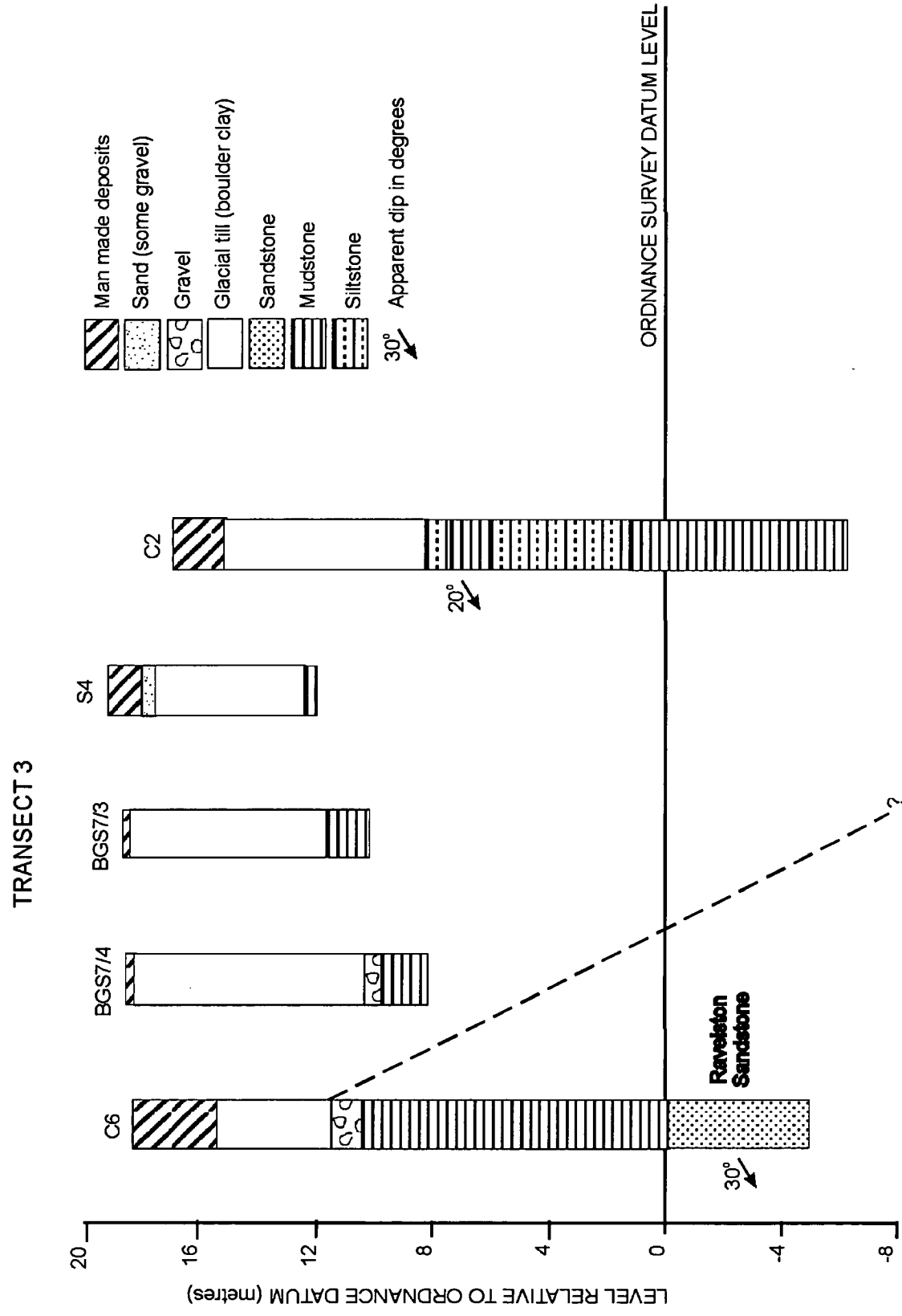

Figure C.3: Borehole logs from Transect 3

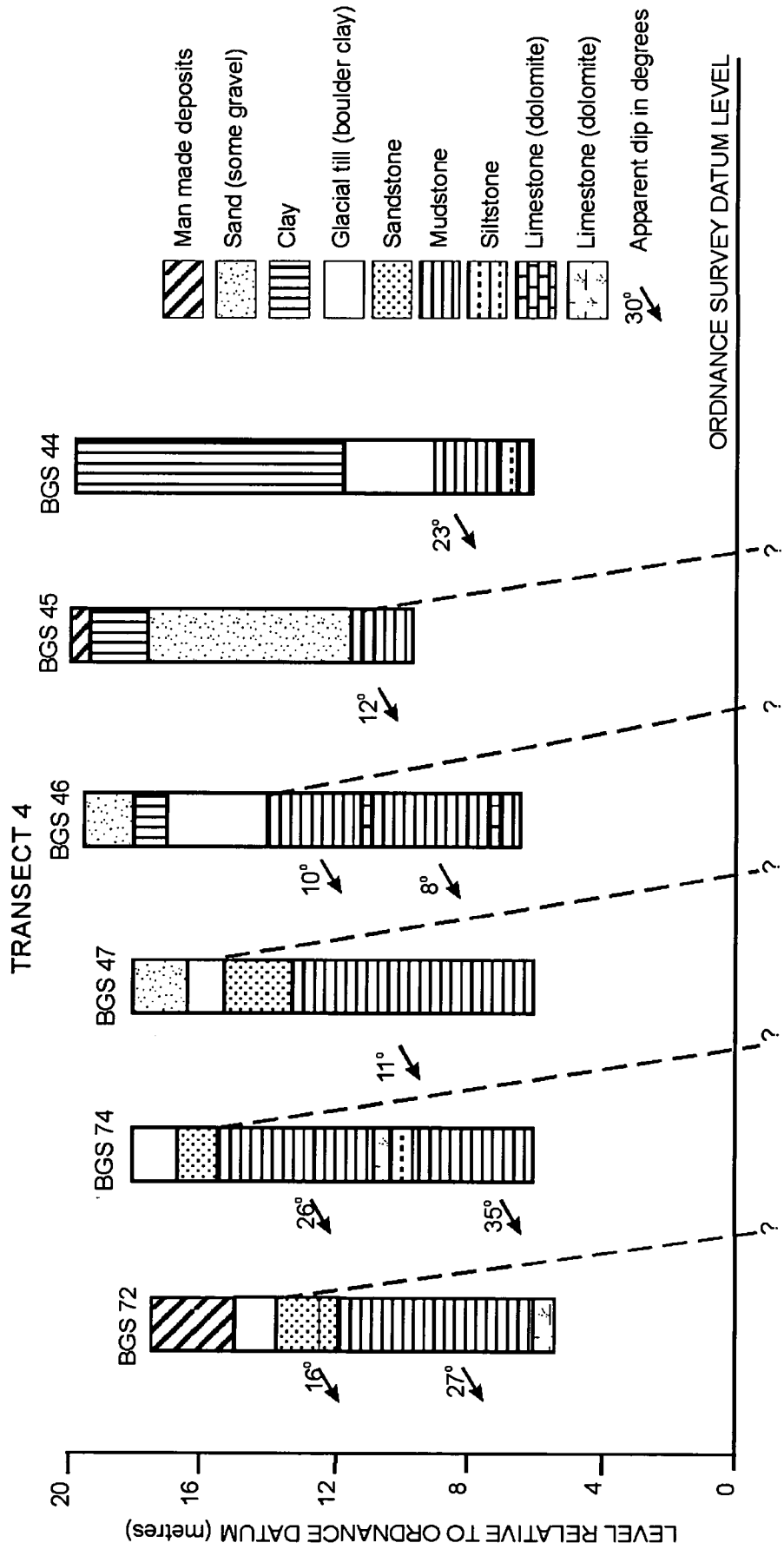

Figure C.4: Borehole logs from Transect 4

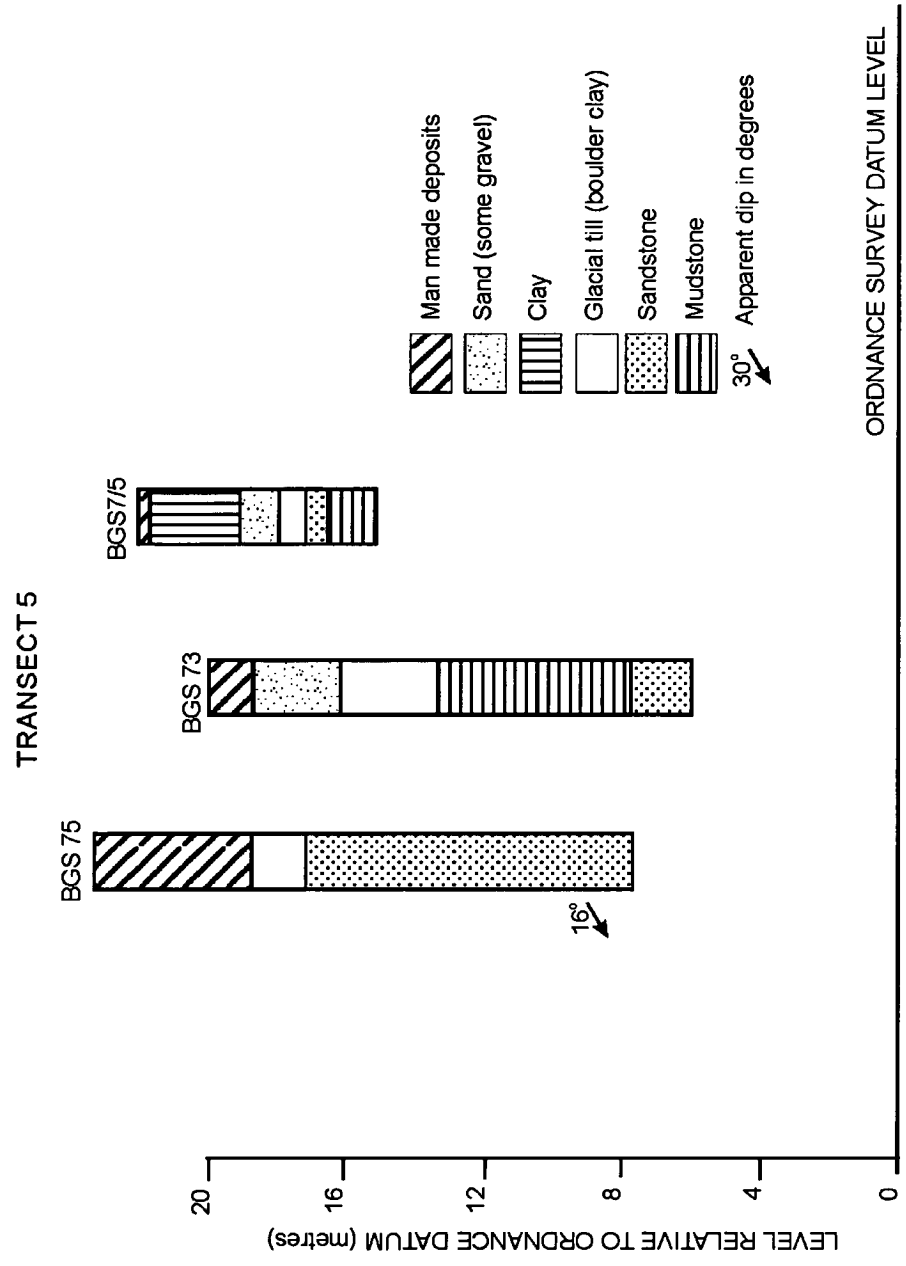

Figure C.5: Borehole logs from Transect 5